Final Report

FDOT Contract No.: BDK75 977-22
UF Contract No.: 00083425, 00087888 & 00104124

Development of LRFD Resistance Factors for Mechanically Stabilized Earth (MSE) Walls

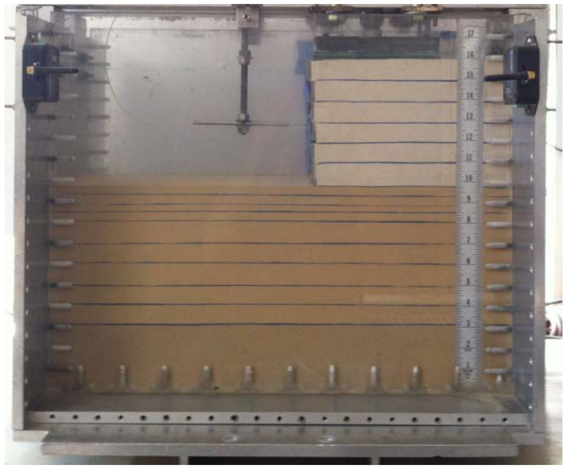

Principal Investigators: Michael McVay
David Bloomquist
Primary Researcher: Scott Wasman
Graduate Research Assistants: Gary Drew
Austin Lovejoy
Chris Pyle
Riley O'Brien

Department of Civil and Coastal Engineering
Engineering School of Sustainable Infrastructure and Environment
University of Florida
P.O. Box 116580
Gainesville, Florida 32611-6580

Developed for the

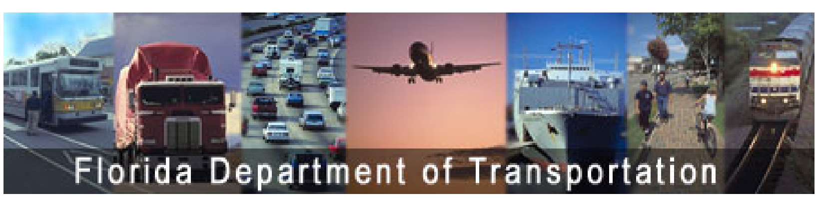

Rodrigo Herrera, P.E., Project Manager; Peter Lai (Retired)

December 2013

DISCLAIMER

The opinions, findings, and conclusions expressed in this publication are those of the authors and not necessarily those of the Florida Department of Transportation or the U.S. Department of Transportation.

Prepared in cooperation with the State of Florida Department of Transportation and the U.S. Department of Transportation.

SI (MODERN METRIC) CONVERSION FACTORS (from FHWA)

APPROXIMATE CONVERSIONS TO SI UNITS

SYMBOL	WHEN YOU KNOW	MULTIPLY BY	TO FIND	SYMBOL
		LENGTH		
in	inches	25.4	millimeters	mm
ft	feet	0.305	meters	m
yd	yards	0.914	meters	m
mi	miles	1.61	kilometers	km

SYMBOL	WHEN YOU KNOW	MULTIPLY BY	TO FIND	SYMBOL
		AREA		
in^2	square inches	645.2	square millimeters	mm^2
ft^2	square feet	0.093	square meters	m^2
yd^2	square yard	0.836	square meters	m^2
ac	acres	0.405	hectares	ha
mi^2	square miles	2.59	square kilometers	km^2

SYMBOL	WHEN YOU KNOW	MULTIPLY BY	TO FIND	SYMBOL
		VOLUME		
fl oz	fluid ounces	29.57	milliliters	mL
gal	gallons	3.785	liters	L
ft^3	cubic feet	0.028	cubic meters	m^3
yd^3	cubic yards	0.765	cubic meters	m^3
NOTE: volumes greater than 1000 L shall be shown in m^3				

SYMBOL	WHEN YOU KNOW	MULTIPLY BY	TO FIND	SYMBOL
		MASS		
oz	ounces	28.35	grams	g
lb	pounds	0.454	kilograms	kg
T	short tons (2000 lb)	0.907	megagrams (or "metric ton")	Mg (or "t")

SYMBOL	WHEN YOU KNOW	MULTIPLY BY	TO FIND	SYMBOL
		TEMPERATURE (exact degrees)		
°F	Fahrenheit	5 (F-32)/9 or (F-32)/1.8	Celsius	°C

SYMBOL	WHEN YOU KNOW	MULTIPLY BY	TO FIND	SYMBOL
		ILLUMINATION		
fc	foot-candles	10.76	lux	lx
fl	foot-Lamberts	3.426	candela/m^2	cd/m^2

SYMBOL	WHEN YOU KNOW	MULTIPLY BY	TO FIND	SYMBOL
		FORCE and PRESSURE or STRESS		
Lbf*	poundforce	4.45	newtons	N
kip	kip force	1000	pounds	lbf
lbf/in^2	poundforce per square inch	6.89	kilopascals	kPa

APPROXIMATE CONVERSIONS TO SI UNITS

SYMBOL	WHEN YOU KNOW	MULTIPLY BY	TO FIND	SYMBOL
LENGTH				
mm	millimeters	0.039	inches	in
m	meters	3.28	feet	ft
m	meters	1.09	yards	yd
km	kilometers	0.621	miles	mi

SYMBOL	WHEN YOU KNOW	MULTIPLY BY	TO FIND	SYMBOL
AREA				
mm^2	square millimeters	0.0016	square inches	in^2
m^2	square meters	10.764	square feet	ft^2
m^2	square meters	1.195	square yards	yd^2
ha	hectares	2.47	acres	ac
km^2	square kilometers	0.386	square miles	mi^2

SYMBOL	WHEN YOU KNOW	MULTIPLY BY	TO FIND	SYMBOL
VOLUME				
mL	milliliters	0.034	fluid ounces	fl oz
L	liters	0.264	gallons	gal
m^3	cubic meters	35.314	cubic feet	ft^3
m^3	cubic meters	1.307	cubic yards	yd^3

SYMBOL	WHEN YOU KNOW	MULTIPLY BY	TO FIND	SYMBOL
MASS				
g	grams	0.035	ounces	oz
kg	kilograms	2.202	pounds	lb
Mg (or "t")	megagrams (or "metric ton")	1.103	short tons (2000 lb)	T

SYMBOL	WHEN YOU KNOW	MULTIPLY BY	TO FIND	SYMBOL
TEMPERATURE (exact degrees)				
°C	Celsius	1.8C+32	Fahrenheit	°F

SYMBOL	WHEN YOU KNOW	MULTIPLY BY	TO FIND	SYMBOL
ILLUMINATION				
lx	lux	0.0929	foot-candles	fc
cd/m^2	candela/m^2	0.2919	foot-Lamberts	fl

SYMBOL	WHEN YOU KNOW	MULTIPLY BY	TO FIND	SYMBOL
FORCE and PRESSURE or STRESS				
N	newtons	0.225	poundforce	lbf
kPa	kilopascals	0.145	poundforce per square inch	lbf/in^2

*SI is the symbol for International System of Units. Appropriate rounding should be made to comply with Section 4 of ASTM E380.
(Revised March 2003)

TECHNICAL REPORT DOCUMENTATION PAGE

1. Report No.	2. Government Accession No.	3. Recipient's Catalog No.
4. Title and Subtitle Development of LRFD Resistance Factors for Mechanically Stabilized Earth (MSE) Walls		5. Report Date December 2013 6. Performing Organization Code
7. Author(s) Michael McVay, David Bloomquist, Scott Wasman, Gary Drew, Austin Lovejoy, Chris Pyle and Riley O'Brien		8. Performing Organization Report No.
9. Performing Organization Name and Address University of Florida – Dept. of Civil and Coastal Engineering Engineering School of Sustainable Infrastructure & Environment 365 Weil Hall – P.O. Box 116580 Gainesville, FL 32611-6580		10. Work Unit No. (TRAIS) 11. Contract or Grant No. BDK75 977-22
12. Sponsoring Agency Name and Address Florida Department of Transportation 605 Suwannee Street, MS 30 Tallahassee, FL 32399		13. Type of Report and Period Covered Final Report 9/15/09 – 9/30/13 14. Sponsoring Agency Code
15. Supplementary Notes		

16. Abstract: Over 100 centrifuge tests were conducted to assess Load and Resistance Factor Design (LRFD) resistance factors for external stability of Mechanically Stabilized Earth (MSE) walls founded on granular soils. In the case of sliding stability, the tests suggest the LRFD Φ values vary from 0.74 to 0.94 and 0.63 to 0.68 using Rankine and Coulomb methods for lateral resultant force, respectively. These values covered wall heights of 8 to 14 ft with variable backfill having $\mu_\phi = 32°$ and $CV_\phi = 11.7\%$. The study also revealed that the load factor for horizontal earth pressure agreed very well with current practice (AASHTO, 2012), i.e. 1.5.

In the case of bearing stability, the tests support Φ = 0.47 and 0.45 (β = 3.09) for foundation soils with $\mu_\phi = 26°$-$30°$ and 31°-33°, respectively, and Φ = 0.65 and 0.68 (β = 2.32); current practice uses Φ = 0.65. The tests also suggest the use of load inclination factors in estimating bearing capacity. The combination of axial and lateral force, i.e., inclined resultant reduces the depth and length of the bearing failure surface, which is reflected in a reduced capacity. From over 200 measurements, the load factor for vertical earth pressure was determined to be 1.87, which is larger than current practice, 1.35 (AASHTO, 2012), but agrees well with values reported by others for internal stability. In the case of bearing stability of MSE walls near slopes, it was found that current prediction methods (Bowles, Vesic, etc.) are too conservative. Moreover, based on observed failures of MSE walls near embankments, slope stability instead of bearing controls their design.

17. Key Words	18. Distribution Statement
MSE Walls, LRFD, Resistance Factors, Load Factors, Soil Variability, Centrifuge, Sliding Stability, Bearing Capacity, Embankments, and Load Inclination	No restrictions.

19. Security Classif. (of this report)	20. Security Classif. (of this page)	21. No. of Pages	22. Price
Unclassified	Unclassified	148	

Form DOT F 1700.7 (8-72) Reproduction of completed page authorized

ACKNOWLEDGMENTS

The researchers would like to thank the Florida Department of Transportation (FDOT) for the financial support to carry out this research as well as the guidance of the project managers. This research could not have been completed without the aid of the State Materials Office (SMO), which provided soil for use in the centrifuge models. Paul Gilbert of Soil Tech Consultants and Wipawi Vanadit-Ellis at the U.S. Army Corp of Engineers Centrifuge Research Center provided loess (Vicksburg Silt) for use in the centrifuge models. Also, The Bridge Software Institute (BSI) at The University of Florida made available sensors and test equipment for the centrifuge tests.

EXECUTIVE SUMMARY

Geotechnical design codes have adopted the reliability-based framework for design of retaining walls. Mechanically Stabilized Earth (MSE) walls are designed with appropriate load and resistance factors to meet internal and external stability for various vehicle loadings for different reinforcement lengths and wall heights. Recommended American Association of State Highway and Transportation Officials (AASHTO) resistance factors for external stability of MSE walls were developed from calibration to the Allowable Stress Design (ASD) Factors of Safety (FS) with no explicit consideration of soil variability and method error in resistance factors. Load factors for vertical and horizontal earth pressures have been recommended by AASHTO (2012); however, the MSE wall system is not considered when estimating soil stresses. For instance, the interaction between the soil and the concrete wall, as well as the forces at the reinforcement-wall connection result in large,-vertical stresses concentrated on the foundation soils under the front edge of the wall. As a result, the soil stress distribution is non-uniform, and the resultant soil force will not be located directly beneath the center of mass of the reinforced section. Currently, AASHTO recommends treating the vertical stress distribution as uniform, which may lead to un-conservative load or resistance estimates. Finally, methods that predict stability of MSE walls on embankments do not agree very well with one another and has led to variability in design and construction cost for many MSE walls in urban transportation settings.

This body of work determines the Load and Resistance Factor Design (LRFD) resistance factors for sliding and bearing of MSE walls where the influence of soil and method variability is considered through numerical and physical modeling (centrifuge). Furthermore, load factors for vertical and horizontal earth pressures are determined and compared to other reported values as

well as current practice. Additionally, the bearing capacity of MSE walls on embankments is investigated using physical models (centrifuge).

The significant findings of the sliding stability analysis are that the LRFD $\Phi = 0.74$ to 0.94 and 0.63 to 0.68 when using Rankine and Coulomb methods, respectively, for assessing lateral resultant forces. These values covered wall heights of 8 to 14 ft and variable backfill soil described by $\mu_{\phi} = 32°$ and $CV_{\phi} = 11.7\%$. In addition, the measured horizontal earth pressure load factor, 1.5, agreed very well with current practice (AASHTO, 2012).

In the case of bearing stability, LRFD $\Phi = 0.47$ and 0.45 ($\beta = 3.09$) for foundation soils with $\mu_{\phi} = 26°$-$30°$ and $31°$-$33°$, respectively, and $\Phi = 0.65$ and 0.68 ($\beta = 2.32$); current practice uses $\Phi = 0.65$. While it's not common to use a load inclination factor, the observed failure surfaces suggest that the inclined resultant essentially reduces the depth and length of a potential failure, which is reflected in the reduced capacity. In the case of load factors for vertical earth pressure, a value of 1.87 agrees well with values reported by others for internal stability in full-scale tests. It is recommend herein that 1.87 be used in practice over the current value of 1.35 (AASHTO, 2012).

The investigation of stability of MSE walls on embankments showed significant conservativeness of bearing capacity prediction methods employing slope correction factors. This conservativeness is attributed to deeper rupture surfaces (as opposed to shallow rupture surface unique to bearing capacity) observed in the centrifuge experiments. Plaxis finite element analysis of MSE walls on embankments also shows deep rupture surfaces, with observed Mohr circles in zone of bearing rupture surfaces, significantly lower than the Mohr-Coulomb strength envelope. The analysis further suggests that overall slope stability analysis, i.e., breaking up the mass into slices and solving the resistance along the bottom and checking the general limit state, i.e., driving vs. resistance analysis (e.g., modified Bishop, simplified Janbu, etc.,) is warranted over any bearing capacity approach.

TABLE OF CONTENTS

LIST OF TABLES

LIST OF FIGURES

CHAPTER 1
INTRODUCTION

1.1 Background

The use of Mechanically Stabilized Earth (MSE) walls has gained wide acceptance throughout the world over the past 40 years in a variety of applications. In the State of Florida, they are most commonly found in bridge abutments and ground elevation needs where right of way is an issue. In addition, they are frequently located in congested urban areas where there are multiple highway interchange overpasses requiring a supplement of natural grade to achieve the required roadway elevation. In these cases, the MSE walls sit atop a sloped soil embankment, set back from the embankment edge. Successful functionality of an MSE wall requires that the soil behind a facing structure is reinforced to create a stable block that carries external loads from earth pressures and traffic. Internal stability must be guaranteed against reinforcement pullout and rupture. Because the reinforced soil essentially becomes a block, external stability against sliding along the ground surface, bearing failure, rotation by overturning, and embankment's slope failure must be considered.

The Florida Department of Transportation (FDOT) has adopted the Load and Resistance Factor Design (LRFD) design approach for retaining walls and is using AASHTO's recommended LRFD resistance factors, Φ, (Figure 1-1) for internal and external wall stability assessment. Current (2012) AASHTO LRFD Φ factors were obtained by backfitting to Allowable Stress Design (ASD) Factor of Safety (FS). Unfortunately, AASHTO fails to account for any soil variability (e.g. Coefficient of Variation, CV of soil properties) as well as the influence of soil spatial correlation (i.e. covariance). For instance, shown in Figure 1 is AASHTO recommended Φ's for bearing and sliding resistance for wall footings.

Wall-Type and Condition		Resistance Factor
Nongravity Cantilevered and Anchored Walls		
Axial compressive resistance of vertical elements		Article 10.5 applies
Passive resistance of vertical elements		0.75
Pullout resistance of anchors [(1)]	• Cohesionless (granular) soils • Cohesive soils • Rock	0.65 [(1)] 0.70 [(1)] 0.50 [(1)]
Pullout resistance of anchors [(2)]	• Where proof tests are conducted	1.0 [(2)]
Tensile resistance of anchor tendon	• Mild steel (e.g., ASTM A 615 bars) • High strength steel (e.g., ASTM A 722 bars)	0.90 [(3)] 0.80 [(3)]
Flexural capacity of vertical elements		0.90
Mechanically Stabilized Earth Walls, Gravity Walls, and Semi-Gravity Walls		
Bearing resistance	• Gravity and semi-gravity walls • MSE walls	0.55 0.65
Sliding		1.0
Tensile resistance of metallic reinforcement and connectors	Strip reinforcements [(4)] • Static loading • Combined static/earthquake loading Grid reinforcements [(4)] [(5)] • Static loading • Combined static/earthquake loading	 0.75 1.00 0.65 0.85
Tensile resistance of geosynthetic reinforcement and connectors	• Static loading • Combined static/earthquake loading	0.90 1.20
Pullout resistance of tensile reinforcement	• Static loading • Combined static/earthquake loading	0.90 1.20
Prefabricated Modular Walls		
Bearing		Article 10.5 applies
Sliding		Article 10.5 applies
Passive resistance		Article 10.5 applies

Figure 1-1 AASHTO table 11.5.6-1 recommended LRFD **Φ** factors for retaining wall stability

Recently a number of researchers (Chalermyanont and Benson, 2005, Babu 2008) have developed reliability based design (RBD) figures and tables for MSE and retaining wall design. For instance, shown in Figure 2 is Chalermyanont and Benson (2005) recommended wall dimensions for MSE walls to resist sliding based on traditional driving and resisting forces, expressed through the FS. Note, it is common to use FS in describing the ratio of resistance to load; however, FDOT practice is to use Capacity Demand Ratio (CDR), which was used for this project.

$$FS_s = \frac{\tau}{P_a} = \frac{\gamma_s HL \tan(\phi)}{0.5\gamma_s H^2 k_a} \qquad \text{Eq. 1-1}$$

where γ_s is the unit weight of soil within MSE backfill, H is the height of the wall, L is the reinforcement length (also the width of the wall) and k_a is the coefficient of active pressure. Figure 2 was developed for an angle of internal friction, ϕ, between 25° and 40° and CV_ϕ from 5% to 20% for different levels of reliability, β or probability of failure, P_f. Similar charts have been developed for sliding and bearing capacity by Babu (2008). Note, Chalermyanont and Benson (2005) presented the coefficient of variation as COV (Figure 1-2).

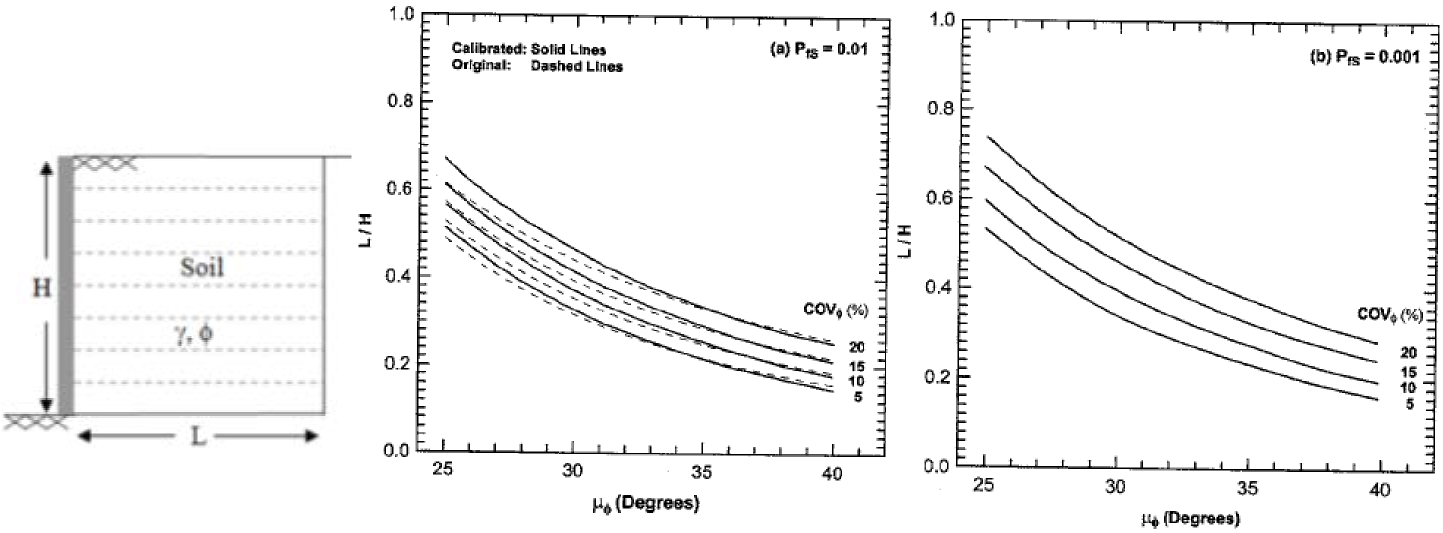

Figure 1-2 Recommended MSE wall L/H as a function of: μ_ϕ and CV_ϕ for P_f of 0.01 and 0.001 (Chalermyanont and Benson, 2005)

Evident from Figure 1-2, the wall design (L/H) is not only affected by the soil's angle of internal friction, ϕ, but also its CV_ϕ, which is not considered in sliding stability given in Figure 1-1. Unfortunately, typical Reliability Based Design (RBD) charts, e.g. Figure 1-2, does not provide AASHTO's LRFD Φ (or associated Factor of Safety, FS – Eq. 1-1) for specific variability (e.g. soil's μ_ϕ, CV_ϕ, etc). However, FS or LRFD Φ may be obtained from the RBD analysis performed for the charts. For instance, shown in Figure 1-3 is a histogram of hundreds of thousands of Monte Carlo Simulations which varied the selected backfill angle of internal friction, ϕ, holding the wall's L/H = 0.5, and the backfill's unit weight at19 kN/m^3 (121 lbs/ft^3) fixed. The variability or histogram is a result of having backfill angle of internal friction modeled a normal distribution with a mean (μ_ϕ) of 30^0 with a CV_ϕ = 10%. For this analysis, the mean of histogram (μ_{FSO}), was 1.212 (i.e. mean factor of safety) which corresponds to an LRFD Φ of 0.83 (1 / μ_{FSO}) similar to Figure 1-2 for sliding. Also associated with the histogram or probability distribution is the probability of failure or the area under the curve for $FS_0 < 1$ which is 0.0178 (P_{fs}, Figure 1-3). Consequently, instead of presenting just L/H influence, a new set of curves may be added to Figure 1-2 representing μ_{FSO} or 1/LRFD Φ. Of interest is the range of LRFD Φ for typical FDOT wall dimension and soil conditions for acceptable failure probabilities.

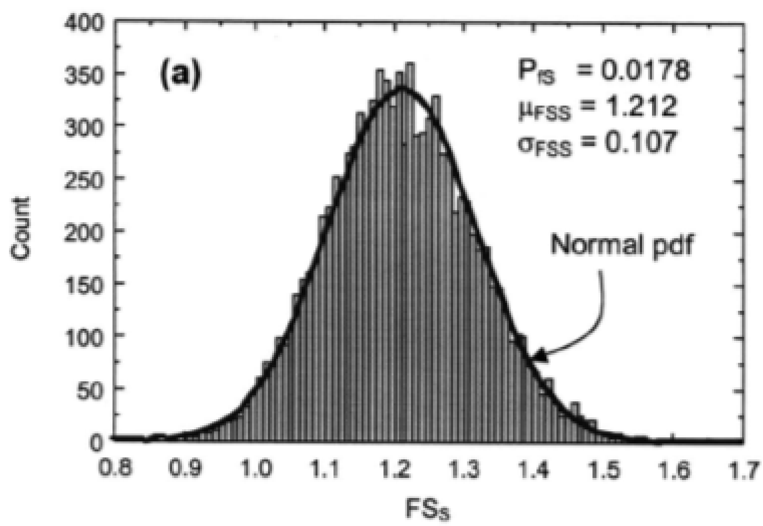

Figure 1-3 Histogram of probability distribution of sliding factor of safety (FS_s) from Chalermyanont and Benson (2005)

Also, affecting the probability of failure (P_{fs}, Figure 1-3) is the accuracy of the histogram and the theory (Eq. 1-1) used to generate the distribution. For instance, if P_a (Eq. 1-1) was generated from Rankine or Coulomb's approach, different μ_{FSS} or 1/LRFD Φ may develop. The latter needs to be checked against field or laboratory data for verification of summary statistics. One way is to collect field cases with known FS or another is to validate the theory through centrifuge testing. Specifically, the wall driving forces could be increased while the resistance is held constant in the centrifuge. The field/centrifuge testing needs to be performed in conjunction with the analysis (Figure 1-3) to identify μ_{FSO} or 1/LRFD Φ for a specific probability of failure, P_{fo}. The work should be performed for external wall stability due to sliding, overturning, bearing and slope stability. In finding LRFD Φ, the influence of backfill soil properties (angle of internal friction, ϕ, variability CV_ϕ, unit weight, γ and variability $CV\gamma$), retained soil properties (ϕ, variability CV_ϕ) and foundation soil properties (ϕ, variability CV_ϕ) should be considered.

Also of concern to FDOT Engineers are the prediction of the bearing capacity of MSE walls near slopes. For instance, Figure 1-4 illustrates the two cases of footings on or near a slope. Of interest is the reduced soil mass in the passive and radial zones and the reduced length of the shear surface along these zones (dashed lines). Bowles (1997) proposed a method to adjust the bearing capacity equation (Eq. 1-2),

$$q_u = \left(c\mathrm{N}_c + \gamma_s D_f N_q C_q + 0.5\gamma_s L N_\gamma C_\gamma\right)\Phi \qquad \text{Eq. 1-2}$$

through the bearing capacity factor, N_γ term (weight influence factor), Eq. 1-3,

$$N'_\gamma = \frac{N_\gamma}{2} + \frac{N_\gamma}{2}\left[R + \frac{b}{2L}(1 - R)\right] \qquad \text{Eq. 1-3}$$

where c = cohesion, γ = total unit weight, D_f = footing embedment depth, C_q, C_γ = correction factors, L = footing width, N_c, N_q, N_γ = cohesion, surcharge and unit weight bearing capacity factors, R = ratio of minimum to maximum K_p, b = distance from front of wall to edge of slope and K_p = coefficient of passive earth pressure.

However, other methods have been proposed (e.g., Meyerhof, Hansen, Vesic) for the bearing capacity factors near slopes. FDOT engineers have shown a comparison of bearing capacity results using Bowles and other non-adjusted factors (Figure 1-5). The figure identifies the influence of distance to the slope crest on the bearing capacity ratio using Bowles as well as Meyerhof, Vesic, Hansen, and Deschenes. Evident from Figure 1-5, there is a factor of 3 differences between the smallest and largest values.

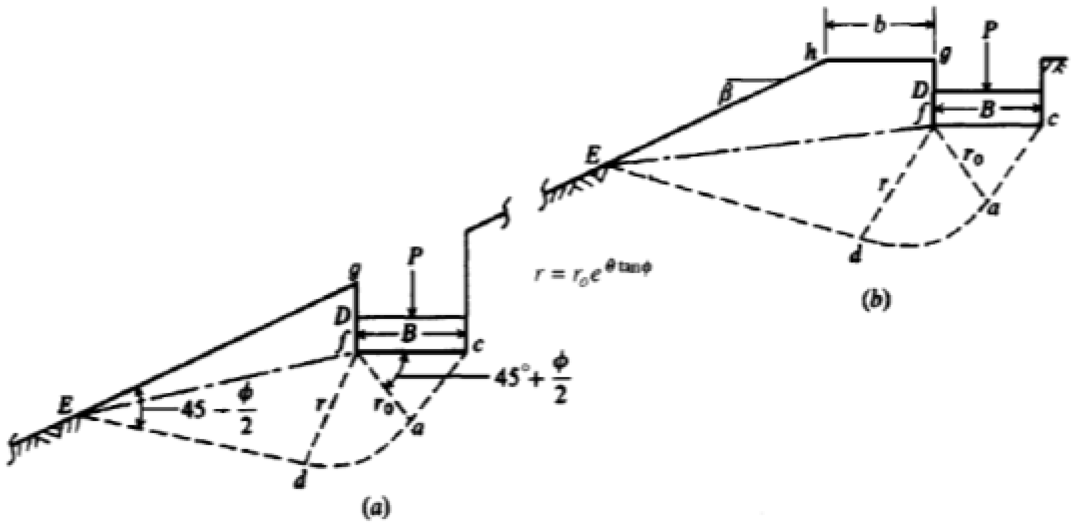

Figure 1-4 Footing (a) on slope and (b) near slope (Bowles, 1997)

As identified earlier, the LRFD resistance factors, Φ, developed by AASHTO (Figure 1-1) were obtained by calibration with Allowable Stress Design (ASD). The true LRFD resistance factors should be obtained from reliability theory through a comparison of experimental with theoretical analysis. For instance, having a sufficient quantity of experimental data (e.g. centrifuge data), i.e. measured data, then the bias (measured/predicted – e.g. Bowles)

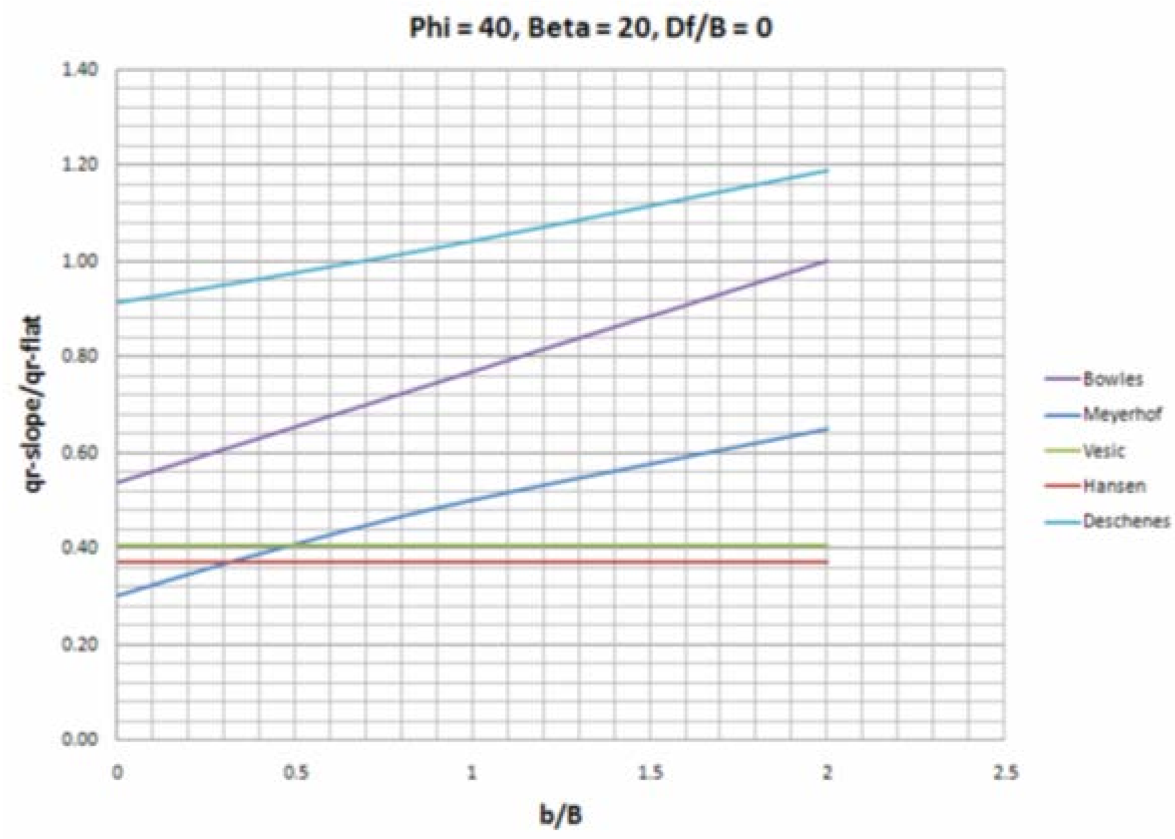

Figure 1-5 Comparison of methods for ratio of bearing capacity to influence of distance to slope, for a beta of 20°

and associated LRFD Φ could be established for certain level of reliability. Interestingly, AASHTO recommends LRFD Φ's of 0.65 for a slope supporting a structural element. Based on Figure 1-5 the latter values are highly unconservative (a difference of a factor of 3). Also from Figure 1-1, the Φ's for bearing capacity from AASHTO does not consider the influence of soil variability both behind and beneath the MSE wall.

1.2 Objective and Supporting Tasks

The primary objective of this research is to develop load and resistance factors for MSE walls subject to sliding and bearing capacity, i.e. external stability. The load and resistance factors will be determined from measured data, collected from centrifuge tests, and, partially, from the field. The load factors will be determined for the vertical and horizontal soil dead loads and the external surcharge loading. The resistance factors will be determined for cases of known soil variability and external surcharge load variability (μ and CV). First, nomographs, similar to those presented by Chalermyanont and Benson (2005), will be developed for a parametric sensitivity analysis to determine the soil properties that are most influential on the wall's reliability. Second, centrifuge tests of MSE walls for sliding and bearing stability will be performed to determine the CV's of load and resistance. For bearing stability, MSE walls near embankments (sloping ground) will be tested in addition to those only on flat ground. Third, based on the CV's observed in the tests, the load factors, γ, and Φ's will be recommended for sliding and bearing stability. Lastly, analytical expressions of the CV's of load and resistance that are a function of the soil properties μ and CV's will be presented for future application.

1.2.1 Task 1 – Identify Typical Design Scenarios, Loadings, and Analytical Approaches

In design of MSE walls, the external stability analysis must consider sliding, overturning, bearing capacity and overall (slope) stability. For each analysis method, typical geometries and loading must be established (e.g., horizontal or sloping backfills, external live loads, etc.). Conventional analysis methods include Rankine and Coulomb for lateral earth pressures and Terzaghi, Meyerhof, Vesic, etc. for bearing capacity. MSE walls use extensible and inextensible types of reinforcement that influence the internal stability. Typical backfill used in the state of Florida have a range of friction angles and must meet limits on the amount of fines for permeability.

1.2.2 Task 2 – Preliminary Assessment of CDR or LRFD Φ for External Wall Stability

Using general FDOT wall layouts, backfill, retained and foundation soil types, along with analytical approaches identified in Task 1, the factor of safety equations for wall sliding, bearing or slope failure will be developed. Next, a matrix of variable wall dimensions, backfill, retained soil and foundation soil will be established along with their expected CV's. Subsequently, using Monte Carlo simulations, each parameter's range and CV will be evaluated to assess the histogram of CDR from which the mean (μ_{CDR} or $1/\Phi$) and variance (σ_{CDR}^2) will be established, along with the probability of failure, P_f. The results of the analysis will be presented in charts.

1.2.3 Task 3 – Centrifuge Testing of Retaining Wall Stability

Centrifuge tests of MSE wall sliding and bearing stability will be performed to establish the histograms of the CDR, load and resistance. Models will be tested in the large centrifuge at the University of Florida in 3 phases: (1) models of sliding stability for a 40 ft tall, L/H =1 prototype wall, (2) models of bearing stability for a 20 ft tall, L/H = 0.5 prototype wall on flat ground, and (3) models of bearing stability for a 20 ft tall, L/H = 0.5 prototype wall near an embankment. Based on the findings from Task 2, the soil parameters and wall dimensions of greatest influence in MSE wall sliding and bearing stability will be tested. Since the purpose is to evaluate the histograms of load and resistance to obtain the μ and CV of each for use in determining each respective Φ, a total of 50 to 60 tests are required.

1.2.4 Task 4 – Comparison of Centrifuge with Analytical Evaluations

Comparison of the results from the centrifuge tests with current conventional methods of sliding and bearing stability estimation will be made. This will provide the method bias, λ, of each conventional method to predict load and resistance and which will subsequently be used in determining the Φ's of each stability case. In the analysis, a change in analytical assumptions (e.g., Rankine versus Coulomb behavior, Meyerhof versus Vesic, etc.) or the introduction of other uncertainties may be required to bring the analytical methods in alignment with experimental.

1.2.5 Supplemental Task 1 – Experimental Program

To evaluate the methods used in design of MSE walls near slopes and histograms of CDR, centrifuge tests will be performed with varying parameters (i.e., ϕ, γ, etc.). The tests will consider two typical slope angles (β), soil properties (ϕ, γ) of the embankment and backfill, distance from the slope (setback = b), presence of water in the embankment, surcharge loading and wall dimensions (L/H). To establish the histograms, it is expected that approximately 60 centrifuge tests will be required.

1.2.6 Supplemental Task 2 – Identify Methods and Assess CDR

Considering slope angles, soil properties of the embankment and backfill, wall distance from slope (setback = b), presence of water and wall dimensions with analytical methods, the distributions of CDR for wall stability will be developed for one or two of the identified analytical approaches (Figure 1-5). If any of the methods have to be modified, the approach will cover the modes of failure encounter in the centrifuge tests. Specific focus on either shallow bearing failure surface or overall deep seated failure surfaces passing through the backfill will be considered. Simulations will be performed using the Monte Carlo method and available software for stability analysis. The resulting distributions of CDR will establish the mean, μ, and coefficient of variation, CV, related to the system and analytical methods.

1.2.7 Supplemental Task 3 – Comparison of Experimental and Analytical CDR Evaluations

Based on the comparison between the results from Supplemental Tasks 1 and 2, it is expected that adjustments in the analytical methods (e.g., bias) will be required. A change in the LRFD Φ for the stability issues investigated will be suggested. Following this, the final μ and CV of CDR or LRFD Φ will be established. Subsequently, equations or charts which represent these as functions of slope angle (β), μ and CV of soil properties (ϕ and γ), wall distance from slope (setback = b) and wall dimensions (L/H) will be developed.

1.2.8 Task 5 – Development of LRFD Φ External Wall Stability and Final Report

Based on the results from Task 4, LRFD Φ's will be established for the cases of external wall stability investigated. These will be expressed as a constant or range for the most critical soil parameters (e.g., μ_ϕ and CV_ϕ) and wall dimensions (e.g., L/H).

Also, the final LRFD Φ for walls near slopes will be established based on the evaluations and consultation with FDOT. Here, careful consideration will be given as to which parameters which have minimal or maximum impact on LRFD Φ. The developed LRFD Φ may be expressed as a constant, a range, or when necessary, a table or monograph based on b, β, μ_ϕ, CV_ϕ, μ_γ or CV_γ.

CHAPTER 2
EXPERIMENTAL PROGRAM

2.1 Introduction

An experimental program was developed to assess the external stability of MSE walls for determination of the LRFD Φ's. This started with a sensitivity study to identify soil properties that were most influential in the sliding, bearing and overturning stability of an MSE walls. Then, a new centrifuge container was designed and built to conduct the experimental tests. Based on size of the container, a model scale was selected (1:40) and tests sensors were selected and obtained to monitor stresses beneath the wall and its movements (lateral and vertical). Finally, granular soil was selected for the MSE study based on the sensitivity analysis, and laboratory tests were performed to assess densities, and angles of internal friction. A discussion each of the tasks involved in the experimental program follows.

2.2 Parameter Sensitivity Study

In order to determine the influence of the soil properties and their variability (CV) on the sliding and bearing stability of the MSE walls, a sensitivity analysis was performed using simulations in Matlab (2009b). The equations describing the loads and resistances for each case were used with randomized soil properties to develop a histogram of capacity demand ratio (CDR). With a sufficient number of simulations, the P_f for each analysis (e.g. mean of ϕ, μ_ϕ) was determined along with its influence.

The wall investigated was 30 ft high with a reinforcement length to wall height ratio (L/H) of 1, retained and backfill soil unit weight of 105 pcf (pound per cubic foot-lb/ft^3) with friction angle of 30°, foundation soil friction angle of 35° and load surcharge (q_s) of 250 psf (pound per square foot-lb/ft^2). The left side of Table 2-1 presents the CV's of the values used in the analyses including a description of the variability of

Table 2-1 Soil properties and surcharge for simulation

Variable	Baseline Parameters		Range of Parameters		Distribution
	(μ)ϕ	CV	(μ)ϕ	CV	
Retained Soil ϕ	30°	10%	20° - 40°	5% - 20%	Lognormal
Retained Soil γ	105 pcf	5%	95 pcf - 120 pcf	5% - 20%	Lognormal
Foundation Soil ϕ	35°	10%	20° - 40°	5% - 20%	Lognormal
Foundation Soil γ	105°	5%	95 pcf - 120 pcf	5% - 20%	Lognormal
Surcharge q_s	250 psf	25%	NA	NA	Lognormal

surcharge. The analysis was carried out with Rankine active earth pressure, and selecting soil parameters randomly using Monte Carlo simulations from a log normal distribution based on μ n and CV identified in the left side of Table 2-1.

The right side of Table 2-1 shows the values and distribution used for the sensitivity study. Each μ and CV parameter is consistent with those reported in research literature (Duncan, 2000; Zevgolis, 2006; Fenton, 2008) as well as from FDOT State Materials Office. Since soil properties and loads are generally non-negative, a lognormal distribution was used as the underlying distribution for each.

2.2.1 Sliding

The stresses that were considered in sliding stability analysis of the MSE wall are shown in Figure 2-1. Inclined surcharge soil is commonly built on the top of the wall to meet elevation requirements and thus should be considered in stability analysis. However, in some AASHTO Load Cases the inclined surcharge may not be present and thus λ and β, the horizontal distance and angle of the inclined surcharge, respectively, are negligible or zero. The critical case considers the external surcharge, q_s, load to act a distance of 2H-L over the backfill.

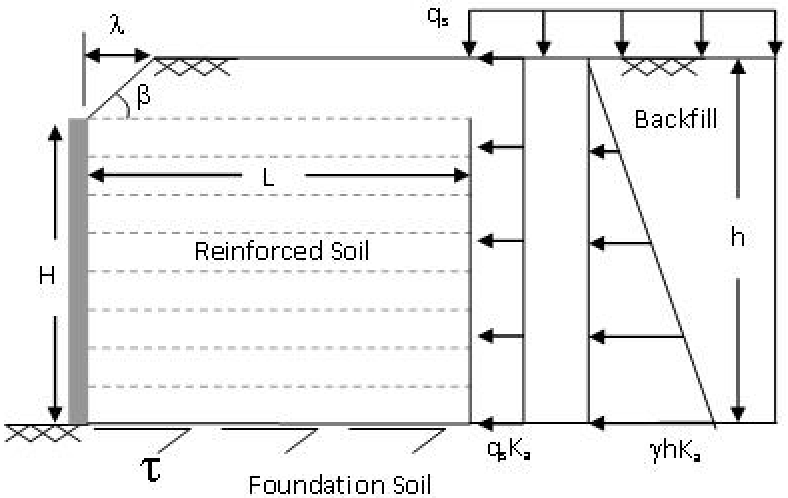

Figure 2-1 MSE wall for sliding stability

Equations 2-1 and 2-2 describe the factored driving force (load) and the factored resisting force, respectively, for the MSE wall shown in Figure 2-1. The load and resistance are factored with the recommended values in the AASHTO LRFD Bridge Design Specifications (2012). The resistance is a function of vertical earth pressure and is factored by the recommended load factor, EV.

$$P_a = K_a(0.5\gamma_s H^2 EH + q_s HLS) \quad \text{Eq. 2-1}$$

where P_a is the force resultant per unit width (factored), γ_s is the total unit weight of backfill, q_s is the surcharge load, h is the height of horizontal earth pressure diagram, K_a is the active earth pressure coefficient (Rankine or Coulomb), EH is the load factor for horizontal earth pressure, and LS is the load factor for surcharge.

The factored shear resistance to along the base of the MSE wall is

$$T = (\gamma_s HLEV \tan(\phi))\Phi \quad \text{Eq. 2-2}$$

where T is the factored shear resistance, γ_s is the total unit weight of backfill, H is the height of reinforced soil (use H if inclined soil is not present), L is the reinforcement length, EV is the load factor for vertical earth pressure, ϕ is the friction angle of drained reinforced or foundation soil (smallest), and Φ is the LRFD resistance factor.

In the sensitivity study, the probability of failure, P_f for sliding is defined from the simulations as the total number of CDR < 1 divided by the total number of CDR values. The CDR of sliding stability analysis is defined as

$$CDR = T/P_a \qquad \text{Eq. 2-3}$$

Figure 2-2 shows the histogram of CDR for sliding (Eq. 2-3) using the baseline parameters (left side of Table 2-1) with Monte Carlo sampling from the soil parameter distributions. One million simulations were performed to obtain the distribution. The latter number of simulations resulted in a CV of P_f that was less than 10% with a standard error less than 0.1% ($\sqrt{\frac{P_f(1-P_f)}{N}}$). The P_f was 0.082% and the CDR had a μ = 1.78, and standard deviation, (σ) = 0.34 (CV = 19%).

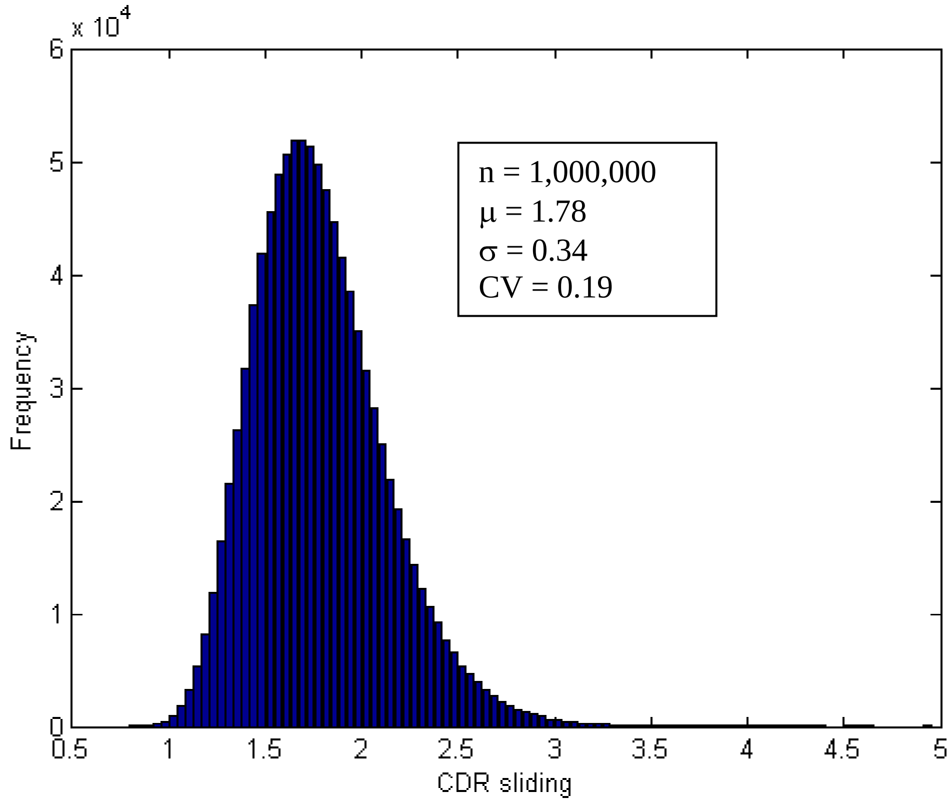

Figure 2-2 Histogram of CDR for MSE wall sliding stability

Once the baseline wall's P_f was established, a sensitivity analysis was performed using the parameters' ranges in Table 2-1 to determine their effect on P_f and identify which parameters should be varied in the centrifuge tests. For the analysis, each parameter was varied (Monte Carlo) and the other held constant from which a distribution of CDR (Eq. 2-3) was developed then the P_f was calculated. For example, the baseline case was analyzed with the retained soil ϕ of 20°, 25°, 30°, 35°, 40° resulting in five distinct values of P_f.

Figure 2-3 shows the influence of the parameters on the P_f. It is evident that the mean unit weight has a small influence on the P_f which is due to the presence of the surcharge load acting above the backfill soil (Figure 2-1). In the case where the surcharge is absent or considered to act over the reinforced soil also, the increase in unit weight has no influence on the P_f due to the fact it appears in both the numerator and denominator of Equation 2-3. The friction angle (ϕ) is shown to have a significant influence on the P_f and it appears to be through the resistance ($\tan(\phi)$) rather than the driving force (K_a). The foundation soil's ϕ has the same influence, since it contributes to the shear resistance in the same manner (i.e., $\tan(\phi)$). The increasing CV for both friction angle (ϕ) and unit weight (γ) results in higher P_f. This is because the lower values become more likely (σ increases since $CV = \sigma/\mu$) which decreases the resisting force and increases the driving force. The analysis suggests that the friction angle of the soils (backfill, and foundation soil) should be varied, but not unit weights in the centrifuge tests.

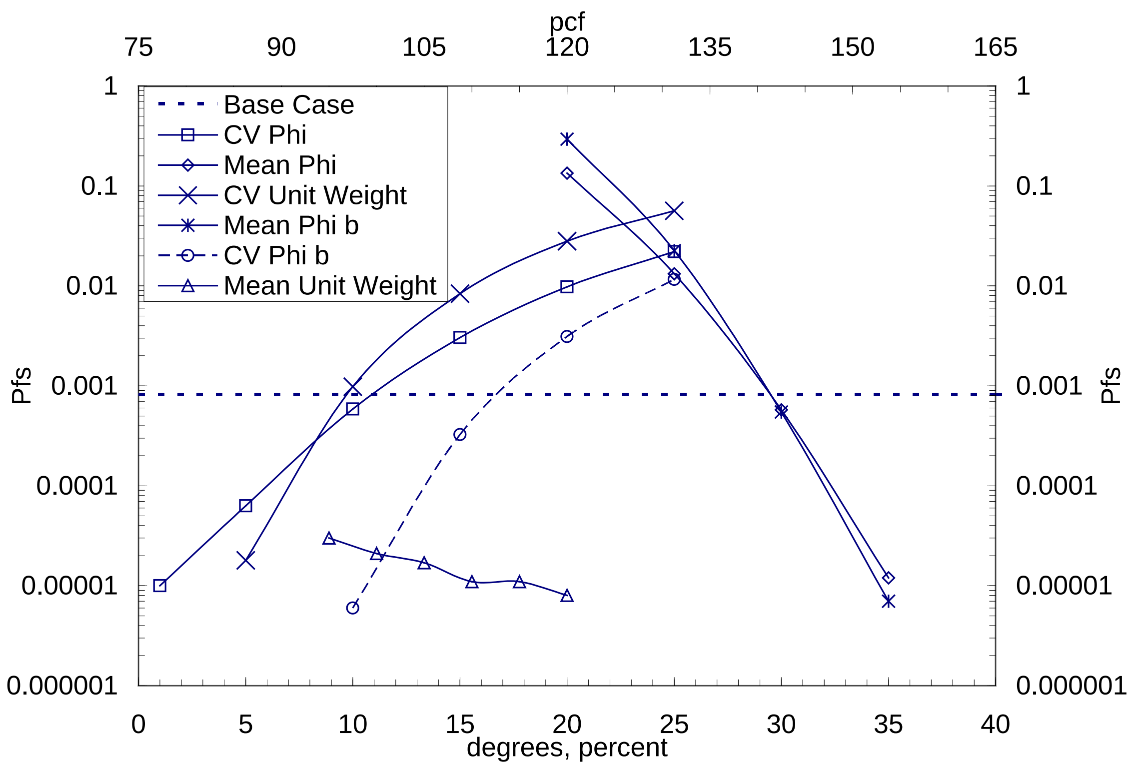

Figure 2-3 Probabilities of failure from sliding stability parametric study

2.2.2 Bearing

The stresses that are considered in the case of bearing stability of an MSE wall are shown in Figure 2-4. The same wall configuration presented for sliding stability is presented here, however, in some cases λ and β are negligible or zero. The critical case considers the external surcharge, q_s, load to act a distance of 2H from the back of the wall facing elements.

Furthermore, the bearing pressure, q_v, is assumed to be uniform over the base of the wall (distance L).

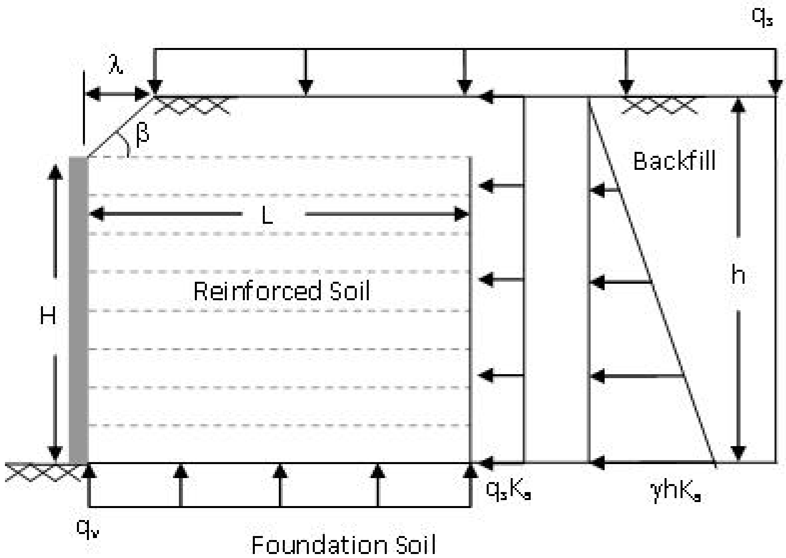

Figure 2-4 MSE wall for bearing stability

Equations 2-4 and 2-5 describe the factored load and factored bearing resistance (capacity), respectively, for the MSE wall in Figure 2-4. The load and resistance are factored with the recommended values in the AASHTO LRFD Bridge Design Specifications (2012).

$$R_v = \gamma_s HLEV + \mathrm{q}_s LLS \qquad \text{Eq. 2-4}$$

where R_v is the factored vertical resultant load, H is the wall height, L is the foundation width (i.e., reinforcement length), EV is the load factor for vertical earth pressure, q_s is the surcharge load, and LS is the load factor for surcharge.

Equation 2-5 is from the factored ultimate bearing capacity of spread footings and is applied to estimate MSE wall bearing resistance.

$$q_u = \left(c\mathrm{N}_c + \gamma_s D_f N_q C_q + 0.5\gamma_s L N_\gamma C_\gamma\right)\Phi \qquad \text{Eq. 2-5}$$

where c is the cohesion, γ is the total unit weight above or below footing depth, D_f is the footing embedment depth, C_q, C_γ are the correction factors for groundwater location, L' is the footing width, N_c, N_q, N_γ are the cohesion, surcharge and unit weight bearing capacity factors and Φ is the bearing resistance factor.

When eccentric loads are present, the foundation width, L, must be reduced to an effective length as shown below.

$$L' = L - 2e \qquad \text{Eq. 2-6}$$

where L' is the effective foundation width, L is the foundation width without eccentric loads, and e is the eccentricity. The eccentricity is a function of the resisting and overturning moments about the toe of the wall (front of facing) and the vertical resultant force.

$$e = \frac{L}{2} - \frac{(M_r - M_o)}{R_v} \qquad \text{Eq. 2-7}$$

The resisting moment is determined from

$$M_r = \gamma_s HLEV\left(\frac{L}{2}\right) \qquad \text{Eq. 2-8}$$

where M_r is the resisting moment, γ_s is the soil's unit weight, H is the wall height, L is the foundation width (i.e., reinforcement length), and EV is the load factor for vertical earth pressure.

The overturning moment is determined from

$$M_o = K_a\left(0.5\gamma_s\frac{H^3}{3}EH + q_s\frac{H^2}{2}LS\right) \qquad \text{Eq. 2-9}$$

where M_o is the overturning moment, γ_s is the soil's unit weight, H is the wall height, EH is the load factor for horizontal earth pressure, q_s is the surcharge load, LS is the load factor for surcharge, and K_a is the active earth pressure coefficient (Rankine or Coulomb).

Simulations of bearing stability for the wall configuration shown in Figure 2-4 were performed with CDR Equation 2-10, The P_f is defined as the total number of CDR < 1 divided by the total number of CDR values.

$$CDR = \frac{q_u}{\left(\frac{R_v}{L'}\right)} \qquad \text{Eq. 2-10}$$

where q_u is the ultimate bearing capacity presented in Equation 2-5 and R_v/L' is the applied bearing pressure described in Equations 2-4 and 2-6. Next, the P_f is defined as the total number of CDR < 1 divided by the total number of CDR values. This is synonymous with the area under the tail of a distribution where the CDR < 1.

Figure 2-5 shows the histogram of CDR for bearing (Eq. 2-10) using the baseline parameters (left side of Table 2-1) with Monte Carlo sampling from the soil parameter distributions. One million simulations were performed to obtain the distribution. This number of simulations was required for a CV of P_f that was less than 10% with a standard error less than 0.1% ($\sqrt{\frac{P_f(1-P_f)}{N}}$). The P_f was 0.1% and the CDR had a mean, $\mu = 6.5$, and standard deviation, $\sigma = 1.3$ (CV = 20%). The histogram for bearing stability showed higher CDR values and a more skewed distribution. The occurrence of the higher values may be due to the higher CV of the backfill soil's angle of internal friction, ϕ. This will be investigated further based on the measured distributions of load and resistance from the centrifuge tests. Where the μ's of $CDR_{measured}$ and $CDR_{predicted}$ differ significantly, the LRFD Φ may have to be adjusted with a corrected bias to ensure an appropriate P_f.

Next, a sensitivity analysis using the parameters in Table 3-1 was performed to identify their effect on P_f and identify the parameters to be studied in the centrifuge tests of bearing stability. The analysis followed the same procedure as discussed previously for the sliding stability. For the analysis, each parameter was varied (Monte Carlo), and the others held constant, from which a distribution was developed along with the P_f.

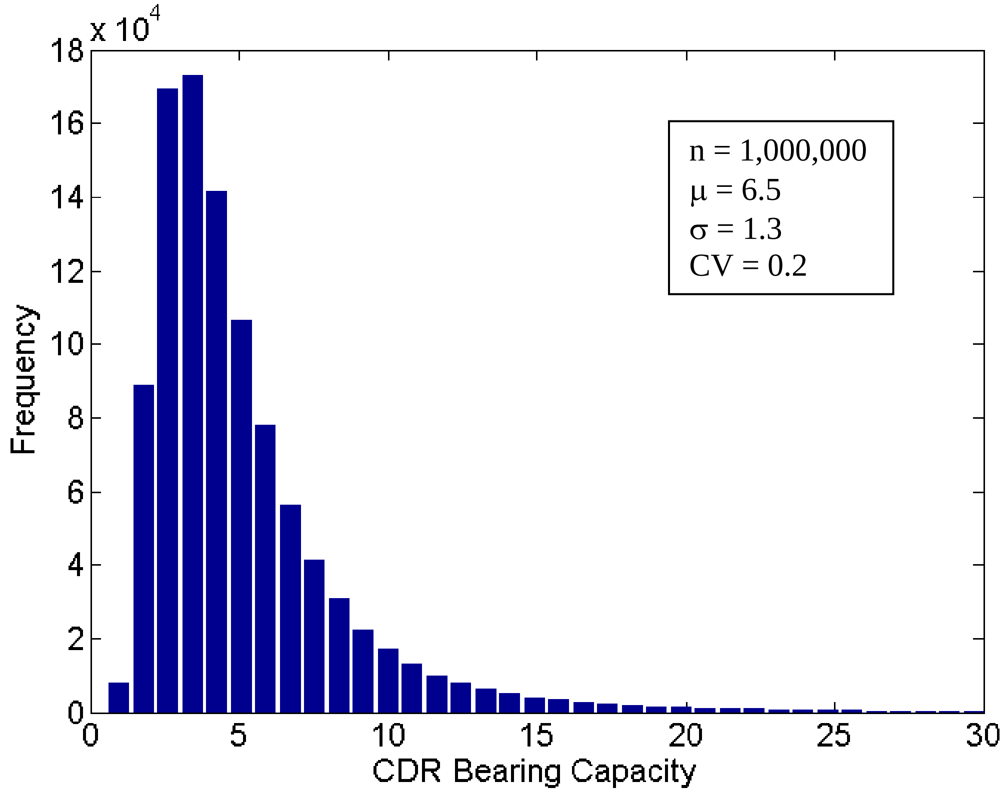

Figure 2-5 Histogram of CDR for MSE bearing capacity

Figures 2-6 and 2-7 show the influence the parameters had on the P_f. Evident is that the μ_ϕ for all soils (foundation soil, fs; reinforced soil, rs; backfill, bf) and the CV_ϕ of the foundation soil, fs, have the greatest influence on the P_f. For the foundation soil, increased μ_ϕ increases q_u, thereby shifting the mean of the CDR to the right and decreasing the P_f; whereas, increased CV_ϕ shifts the mean CDR to the left and increases the P_f. The increased P_f (larger area under tail < 1) is due to more frequent values of low ϕ (σ increases since $CV = \sigma/\mu$) resulting in smaller N_q and N_γ terms in Eq. 2-5. For the retained soil (reinforced soil and backfill), increased μ_ϕ decreases M_o through K_a and results in decreased eccentricity and thereby, larger L'. This shifts the mean

CDR to the right decreases the P_f. The foundation and retained soil's CV_γ and retained soil's CV_ϕ have a smaller influence on P_f, changing it less than an order of magnitude. The analysis suggests that the μ_ϕ of all soils (foundation and retained) and the foundation soil's CV_ϕ should be varied in the centrifuge tests.

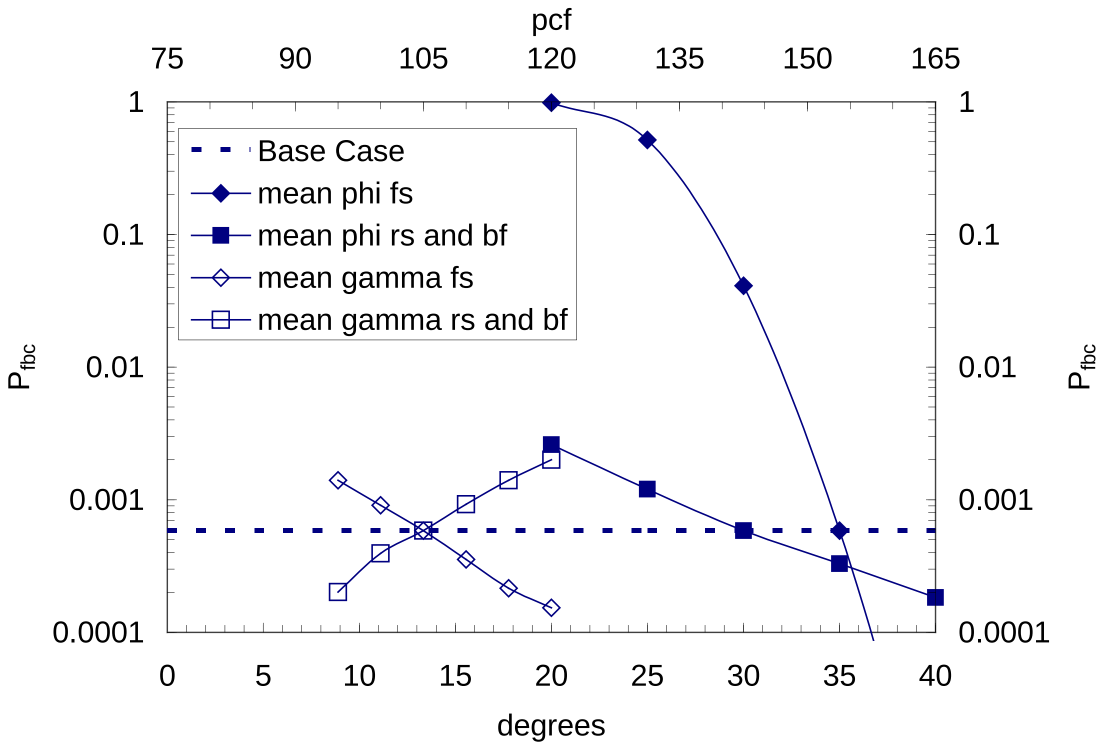

Figure 2-6 P_f from bearing stability parametric study: varied mean values

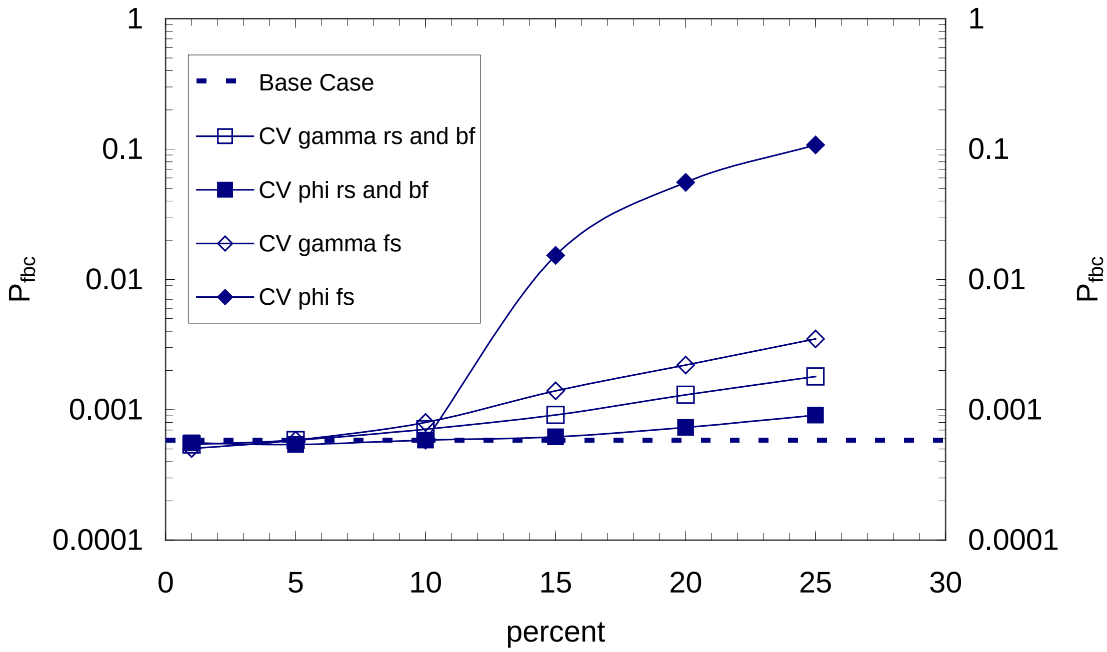

Figure 2-7 P_f from bearing stability parametric study: varied CV values

2.2.3 Overturning

The overturning stability of an MSE wall is dependent on the moment that resists the overturning moment. For the MSE wall shown in Figure 2-4, the factored resisting and overturning moments are given in Equations 2-8 and 2-9, respectively. Each is per unit length of wall and includes the influence of q_s in the overturning but not in the resisting (i.e., isn't considered to act over the reinforced soil), i.e. recommended procedure by the FDOT Structures Design Guidelines (SDG) (2013). Equation 2-11 is the CDR for overturning. Note, an LRFD Φ is not applied in overturning to the resisting moment terms, as currently there isn't a value suggested.

CDR = Mr / Mo   Eq. 2-11

Figure 2-8 shows the histogram of CDR for overturning (Eq. 2-11) using the baseline parameters (left side of Table 2-1) with Monte Carlo sampling from the soil parameter distributions. One million simulations were performed to obtain the distribution. The number of simulations was required for a CV of P_f that was less than 10% with a standard error less than

0.1% ($\sqrt{\frac{P_f(1-P_f)}{N}}$). The P_f was 0.03% and the CDR had a μ = 1.62, and standard deviation, (σ) = 0.24 (CV = 15%).

Next, a sensitivity analysis using the parameters in Table 2-1 was performed to identify their effect on P_f and identify the parameters to be studied in the centrifuge tests. The analysis followed the same procedure as discussed previously for the sliding and bearing stability.

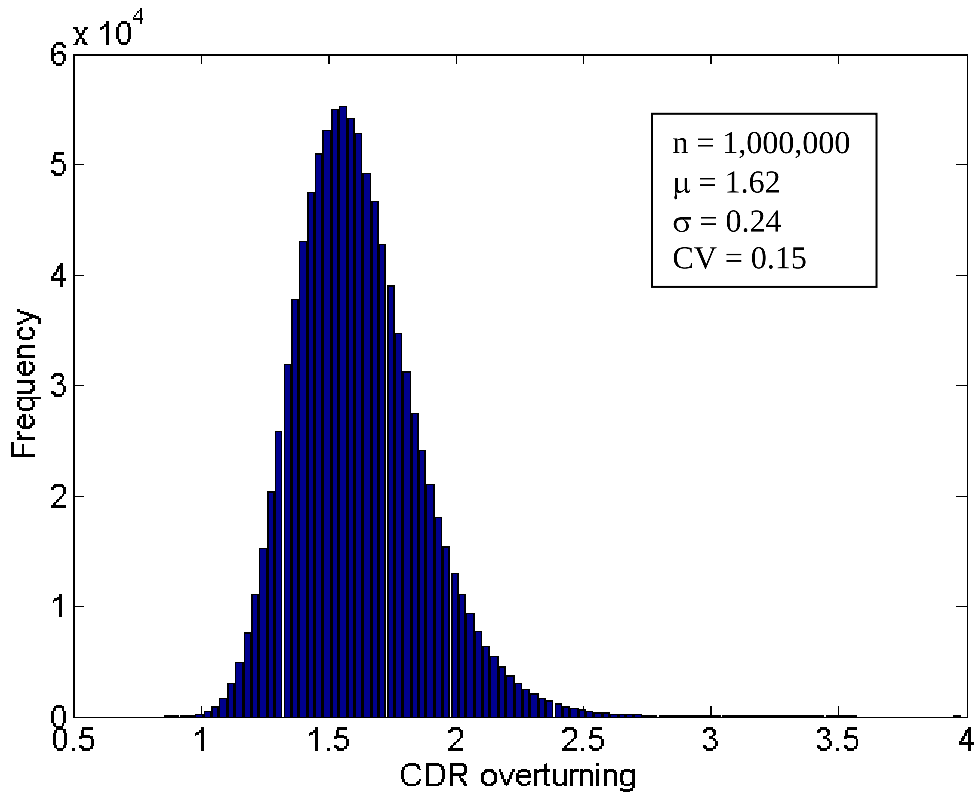

Figure 2-8 Histogram of CDR for MSE overturning

Figure 2-9 shows the parameters used in the overturning stability and their influence on the P_f. As overturning is only a function of the reinforced soil and backfill soil, it was found that the greatest influence on CDR was from the mean and CV of ϕ in the backfill and the CV of reinforced soil and backfill soil (treated herein as the same material). The mean value of phi, ϕ, influences the overturning moment or driving force through the Ka term and it decreases the P_f. As shown with the bearing sensitivity study, the increase in CV of phi, ϕ, and gamma results in an increased likelihood of lower values sampled from the distribution (log-normal).

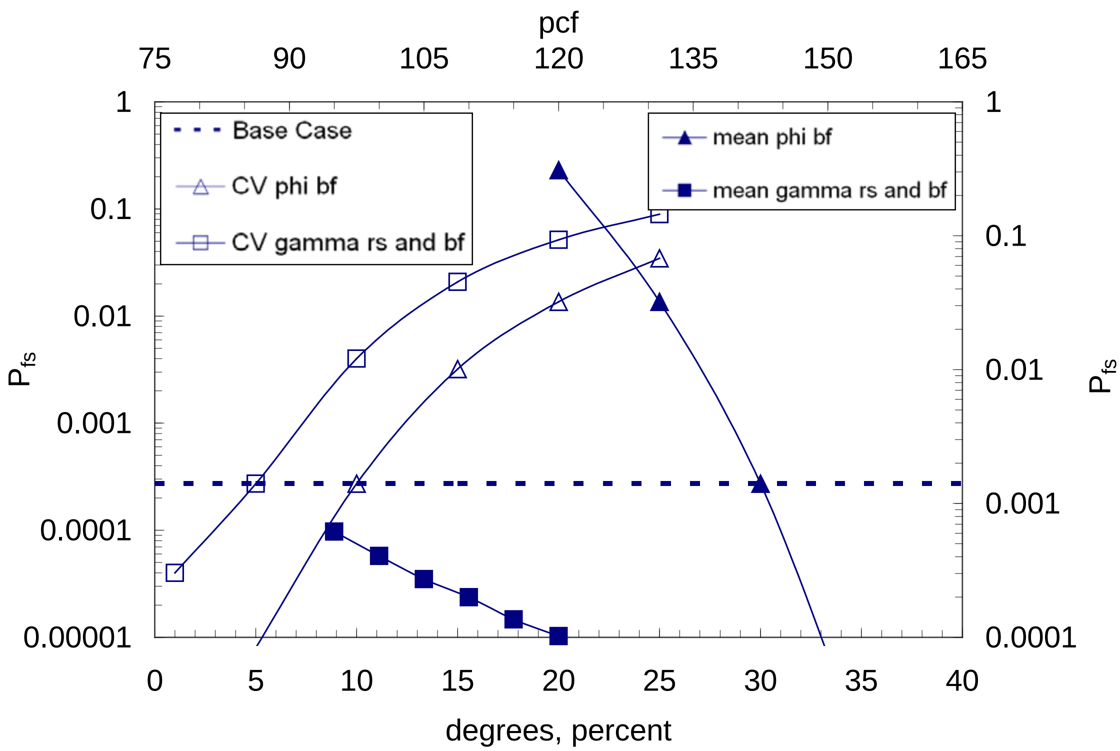

Figure 2-9 Probabilities of failure from sensitivity study on overturning: varied μ and CV values

2.3 Centrifuge Test Setup and Models

2.3.1 UF's Large Centrifuge

The UF centrifuge used in this study was constructed in 1987 as part of a project to study the load-deformation response of axially loaded piles and pile groups in sand (Gill, 1988). Throughout the years several modifications have been undertaken to increase the payload capacity of the centrifuge. Previously, electrical access to the centrifuge was only provided by four 24-channel electrical slip-rings. Recently, this was supplemented with wireless nodes for monitoring instruments in the centrifuge container. Pneumatic and hydraulic access is provided by a three port hydraulic rotary union manufactured by the Deublin Company. The rotating-arm payload on the centrifuge is balanced by fixed counterweights that are placed prior to spinning the centrifuge. Aluminum C channels support both the pay-load and counter-weights in the centrifuge (Figure 2-10).

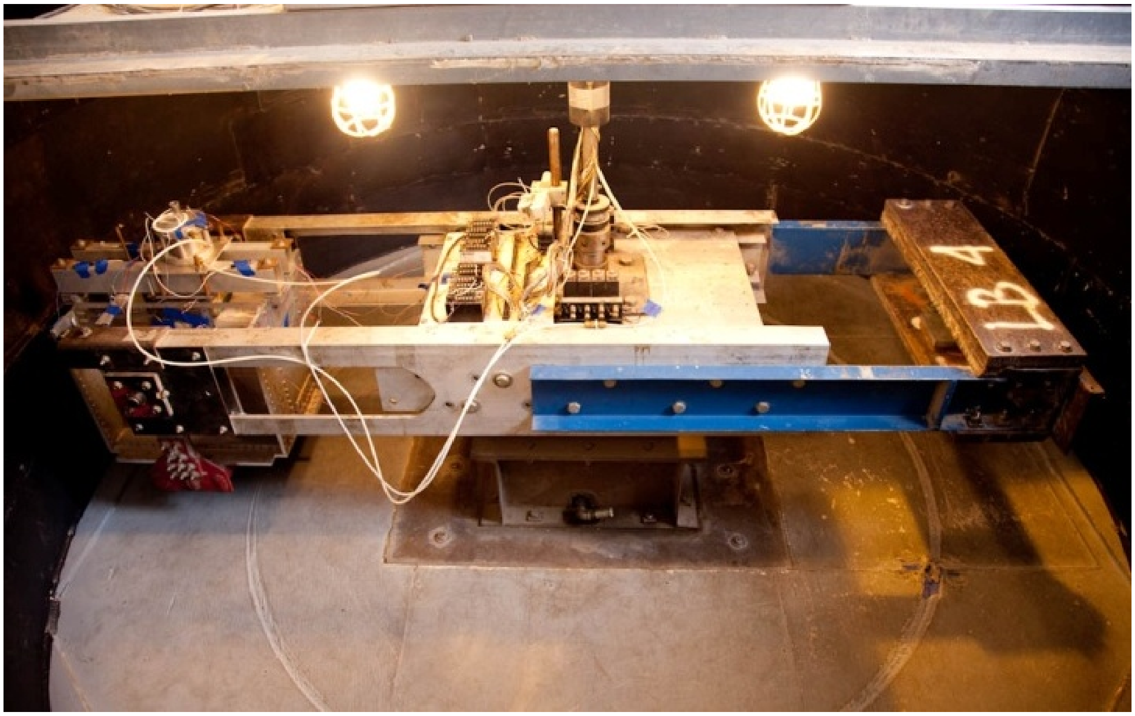

Figure 2-10 University of Florida's large geotechnical centrifuge

On the pay-load side (Figure 2-10), the aluminum C channels support the swing-up platform, through shear pins. The latter allows the model container to rotate as the centrifugal force increases with increasing rotations per minute (rpm). The platform (constructed from A36 steel), and connecting shear pins were load tested with a hydraulic jack in the centrifuge. The test concluded that both the swing up platform and shear pins were safe against yielding if the overall pay-load was less than 12.5 tons (Molnit, 1995).

2.3.2 Theory of Similitude

Laboratory modeling of prototype structures has seen a number of advances over the decades. Of interest are those, which reduce the cost of field-testing as well as reduce the time of testing. Additionally, for geotechnical engineering, the modeling of in situ stresses is extremely important due to soils' stress dependent nature (stiffness and strength). One way to reproduce the latter accurately in the laboratory is with a centrifuge.

A centrifuge generates a centrifugal force, or acceleration based on the angular velocity which a body is traveling. Specifically, when a body rotates about a fixed axis each particle travels in a circular path. The angular velocity, ω, is defined as $d\theta/dt$, where θ is the angular position, and t is time. From this definition, it can be implied that every point on the body will have the same angular velocity. The period T is the time for one revolution, and the frequency f is the number of revolutions per second (rev/sec). The relation between period and frequency is $f = 1/T$. In one revolution, the body rotates 2π radians or

$$\omega = \frac{2\pi}{T} = 2\pi f \qquad \text{Eq. 2-12}$$

The linear speed of a particle (i.e., $v = ds/dt$) is related to the angular velocity, ω, by the relationship $\omega = d\theta/dt = (ds/dt)(1/r)$ or

$$v = \omega \mathrm{r} \qquad \text{Eq. 2-13}$$

An important characteristic of centrifuge testing can be deduced from Eqs. 2-12 and 2-13: all particles have the same angular velocity, and their speed increases linearly with distance from the axis of rotation (r). Moreover, the centrifugal force applied to a sample is a function of the revolutions per minute (rpm) and the distance from the center of rotation. In a centrifuge, the angle between the gravitational forces, pulling the sample towards the center of the earth, and outward centrifugal force is 90°. As the revolutions per minute increase so does the centrifugal force. When the centrifugal force is much larger than the gravitational force the normal gravity can be neglected. At this point the model will in essence feel only the "gravitational" pull in the direction of the centrifugal force. The earth's gravitational pull (g) is then replaced by the centrifugal pull (a_c) with the following relationship;

Centrifugal acceleration; $A = r\left(\frac{\pi \cdot rpm}{30}\right)^2$ Eq. 2-14

where $rpm = \frac{30}{\pi}\sqrt{\frac{a_c}{r}}$ Eq. 2-15

Scaling factor; $N = \frac{a}{g}$ Eq. 2-16

$N = \frac{\sqrt{a_c^2 + g^2}}{g^2}$ Eq. 2-17

If $a_c >> g$, $N = \frac{a_c}{g}$ Eq. 2-18

where a is the total acceleration, g is the normal gravitational acceleration, a_c is the centrifugal acceleration, rpm is the number of revolutions per minute, and r is the distance from center of rotation.

The scaling relationship between the centrifuge model and the prototype can be expressed as a function of the scaling factor, N (Eq. 2-18). It is desirable to test a model that is as large as possible in the centrifuge, to minimize sources of error (boundary effects, etc.), as well as grain size effects with the soil. With the latter in mind, and, requiring the characterization of MSE walls with heights of at least 20 ft, the following rationale was employed to determine the appropriate centrifuge g level and angular speed, ω.

The inside depth of the sample container was 18 inches which dictated the model total height. To model a 20 ft high prototype wall, 40 gravities would result in a model wall height of 6 inches, and allow 12 inches for modeling of the foundation soil. For L/H = 0.5, L = 3 inches ensures 4L (i.e., 4B) below the wall to minimizing boundary effects as well as allow bearing rupture surface to develop. Spinning the centrifuge at higher or lower gravities would imply the model would either have to be smaller, or too large to fit in the container.

Based on Equation 2-18, a number of important model (centrifuge) to prototype (field) scaling relationships have been developed (Taylor, 1995). Shown in Table 2-2 are those, which apply to this research. Two significant scaling relationships emerge: (1) Linear Dimension are scaled 1/N (prototype length = N*model length), (2) Stresses are scaled 1:1. The first significantly decreases the size of the experiment, which reduces both the cost and time required to run a test. The second relationship ensures that the in situ field stresses and model stresses are 1:1. Note, the effective stress controls both the stiffness and strength of the soil.

Table 2-2 Centrifuge scaling relationships (Taylor, 1995)

Property	Prototype	Model
Acceleration (L/T^2)	1	N
Dynamic Time (T)	1	1/N
Linear Dimensions (L)	1	1/N
Area (L^2)	1	$1/N^2$
Volume (L^3)	1	$1/N^3$
Mass (M)	1	$1/N^3$
Force (ML/T^2)	1	$1/N^2$
Unit Weight (M/L^2T^2)	1	N
Density (M/L^3)	1	1
Stress (M/LT^2)	1	1
Strain (L/L)	1	1
Moment (ML^2/T^2)	1	$1/N^3$

2.3.3 Model Containers

Two centrifuge containers were designed/constructed for running the experimental tests at 100 G (N = 100 or a_c = 100 x g). Both were made from 6061 aluminum alloy with an acrylic glass viewing window, with a shear and bending factor of safety of 2. Visual Analysis structural design software was used to aid in the determination of bending of the acrylic glass plates.

Connections were designed for bolt shear and pullout using a reduction factor of 0.75 and a factor of safety of 2. The aluminum container connections were made using A490 structural steel grade 8 bolts and the acrylic plate is fastened with A286 superalloy stainless steel bolts. Box A, designed with a single viewing window, has the inner dimensions 22 in x 7-7/8 in x 14 in (L x W x H) and Box B, which has two viewing windows, has the inner dimensions of 22 in x 8 in x 18 in.

2.3.4 Data Acquisition System

The centrifuge was updated to a wireless data acquisition system for this research project. Original equipment included 96 slip ring channels; however, these were prone to noise in the signal due to environmental dust. Figure 2-11 shows a MicroStrain V-Link wireless sensor node and receiver station. A total of 3 nodes were used for each test and mounted on the test container to monitor sensors in-flight and simultaneously transmit data to the host computer at a rate of 10 Hz (samples/second). Each node had 4 analog channels that could monitor differential voltage output and up to 10 channels were used to monitor: a) 1 load cell, b) 4 soil stress sensors and c) 4 LVDTs.

Figure 2-11 MicroStrain V-Link node and receiver

2.3.5 Instrumentation

2.3.5.1 Pneumatic Loading Device

An Omega 10,000 lb compression load cell (Figure 2-12) was used to measure surcharge load applied to the back of the MSE wall. It was placed in-line with a pneumatic piston supplied with air through a hydraulic rotary union at the center of the centrifuge (Figure 2-10). The air pressure was controlled through a valve near the supply and monitored using a pressure gauge.

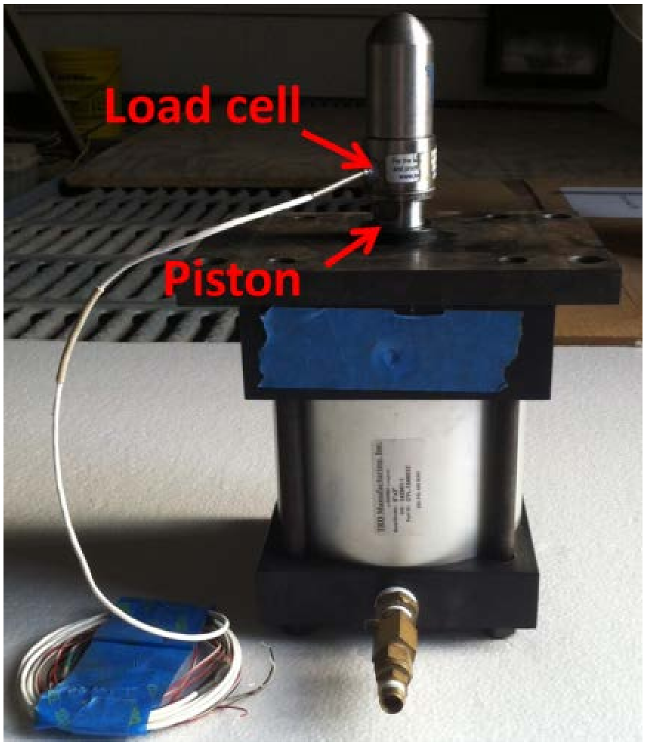

Figure 2-12 Pneumatic piston with compression load cell

2.3.5.2 Linear Variable Differential Transformer (LVDT)

The MSE model wall's horizontal and vertical movement was monitored using MicroStrain's miniature LVDTs which had a 1 inch range (Figure 2-13). Each LVDT was attached to a rigid support frame and oriented horizontally and vertically.

Figure 2-13 MicroStrain's miniature LVDT-1 inch Range

2.3.5.3 Soil Stress Sensors

Of great interest in external MSE stability are the bearing stresses beneath the reinforced section (L in Figures 2-1 and 2-4) of the model wall (Figure 2-14). For instance, with the bearing stresses and the wall's vertical displacement, a load-displacement curve is developed to identify the wall's bearing capacity. The latter required that stress sensors be embedded within the foundation soil, so size and stiffness effects had to be considered. Due to scaling laws, small embedded gauges had to be used in order to fit within the footprint of the MSE wall (L). Miniature, low profile pressure sensors (Figure 2-15) manufactured by Sensorworks (shown in Figure 2-15) and Honeywell (similar to Figure 2-15 but not shown here) were selected to use in the models. All sensors have a stainless steel diaphragm surface with a semi-conductor Wheatstone bridge (4 active strain gauges) bonded to the interior surface. The sensors are 1 – 1.5 mm thick and 7.5 mm in diameter (6 mm diameter active surface).

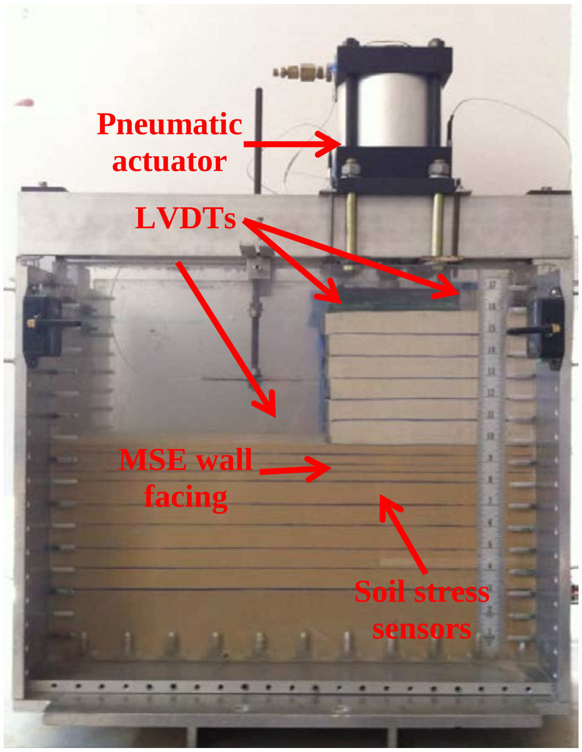

Figure 2-14 Setup of MSE wall model in test container

Figure 2-15 Soil stress sensor – 250 psi

Dave and Dasaka (2011) compiled the factors that affect output from earth pressure cells (soil stress sensors) and suggested correction methods. Many previous studies of such effects (Taylor, 1945; Monfore, 1950; Loh, 1954; Askegaard, 1963; Tory and Sparrow, 1967; Labuz and Theroux, 1999) concluded that when the stiffness of the diaphragm is larger than the stiffness of the medium, the stress output is larger than the medium’s stress (over-registration). And when the stiffness is less than that of the medium, under-registration occurs. Further, sensor thickness also effects the redistribution of stresses at the edges and low profile sensors have less effect. Dave and Dasaka (2011) suggest a sensor aspect ratio (thickness/outer diameter) < 1/5. Table 2-3 has the measured ratios for the soil stress sensors used in this study which satisfy Dave and Dasaka (2011) suggested correction methods.

Table 2-3 Factors affecting measurements with embedded sensors in centrifuge tests

Factor	Required ratios	Measured Ratios
Aspect ratio	T/D < 1/5 (Experimentation Station, 1944) < 1/10 (Dunnicliff, 1988)	1/7.5 – 1.5/7.5 < 1/5
Active diameter	$d/D_{50} > 10$	6/0.2 > 10
Sensor-soil stiffness ratio	> 0.5	28.5 x 10^3 ksi/(0.6 – 4 ksi) > 0.5
Active diameter/Deflection	$d/\Delta > 2000 - 5000$	6/0.002 > 2000

2.3.6 Soil Stress Sensor Calibration

Each sensor's sensitivity (mV/psi) was initially determined by the manufacturer through calibration in a pressure chamber (i.e., uniform fluid pressure). Since, the sensors were to be used in 40% - 90% relative density uniform dry soil with D_{50} = 0.2 mm (5.1 in), it was decided to calibrate under the same conditions. Labuz and Theroux (2005) designed a calibration apparatus for diaphragm type earth pressure cells that included soil overburden and applied uniform pressures up to 100 psi. The calibration of the sensors in this study utilized the centrifuge and the ability to increase the soil unit weight (increased G-levels) which creates the increased overburden pressures (i.e., $\sigma v = N_s\, g\, \rho s\;\; Z$). Figure 2-16 shows sensitivity measurements from the calibration of the sensors in Figure 2-13 under soil overburden and under fluid pressure. This proved to be an extremely effective and efficient method for laboratory calibration of a pressure sensor and has been performed under fluid (water) pressure by Feld et. al. (1991).

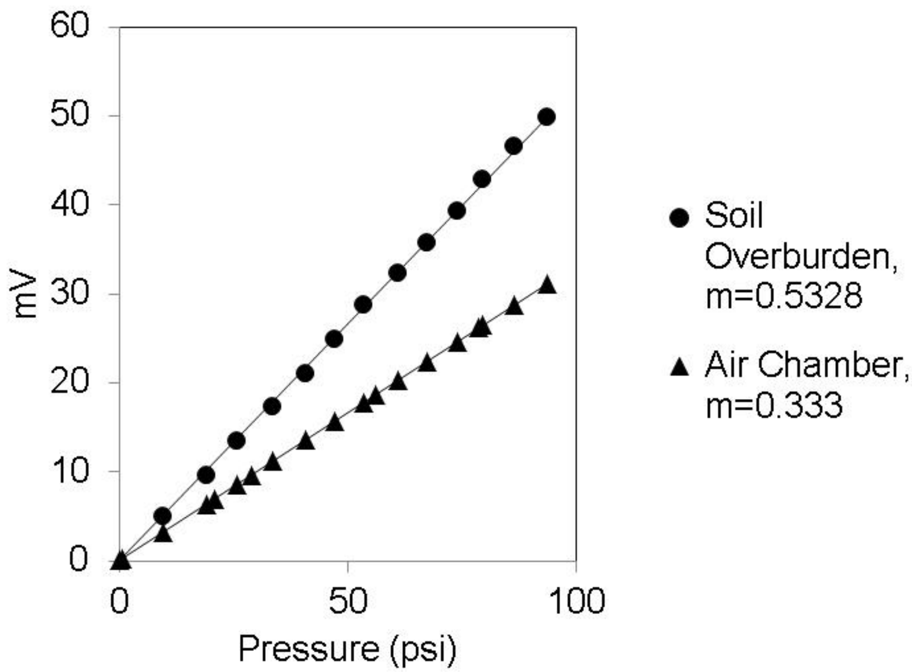

Figure 2-16 Soil stress sensor sensitivities from calibrations (m = slope)

2.3.7 Soil Description and Preparation

In order to model a range of granular soils with different angles of internal friction, soils native to Florida (silty-sands) and Mississippi (loess) were utilized. Each soil had a different grain size distribution and different unit weight which investigated through sieve analysis and vibratory compaction. Table 2-4 presents the uniformity coefficient, C_u, and coefficient of curvature, C_c, for each of the soils [all classified as poorly graded (ASTM, 2007)]. Soil 15 (loess) had 98% passing the #200 standard US sieve (0.075 mm) or predominately in the silty range of the gran size distribution. The maximum and minimum unit weights in Table 2-4 were determined based on vibratory compaction with loose placement according to ASTM D4253 and D4254 (2006), respectively for clean sands with < 15% passing the No. 200 US Standard Sieve. For soils with > 15% passing No. 200 US Standard Sieve, the standard Proctor compaction test (ASTM D698, 2007) was used to determine the maximum unit weight. The corresponding void ratios for each soil are given in Table 2-4.

Table 2-4 Properties of model soils

Soil	Uniformity Coefficient C_u	Coefficient of Curvature C_c	Dry Unit Weight (pcf)		Void Ratio		Friction Angle (degrees)	
			min	max	max	min	min	max
1	2.5	0.82	86.6	102	0.91	0.64	30	39
3	2.5	1.2	92.4	110.9	0.78	0.48	29	38
10	2.2	0.96	90.5	114.8	0.83	0.44	30	36
11	2.2	0.75	89.2	109.2	0.85	0.51	30	38
12	2.8	0.9	87.4	115.4	0.90	0.43	26	41
13	2.3	1.3	78	117.3	1.11	0.41	25	39
16	1.9	0.83	83.6	103	0.98	0.60	32	43
15	*98% passing #200 sieve		60.5	104.8	1.86	0.58	20	33

The centrifuge model preparation consisted of pluviation of the dry soil through a 19 mm (¾ in) diameter flexible tube with standard No. 7 (2.80 mm) U.S. sieve screen at the top. The pluviation drop height was 51 mm (2 in) from the soil surface to the sieve. Soil was placed in layers (12.2 mm), vacuumed to create a flat surface and then uniformly densified with dead weights. For each layer, mass and thickness was recorded to obtain the unit weight.

The friction angle of each soil was determined through relationships between unit weight (measured in the centrifuge container) and results from direct shear testing. For the latter tests, the soil was sheared at relative densities greater than 50% and normal stresses between 9 psi and 72 psi. Table 2-4 lists the minimum and maximum unit weights tested and the associated friction angles.

CHAPTER 3
LOAD AND RESISTANCE FACTORS FOR SLIDING STABILTY

3.1 Introduction

One of the external stabilities that must be checked for an MSE wall is sliding. In evaluating wall sliding, both the forces acting on the back of the wall (i.e. driving) and shear resistance on the foundation soil must be evaluated. Measurements of the lateral soil stress distribution permitted the determination of the lateral resultant force (i.e., driving force) for comparison to Rankine's and Coulomb's theory and calculation of the load bias. Measurements of the vertical soil stress on the plane of sliding permitted the determination of the shear strength (i.e., resistance) for calculation of the resistance bias. The CV of load and resistance (i.e., CV_Q and CV_R) were determined in addition to the observed P_f for different wall heights and soil variability (μ_ϕ, μ_γ, CV_ϕ, CV_γ). With these results the LRFD Φ for sliding stability was calculated. A discussion of each follows.

3.2 MSE Wall Model for Sliding Stability

The MSE wall model was designed at a scaling factor, N_s, of 60. The wall facing was a ceramic glass tiles grouted with hot glue, which allows for flexibility between joints. The model height (H) was 5.75 inches and each tile is 0.875 inch by 0.875 inch, which at a scale of 60 correlates to a prototype wall height of 28.75 ft with facing units 4.4 feet by 4.4 feet. Figure 3-1 shows the wall with carbon steel strand reinforcements (f'_y=35,000 psi) with a cross-section 0.25 inches wide by 0.009 inches thick. The steel strands were anchored to the wall with 90° angle mounts and thermo set two-part high strength epoxy (f'_y=2,324 psi). Bending of the wall face was limited by utilizing adhesive strands on the rear and front of the facing.

Figure 3-1 Rear view of MSE wall with reinforcement

The wall's internal stability was checked based on the AASHTO LRFD Bridge Design Specifications (2012) using the recommended load and resistance factors γ_{EH} = 1.5, $\Phi_{pullout}$ = 0.90, and $\Phi_{rupture}$ = 0.75, respectively. For pullout stability, the recommended active and resistant zones were defined by the inextensible reinforcement case. The load was calculated using the simplified method with the vertical tributary reinforcement spacing (S_v) = 1.5 in and a dimensionless earth pressure coefficient (K_r) = $1.7K_a$ to $1.68K_a$. The pullout friction factor (F*) was determined from direct shear tests of the backfill against carbon steel. For rupture stability, the applied lateral load was based on Rankine's analysis (i.e., no wall-soil friction). Based on results of load tests performed on sections of a wall, the connection strength was 2,324 psi. The complete dimensions of the MSE wall model and properties of the materials are: S_v = 1.5 in, S_h = 2.0 in, # rows = 6, w_r = 0.25 in, t_r = 1.25 (10^{-2}) in, K_r = $1.7K_a$ to 1.68 K_a, L = 6 in (L/H =

1), f'_y strips = 35,000 psi, f'_y epoxy = 2,324 psi, H = 6 in, W = 8 in, and $\gamma_{facing\ panels} \approx 174$ pcf.

Figure 3-2 shows the stages of the model wall construction where the wall was placed in segments and the backfill was pluviated in layers of uniform density. Soil stress sensors were oriented laterally at three elevations behind the reinforcement. Figure 3-3 illustrates the backfill where each layer had different measured density and friction angles, which gives the known variability (i.e., CV) of each.

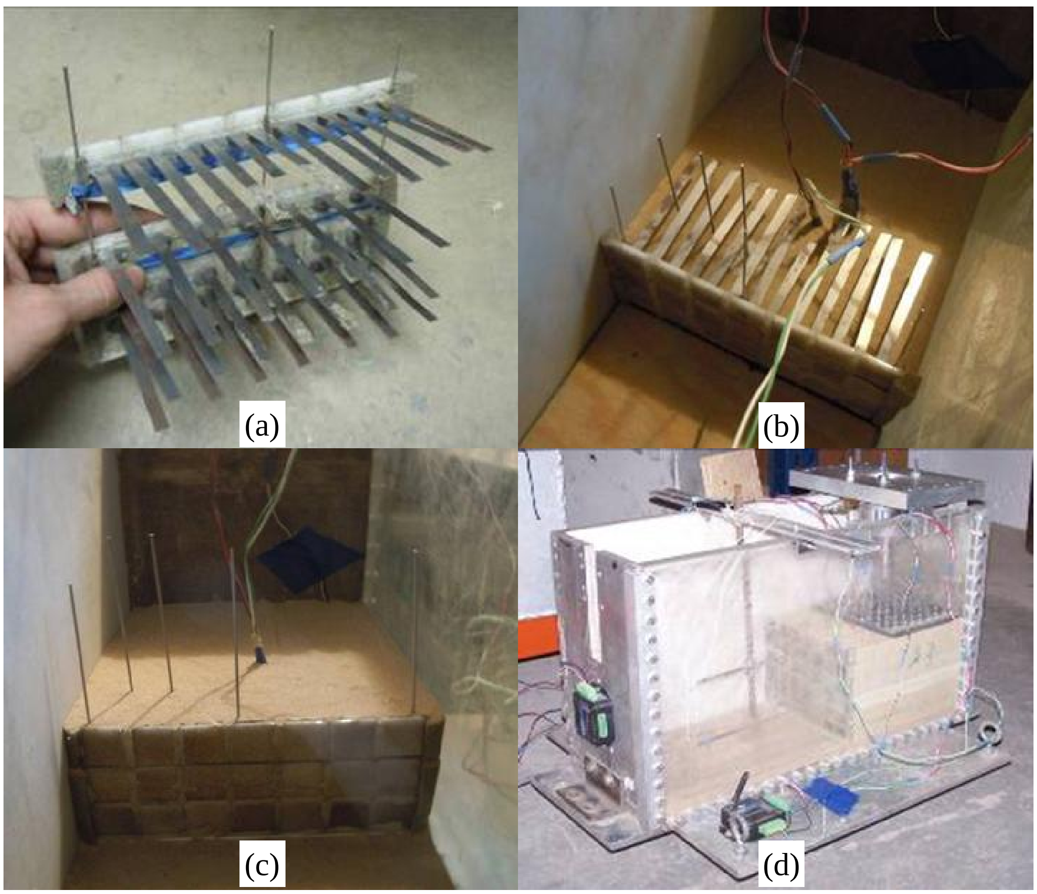

Figure 3-2 Stages of model wall: (a) segmented model wall, (b) segmented model wall during construction, (c) buried segmented model wall and (d) completed segmented model wall ready for test

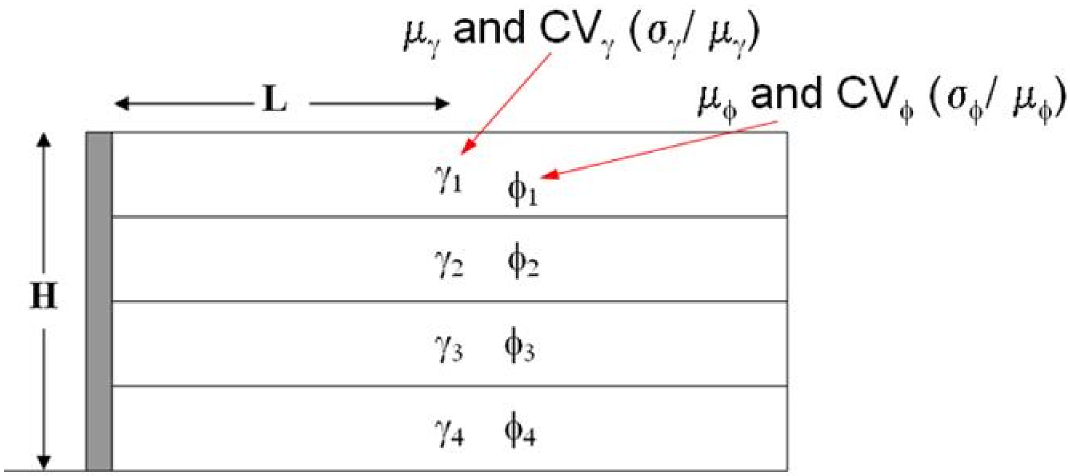

Figure 3-3 Layering process to obtain μ and CV of backfill properties

3.3 Centrifuge Tests of Sliding Stability

Table 3-1 presents the backfill properties and associated variability for L/H =1 models. Based on the soil's unit weight measured in the centrifuge container, the friction angles shown were found from direct shear tests. Unit weights ranged from 91.3 pcf to 95.9 pcf, angle of internal friction varied from 29° to 36.8°, and CV_{ϕ} ranged from 0.013 to 0.14. Overall, 23 model tests allowed for a total of 60 CDR values to be obtained, which were compared with the analytical results for assessment of load and resistance bias.

To have confidence in the P_f, sufficient number of data (CDR) had to be collected such that there was confidence in the CV of the distribution. To verify this, bootstrapping was performed, and the results are shown in the Table 3-2. Agreement between the mean of the bootstrap variance ($\mu_{bst\text{-}var}$) and the variance of the sample set (VAR_{CDR}) indicated sufficient numbers of CDR values. Additionally, the error associated in the variance, identified by the variance of the bootstrapped variance is an order of magnitude smaller than the variance (VAR_{CDR}), suggesting that the employed distribution and statistical descriptors (i.e. mean and variance) are acceptable.

Consequently, using the μ_ϕ and CV_ϕ, a number of best fit distributions of the data were investigated.

Table 3-1 Centrifuge model tests (L/H =1) backfill statistical descriptors

Test	μ_γ (pcf)	CV_γ	μ_ϕ (degree)	CV_ϕ
1A	93.8	0.049	32.3	0.14
2A	95.9	0.075	35.5	0.14
3A	91.4	0.071	32.3	0.14
4A	93	0.061	31.8	0.11
5A	92.6	0.06	31.8	0.09
6A	91.3	0.052	31	0.065
7A	94.5	0.043	36.8	0.013
8A	93.8	0.056	32.5	0.16
9A	95.7	0.069	32.7	0.116
10A	93.8	0.042	29	0.05
11A	93.4	0.051	29.5	0.044
12A	93.1	0.033	29	0.05
13A	93.13	0.033	29	0.049
14A	93.1	0.033	31.5	0.117
15A	93.1	0.033	31.5	0.117
16A	91.6	0.032	31.5	0.117
17A	91.6	0.026	31.5	0.117
18A	103.7	0.06	35.7	0.11
19A	110.2	0.044	45.7	0.114
20A	104.8	0.013	41.3	0.096
21A	101.4	0.056	35.6	0.148
22A	103.9	0.027	39.8	0.066
23A	104.8	0.03	40.7	0.08

Table 3-2 Summary statistics of backfill and bootstrap results with associated P_f

Set	μ_ϕ	CV_ϕ	$\mu_{bst\text{-}var}$	VAR_{CDR}	$VAR_{bst\text{-}var}$	P_f (%)
CDR1	32	0.13	2.814	2.9	0.353	1.2
CDR4	29	0.05	0.159	0.171	0.00198	1
CDR5	32.3	0.11	1.413	1.556	0.09806	1

Figure 3-4 shows the cumulative distribution for CDR5 (μ_ϕ of 32° and an average CV_ϕ of 11%) of the experimental data. Plotted against the data are the lognormal and inverse gaussian cumulative distributions for fit comparisons. Based on a Kolmogorov-Smirnov (KS) two sample goodness of fit test for each CDF, neither could be rejected at the 5% level of significance. The inverse gaussian CDF was a slightly better fit; however, as Figure 3-4 shows the lognormal CDF fits approximately the same based on visual verification. Thus, this suggests the resistance and load are lognormal distributed and can be approximated as such with their μ and CV. The P_f associated with a CDR of 1.0 were determined graphically (Figure 3-4) or more precisely evaluated from the inverse gaussian CDF with CDR = 1.0 and was approximately 1% (0.01). Fit tests of CDR1 and CDR4 resulted in the Inverse Gaussian CDF as the best fit and assessments of their P_f were made as described for CDR5 and reported in Table 3-2.

Table 3-3 shows the measured and predicted resistances and loads for 3 cases of wall heights with the same backfill conditions. The predicted resistance is calculated based on Equation 3-1 and the predicted Rankine and Coulomb loads are calculated based on Equation 3-2, respectively for each K_a.

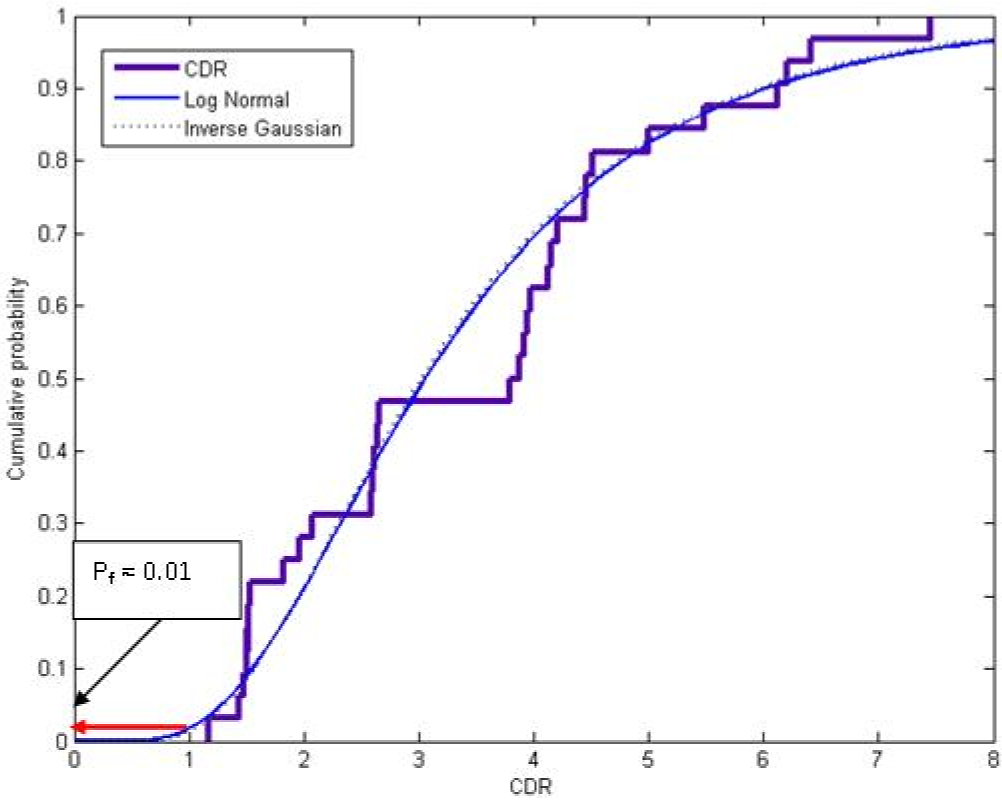

Figure 3-4 Cumulative distributions of CDR5 of sliding for μ_ϕ = 32° and CV_ϕ = 11.7%

$$\tau = \gamma_s HL \tan(\phi) \qquad \text{Eq. 3-1}$$

$$P_a = K_a(0.5\gamma_s H^2 + q_s H) \qquad \text{Eq. 3-2}$$

where τ is the shear resistance, γ_s is the total unit weight of backfill, H is the height of reinforced soil, L is the reinforcement length, ϕ is the friction angle of reinforced soil or foundation soil (smallest), P_a is the force resultant, q_s is the surcharge load, and K_a is the active earth pressure coefficient (Rankine or Coulomb). The bias (measured/predicted) is shown for each test (resistance, $\lambda_{R,}$ and load, λ_L) from which the mean bias is calculated for each group of wall heights.

Table 3-3 Measured and predicted resistances and loads and bias factors

Wall Height (ft)	Resistance			Load				
					Predicted		λ_L	
	Measured (lb/ft)	Predicted (lb/ft)	λ_R	Measured (lb/ft)	Rankine (lb/ft)	Coulomb (lb/ft)	Rankine	Coulomb
8	6141.73	4704.69	1.31	3214.35	1485.81	1164.67	2.16	2.76
	505.87	3128.53	0.16	1075.63	1534.11	1222.81	0.70	0.88
	3974.73	3204.63	1.24	1381.38	1572.36	1253.83	0.88	1.10
	5147.58	3935.05	1.31	1418.87	1415.60	1110.09	1.00	1.28
	6141.73	4704.69	1.31	3214.35	1485.81	1164.67	2.16	2.76
	620.16	230.29	2.69	831.95	1288.66	1034.95	0.65	0.80
	6370.07	4833.54	1.32	5805.69	1476.83	1157.45	3.93	5.02
	1571.38	2453.11	0.64	933.78	1469.89	1348.28	0.64	0.69
	2509.74	2683.51	0.94	1353.44	1629.80	1482.08	0.83	0.91
11	1133.80	5260.43	0.22	2167.65	2620.78	2090.06	0.83	1.04
	853.45	5561.83	0.15	1540.51	2494.66	1987.64	0.62	0.78
	6111.79	5697.12	1.07	1917.78	2561.44	2041.65	0.75	0.94
	7666.96	6995.65	1.10	2009.35	2295.37	1800.04	0.88	1.12
	9161.92	8363.89	1.10	4531.80	2408.29	1888.59	1.88	2.40
	1141.65	345.43	3.31	1498.32	2542.49	2042.65	0.59	0.73
	9502.55	8592.96	1.11	8755.76	2392.07	1875.72	3.66	4.67
	2404.23	4357.31	0.55	1371.09	2404.67	2206.62	0.57	0.62
	3551.98	4766.56	0.75	1954.04	2659.51	2419.91	0.73	0.81

Table 3-3 Continued

Wall Height (ft)	Resistance			Load				
					Predicted		λ_L	
	Measured (lb/ft)	Predicted (lb/ft)	λ_R	Measured (lb/ft)	Rankine (lb/ft)	Coulomb (lb/ft)	Rankine	Coulomb
14	1480.23	8219.43	0.18	2828.91	3874.35	3088.76	0.73	0.92
	1324.91	8690.36	0.15	2047.91	3680.68	2931.80	0.56	0.70
	8517.28	8901.75	0.96	2469.77	3783.90	3015.15	0.65	0.82
	10504.40	10930.71	0.96	2719.60	3379.90	2650.58	0.80	1.03
	3311.16	6814.19	0.49	1894.67	3563.79	3271.20	0.53	0.58
	4617.51	7454.19	0.62	2605.08	3934.57	3581.59	0.66	0.73

3.4 Horizontal Earth Pressure Load Factor

For each centrifuge test, the model was spun up to the test acceleration level (N_s = 60g), and lateral soil stresses at the back of the reinforced soil were measured and recorded. Since many tests were performed (23), a large sample population of measured soil stresses was acquired which may be used to estimate/validate the load factor for vertical earth pressure for reinforced soil.

The load factor can be calculated with the following expression (Nowak, 1995)

$$\gamma = \lambda(1 + nCV) \qquad \text{Eq. 3-3}$$

where γ is the load factor, λ is the load bias (measured/predicted), n is a constant and CV is of the load bias. The constant, n, is chosen such that the probability of exceeding any factored load is always the same. In the AASHTO LRFD bridge design code (2012), a value of n = 2 is used for the strength limit state (Nowak, 1995).

The horizontal dead load in an MSE wall analysis may be a determined from the soil's vertical effective stress, σ_v', at an elevation and the earth pressure coefficient (i.e., K_a).

$$\sigma_H' = \sigma_V' K_a \qquad \text{Eq. 3-4}$$

where K_a is the coefficient of active earth pressure based on the Rankine or Coulomb method. AASHTO (2012) recommends a load factor of 1.5 for horizontal earth pressure and is generally assumed to be conservative for the factored load. However, it may not be accurate for MSE walls due to effects of the reinforcement in the soil.

A data set of 148 measured lateral resultant force collected from all centrifuge tests performed for L/H =1 was used to calculate the load factor for horizontal earth pressure. The predicted lateral resultant force due to the non-uniform soil pressure based on Rankine's and Coulomb's methods were calculated for each of the 148 measured values. Using $n = 2$ in Equation 3-3 (Allen et al., 2005), a new load factor of 1.52 was calculated using Rankine's method and its influence on the load is shown in Figure 3-5 where it is applied to the nominal predicted values (Eq. 3-4). The mean load bias was 0.70 and the CV of the load bias was 0.62. Considering Coulomb's method, a new load factor of 1.63 was calculated and its influence on the load in shown in Figure 3-6 where it is applied to the nominal predicted values. The mean load bias was 0.78 and the CV of

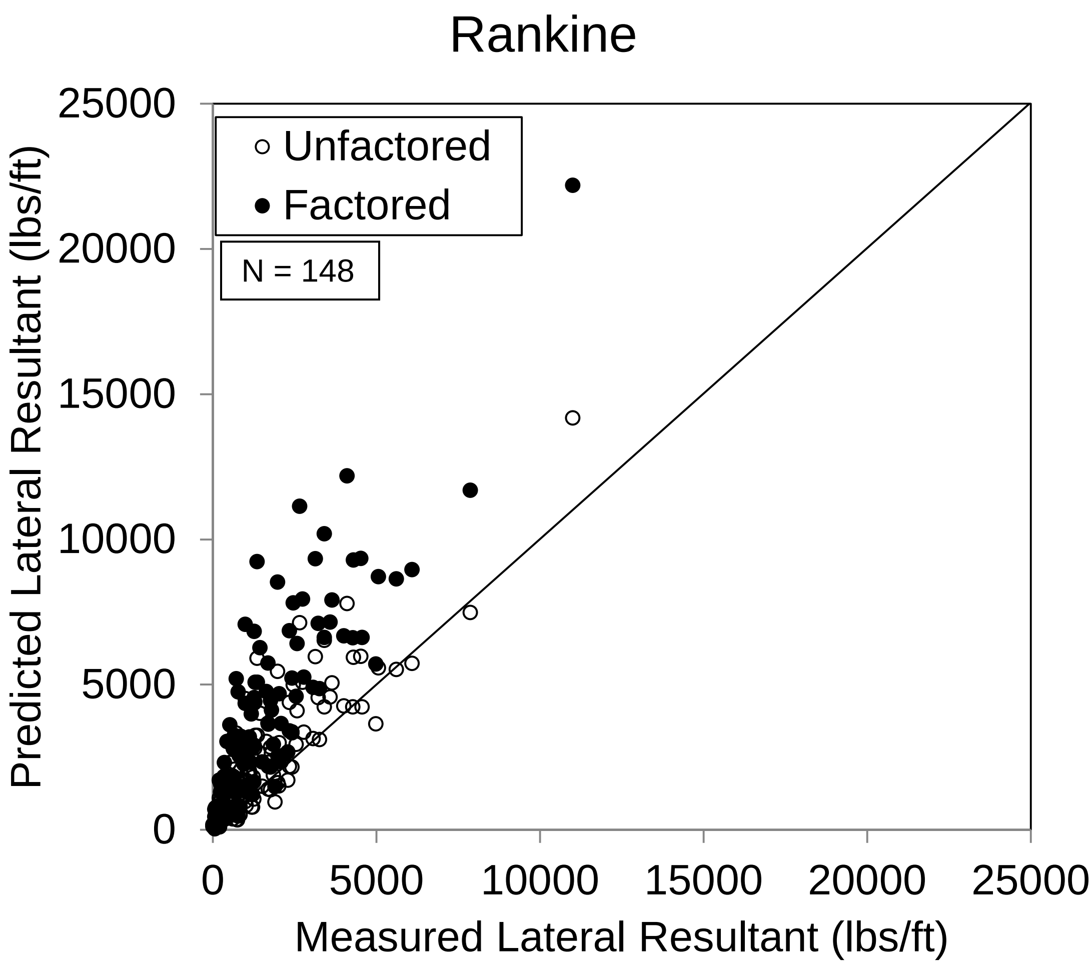

Figure 3-5 Unfactored and factored predicted lateral resultant forces versus measured lateral resultant force based on Rankine analysis

the load bias was 0.56. The effect in both cases is to bring most of the loads above the 1:1 line, which is the desired result. The current recommended value of 1.5 (AASHTO, 2012) is more in line with the load factor based on Rankine's method.

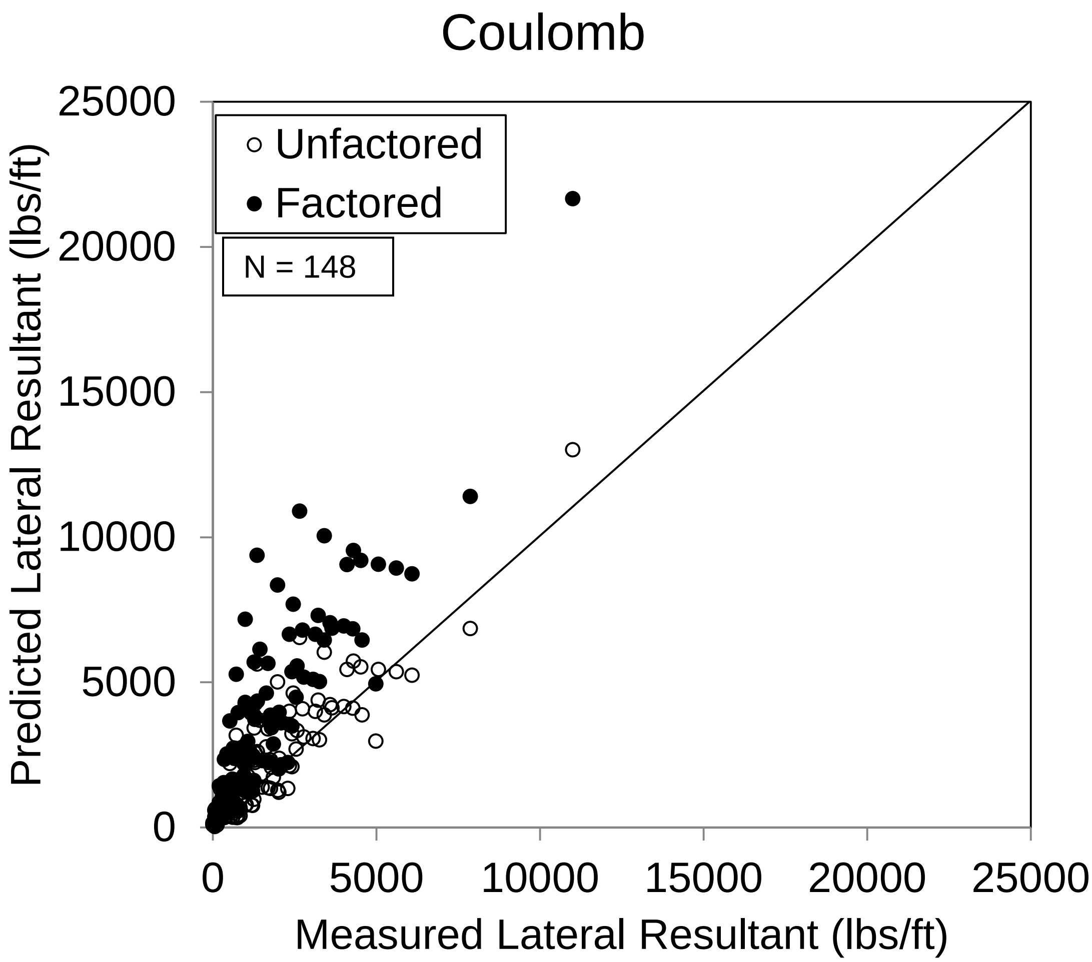

Figure 3-6 Unfactored and factored predicted lateral resultant forces versus measured lateral resultant force based on Rankine analysis

3.5 Resistance Factors for Sliding Stability

Equation 3-5 is the LRFD Φ equation as presented by the FHWA (2001) and Styler (2006). Variability in the resistance and loads is represented through CV_R and CV_Q and bias in each are represented through the λ factors. The CV_Q can be represented in terms of its dead and live load CV components as shown in Equation 3-6.

$$\varphi = \frac{E[\lambda_R] \cdot \sqrt{\frac{\left(1 + CV_Q^2\right)}{\left(1 + CV_R^2\right)}} \cdot (\gamma_D \cdot q_D + \gamma_L \cdot q_L)}{(E[\lambda_D] \cdot q_D + E[\lambda_L] \cdot q_L) \cdot e^{\beta_T \sqrt{\ln\left[\left(1+CV_R^2\right)\left(1+CV_Q^2\right)\right]}}} \qquad \text{Eq. 3-5}$$

$$CV_Q^2 = \frac{q_D^2 \cdot E[\lambda_D]^2 \cdot CV_D^2 + q_L^2 \cdot E[\lambda_L]^2 \cdot CV_L^2}{q_L^2 \left(\frac{q_D^2}{q_L^2} \cdot E[\lambda_D]^2 + 2 \cdot \frac{q_D}{q_L} \cdot E[\lambda_D] \cdot E[\lambda_L] + E[\lambda_L]^2\right)} \qquad \text{Eq. 3-6}$$

where $E[\lambda_R]$ is the mean resistance bias factor, CV_Q is the coefficient of variation in the load, CV_R is the coefficient of variation in the resistance, q_D is the mean dead load, q_L is the mean live load, γ_D is the dead load factor, γ_L is the live load factor, β_T is the target reliability index, λ_D is the mean dead load bias factor, λ_L is the mean live load bias factor, CV_D is the coefficient of variation in the dead load, and CV_L is the coefficient of variation in the live load.

Presented in Tables 3-4 and 3-5 are the computed LRFD ϕ based on models that had the same mean and CV of the soil friction angle. Based on the sensitivity analysis for these cases, the soil friction angle was the most significant parameter and significantly influenced the driving force or lateral load on the wall. Load factors considered for these calculations are case strength 1a from the AASHTO LRFD recommended values. Based on the measured values of the soil properties and the bias values in the load and resistance, Φ values range for the Rankine case (Table 3-4) of lateral force varied from 0.74 to 0.94 for the wall heights tested (Table 3-1). Values for the Coulomb case (Table 3-5) of lateral force ranged from 0.62 to 0.67 for the wall heights tested. Bias factors of total load were determined using the Rankine and Coulomb equations for K_a.

Table 3-4 Calculated Φ values based on Rankine's loading (backfill: μ_ϕ = 32° and CV_ϕ = 11.7%)

Wall Height (ft)	No. Values (n)	Measured Resistance		Measured Load		Bias = (Measured/Predicted)			Load Factors			Φ
		μ_R (lb/ft)	CV_R	μ_Q (lb/ft)	CV_Q	λ_R	λ_D	λ_L	γ_{EV}	γ_{EH}	γ_{LS}	
8	9	2891.90	0.81	1908.10	0.60	1.21	1.4	1.2	1	1.5	1.75	0.79
11	9	4338.90	0.80	2799.63	0.81	1.04	1.17	1.2	1	1.5	1.75	0.94
14	6	4671.10	0.76	2504.57	0.16	0.6	0.7	1.2	1	1.5	1.75	0.74

Table 3-5 Calculated Φ values based on Coulomb's loading (backfill: μ_ϕ = 32° and CV_ϕ = 11.7%)

Wall Height (ft)	No. Values (n)	Measured Resistance		Measured Load		Bias = (Measured/Predicted)			Load Factors			Φ
		μ_R (lb/ft)	CV_R	μ_Q (lb/ft)	CV_Q	λ_R	λ_D	λ_L	γ_{EV}	γ_{EH}	γ_{LS}	
8	9	2891.90	0.81	1908.10	0.60	1.21	1.8	1.2	1	1.6	1.75	0.63
11	9	4338.90	0.80	2799.63	0.81	1.04	1.46	1.2	1	1.6	1.75	0.64
14	6	4671.10	0.76	2504.57	0.16	0.6	0.8	1.2	1	1.6	1.75	0.68

3.6 Observations and Findings of MSE Sliding Analysis

In conclusion, 23 centrifuge tests of MSE wall sliding stability were performed and the loads and resistances were measured for comparison to predictions. The tests provided 146 measurements of lateral resultant load, from which load factors for horizontal earth pressure was calculated for the Rankine and Coulomb methods. The CV's of load and resistance, along with each one's bias, were determined for three MSE wall heights. These results were then used to calculate the LRFD Φ for each case. The observations and findings are summarized below:

- Load factors for horizontal earth pressure based on Rankine's and Coulomb's method of determining lateral resultant load were determined to be 1.52 and 1.63, respectively. Currently, AASHTO (2012) recommends a load factor of 1.5 for all predictions of lateral resultant load in MSE walls.
- Based on the results, LRFD Φ values were calculated to be 0.74 to 0.94 for the Rankine load case, and 0.63 to 0.68 for the Coulomb load case. The Coulomb method leads to more conservative Φ's and are suggested for the soil conditions and wall heights tested.
- Furthermore, Coulomb accounts for a reduction in the lateral resultant load due to friction between the soil particles, which is the case in the prototypes.

CHAPTER 4
LOAD AND RESISTANCE FACTORS FOR BEARING STABILTY

4.1 Introduction

This chapter reports on MSE centrifuge tests of bearing failure of walls founded on horizontal (flat) ground surfaces. The results were used to 1) validate the traditional force polygon representing the forces acting behind and over the MSE wall; and 2) assess the bearing resistance of the wall as a function of backfill and foundation soil properties (e.g. μ_ϕ, CV_ϕ). It was also found from the measured soil stresses/forces, that the AAHSTO load factors for vertical dead load were un-conservative due to wall weight acting on the foundation soil. Using revised load and inclination factors along with bearing capacity factors (Vesic, Hansen, Meyerhof, etc.) for cohesionless soil, LRFD Φ's for MSE walls subject to bearing failure were developed.

4.2 MSE Wall Models Used for Bearing Stability Experiments

The MSE model height was 152 mm (6 in), i.e. 1/40th the size of the prototype (6.1m), with 6 levels of non-extensible carbon steel strips as the soil reinforcement (Figure 4-1). The straps were attached to the back of facing panels with high strength epoxy and their surface covered with 80 grit sand paper to increase shear resistance (internal stability). The facing panels were 23 mm (0.9 in) square ceramic glass tiles; the length of each steel reinforcement was 75 mm (3 in) for an L/H = 0.5, Figure 4-1.

The wall's internal stability was checked based on the AASHTO LRFD Bridge Design Specifications (2012) using the recommended load and resistance factors γ_{EV} = 1.35, $\Phi_{pullout}$ = 0.90, and $\Phi_{rupture}$ = 0.75, respectively. For pullout stability, the

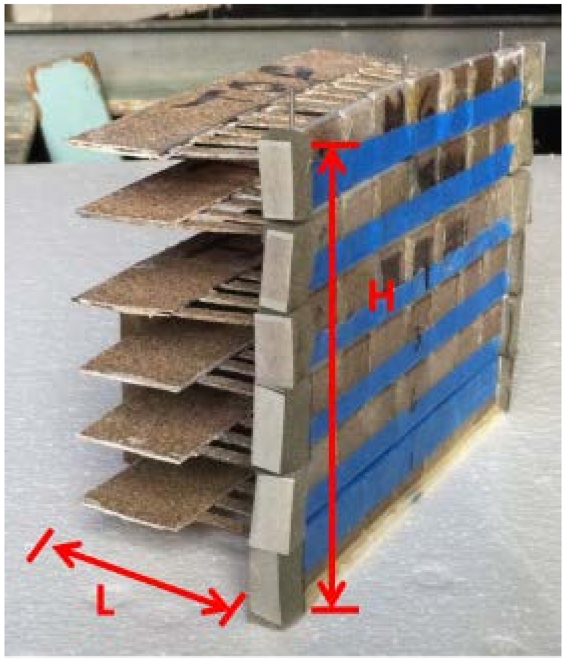

Figure 4-1 MSE wall model reinforcement strips and facing panels

recommended active and resistant zones were defined by the inextensible reinforcement case. The load was calculated using the simplified method with the vertical tributary reinforcement spacing (S_v) = 0.78 in and a dimensionless earth pressure coefficient (K_r) = 1.7K_a to 1.68K_a. The pullout friction factor (F*) was determined from direct shear tests of the backfill against the 80 grit sand paper. This varied from 0.62 to 0.84 for the different backfill densities used in the tests. For rupture stability, the applied lateral load was based on Rankine's analysis (i.e., no wall-soil friction). Based on results of load tests performed on sections of a wall, the connection strength was 2,324 psi. The complete dimensions of the MSE model wall and soil parameters were: S_v = 0.78 in, S_h = 0.47 in, # rows = 6, w_r = 0.25 in, t_r = 1.25 (10^{-2}) in, K_r = 1.7K_a, L = 3 in, f'_y strips = 35,000 psi, f'_y epoxy = 2,324 psi, H = 6 in, W = 8 in, and $\gamma_{facing\ panels} \approx$ 174 pcf.

4.3 Centrifuge Tests of Bearing Stability

4.3.1 Results and Analysis

The centrifuge tests involved spinning the model up to the test acceleration of 40g then applying surcharge, q_s, in increments while the wall's bearing stresses and vertical movements were monitored and recorded. The load-displacement response of the MSE wall was plotted during the test to determine if failure conditions had been reached, as well as termination of the test. Table 4-1 gives the statistical descriptors (μ and CV) of backfill and foundation soil's unit weights, γ, and friction angles, ϕ, for 35 centrifuge experiments performed

Figure 4-2 shows the centrifuge measured load-displacement curves for the case of foundation soil μ_ϕ between 28° and 30°. Grouping of the load-displacement responses based on the foundation soil's friction angle (represented as a μ_ϕ in each test) follows from the sensitivity study herein and Chalermyanont and Benson (2005), which showed the μ_ϕ as having the greatest influence on the bearing limit state analysis. The differences in the load-displacements plots are attributed to the mean unit weights, $\mu_{\gamma s}$. Note, the backfill soil γ has a strong influence on its' angle of internal friction and lateral pressure behind the reinforced soil (MSE wall), influencing both the magnitude of soil pressure at the base, as well as the eccentricity of the resultant force used in bearing capacity analysis (i.e., effective foundation width term).

The bearing resistance of each test, $V_{measured}$ (lbs/ft), was determined from the load-displacement curves (Figure 4-2) where the slope of each curve reached a steady or minimum value. However, a few of the tests did not exhibit failure due to high strength of the foundation soil ϕ (tests 24, 25, and 26), others experienced sensor malfunction (tests 8, 17, and 18); neither set was included in the final LRFD Φ assessment. Table 4-2 lists the surcharge, q_s, at failure and the corresponding $V_{measured}$ from each test. The tests

Table 4-1 Summary of backfill and foundation soils in centrifuge tests

Test	Backfill				Foundation Soil			
	Unit Weight (pcf) $(\mu)_\gamma$	Unit Weight CV_γ (%)	Friction angle (°) $(\mu)_\phi$	Friction angle CV_ϕ (%)	Unit Weight (pcf) $(\mu)_\gamma$	Unit Weight CV_γ (%)	Friction angle (°) $(\mu)_\phi$	Friction angle CV_ϕ (%)
1	99	5.7	32	17.3	93	14.3	29	19.6
2	97	5.8	31	12.7	93	10.4	28	14.6
3	97	6.8	31	19.4	94	10.1	30	14.1
4	99	3.7	32	11.3	94	12.2	30	13.3
5	95	7.1	29	21.4	94	13.2	29	19.3
6	95	6.9	33	5.6	97	14.2	31	15.6
7	97	4.5	32	7.8	96	11.3	30	12.6
8	95	6.6	32	4.1	101	10.0	34	17.3
9	97	6.2	32	13.1	94	9.6	29	13.2
10	93	5.8	30	10.2	98	11.6	29	19.7
11	97	6.1	32	21.1	97	10.9	32	16.7
12	95	6.1	31	9.5	100	11.1	33	22.5
13	96	5.9	32	13.2	97	7.4	30	10.2
14	97	6.6	31	17.0	98	11.6	31	13.3
15	96	7.0	30	20.0	100	5.3	32	8.3
16	96	7.7	30	11.6	99	10.1	29	22.0
17	98	4.8	32	7.0	93	6.3	28	15.0
18	98	4.7	33	11.8	98	7.2	31	9.9
19	98	4.9	32	10.6	98	4.0	31	6.9
20	98	4.7	32	10.8	99	9.5	31	12.4
21	98	5.6	32	6.8	100	3.2	32	6.0
22	101	7.7	35	12.5	98	4.2	31	8.1
23	104	5.7	38	8.5	104	5.4	33	8.9
24	105	6.2	38	7.7	103	8.2	34	17.4
25	105	3.7	38	8.6	104	5.4	34	14.0
26	103	5.2	38	7.4	104	5.9	34	15.0
27	104	4.1	39	4.2	99	9.8	31	11.4
28	108	6.9	39	3.8	92	10.9	29	13.3
29	105	5.0	39	5.0	91	14.0	28	16.0
30	96	3	32	6	83	18	26	20
31	96	4	31	6	90	14	27	15
32	98	3	37	8	84	16	26	18
33	98	1	38	3	87	13	27	16
34	97	1	37	2	87	9	27	13
35	98	1	37	3	85	14	27	17

Table 4-2 Centrifuge test's foundation soil mean friction angles, surcharge loads and measured vertical resultant force (V_{meas}) at capacity

Test	Friction Angle $\mu_{\phi fs}$	Surcharge q_s (psf)	V_{meas} (kips/ft)
1	29	960	15.7
2	28	1025	15.6
3	30	1000	13.5
4	30	1210	16.0
5	29	1320	17.3
6	31	1340	17.0
7	30	1400	19.9
9	29	1220	12.1
10	29	800	16.8
11	32	1790	19.6
12	33	1990	19.0
13	30	2280	25.6
14	31	1399	18.0
15	32	930	11.2
16	29	1220	11.7
19	31	1210	11.3
20	31	320	11.9
21	32	1250	15.5
22	31	1030	11.4
23	33	1170	15.8
27	31	776	12.4
28	29	628	10.3
29	28	2634	33.0
30	26	3769	37.1
31	27	2671	32.7
32	26	4040	39.6
33	27	2839	30.8
34	27	4514	38.4
35	27	4623	39.8

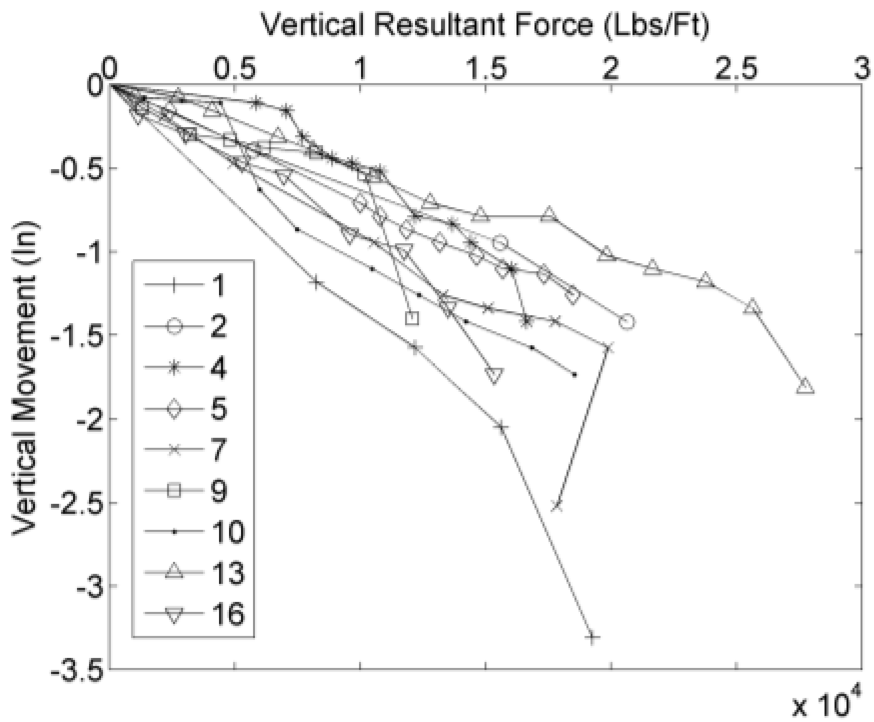

Figure 4-2 Load settlement curves for MSE walls with foundation soil μ_ϕ = 28°-30°

were then grouped into to two ranges of mean strength, μ_ϕ of the foundation soil: 26° - 30° and 31° - 33°. Figures 4-3(a) and (b) show the cumulative distributions of the vertical resultant force (i.e., capacity) and fitted lognormal cumulative distribution functions for eachrange. The lognormal models could not be rejected at a level of significance of 5% as indicated by the Kolmogorov-Smirnov goodness of fit test, (p = 0.75 and 0.93, respectively). Further testing on the tails of the cdfs at a level of significance 5% with the Anderson-Darling goodness of fit test indicated the lognormal models could not be rejected (p = 0.25 and 0.5, respectively). These two ranges were subsequently used in determining the associated Φ's.

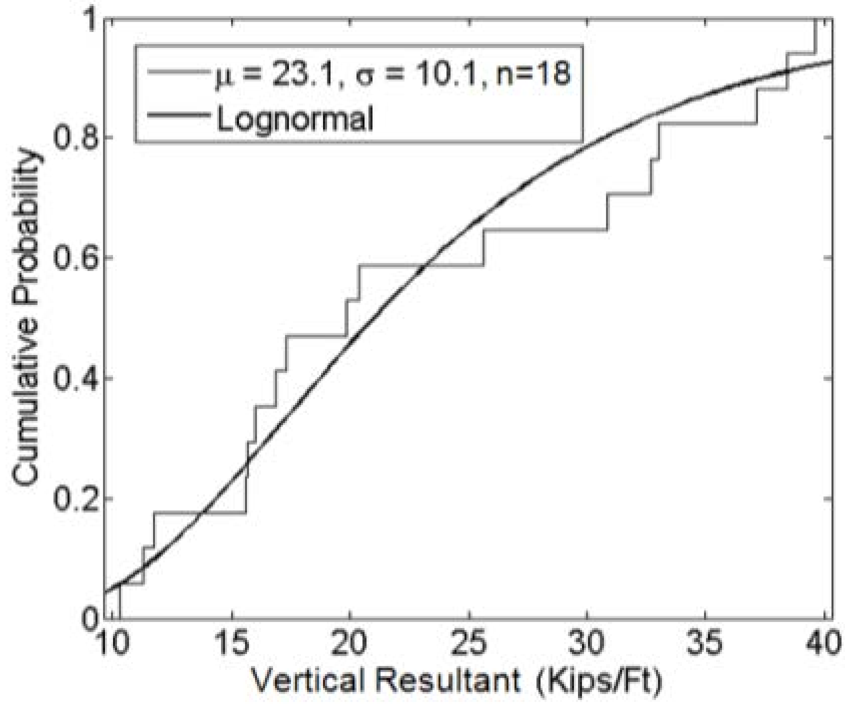

(a)

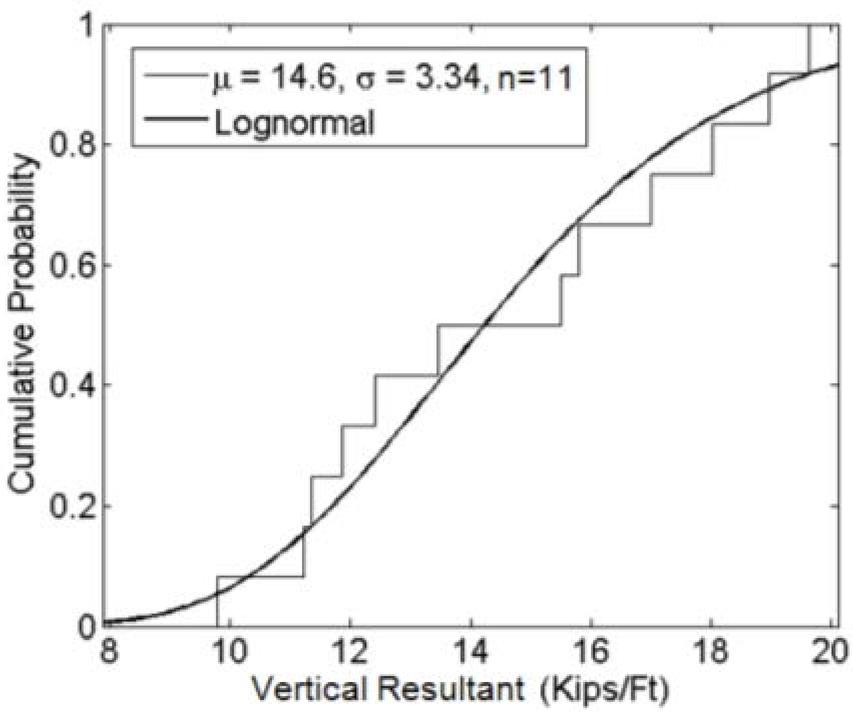

(b)

Figure 4-3 Empirical and lognormal model distribution functions for the capacities from centrifuge tests with foundation soil (a) μ_ϕ = 26°-30° and (b) μ_ϕ = 31°-33°

4.3.2 Force Equilibrium

Validation of the measured vertical resultant force ($V_{measured}$) in each test was performed based on the MSE wall and soil wedge diagram shown in Figure 4-4. W_1 is weight of backfill soil (F/L), W_2(F/L) is the weight of reinforced soil, W_3 is weight of wall, Q_s is resultant of surcharge load (F/L), ϕ_{bf} is angle of internal friction of backfill, and , ϕ_{fs} is angle of internal friction of supporting foundation soil. S_1 and S_2 are shear forces (F/L) developed in the backfill and supporting foundation soil. The resultant polygon of forces acting on soil wedges is shown in Figure 4-5. Of interest is the calculated vertical force, $V_{calculated}$ (Equation 4-1) using measured soil properties (Table 4-1) versus the measured vertical force, $V_{measured}$ from the centrifuge test, Table 4-2. Figure 4-6 shows $V_{measured}$ vs. $V_{calculated}$ for all the data. Evident is the good correlation between measured and predicted ($R^2 = 0.85$), indicating accuracy in the measurements, as well as ensuring confidence in the use of the measured data to calculate the CV_R needed for assessment of LRFD Φ.

$$V\left(\frac{F}{L}\right) = \left[\frac{W_1 + W_2 + W_3 + Q_S}{\frac{\sin(\delta)}{\tan(\theta - \phi)} + \cos(\delta)}\right] \cos(\delta) \qquad \text{Eq. 4-1}$$

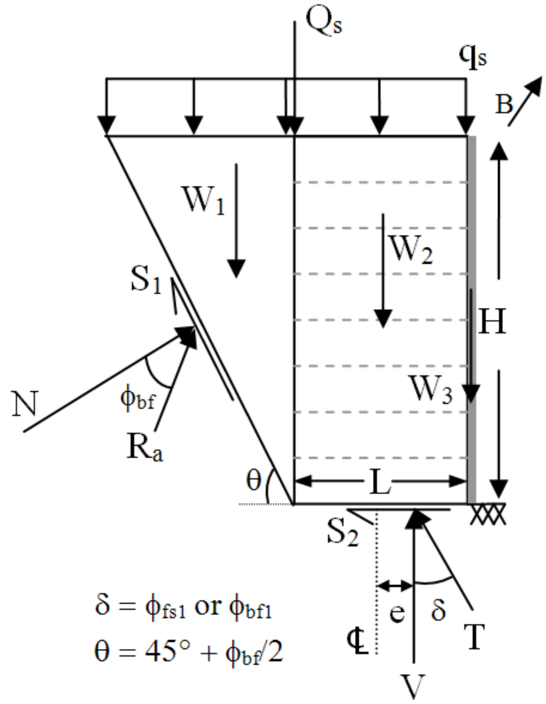

Figure 4-4 Force diagram for MSE wall and soil wedge

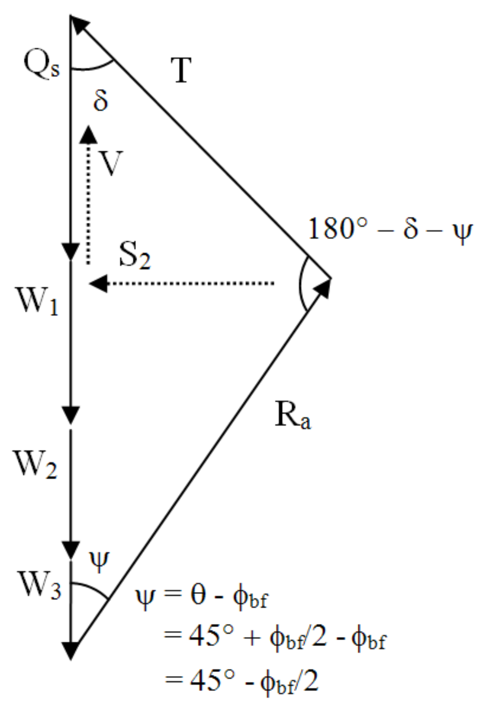

Figure 4-5 Force polygon for MSE wall and soil wedge

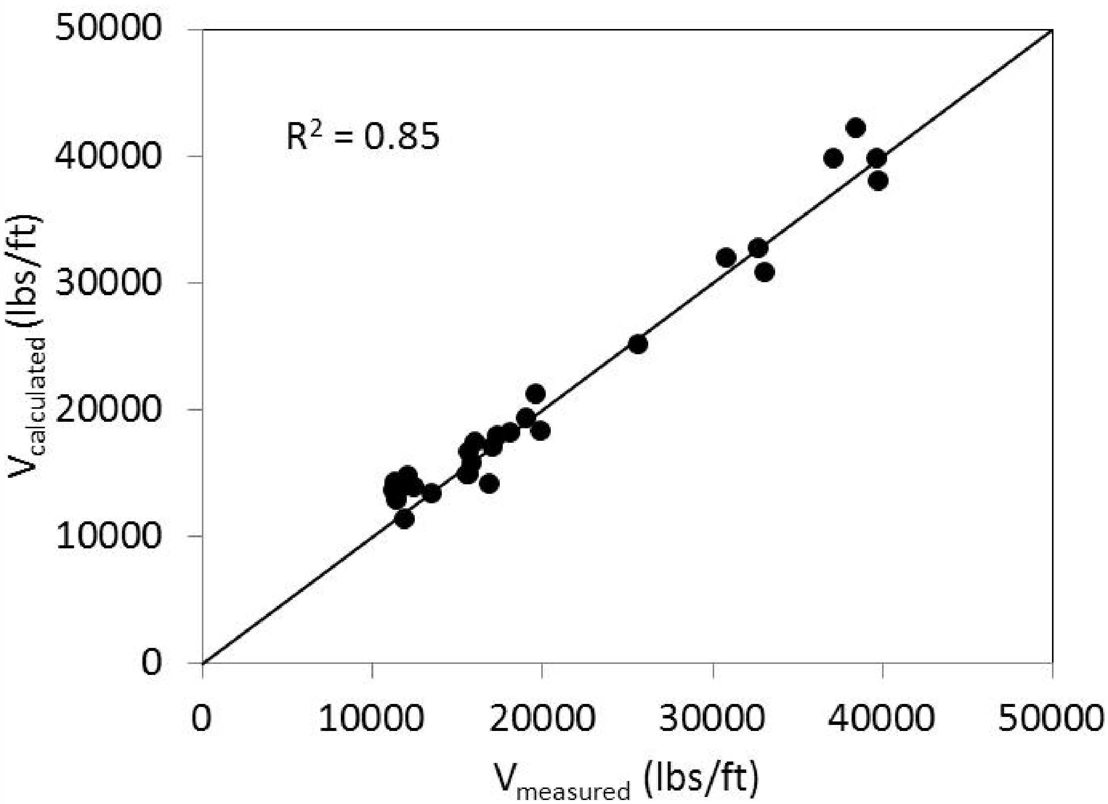

Figure 4-6 $V_{calculated}$ versus $V_{measured}$ for all MSE wall tests ($\mu_{\phi fs}$ = 26°-33°)

4.3.3 Effects of Load Inclination

Perloff and Baron (1976) discussed the effects to a foundation's bearing capacity when there is an eccentric load inclined at some angle (δ) from the vertical. The combined effect of inclined load and eccentricity is to change the depth of the rupture surface depending on the direction of the horizontal component of the inclined load with the eccentricity. In the case where the eccentricity and load inclination act in the same direction, the length of the bearing rupture surface can be greatly reduced. Sokolovski (1960) developed an analytical expression for the rupture surface as a function of the foundation soil's ϕ and inclination of load, δ. For δ from 0° to 20°, Sokolovski (1960) showed a reduced depth of the bearing rupture surface from 0.78L to 0.3L, respectively.

At the same time, the lateral extents of the bearing rupture surface changed from 1.9L to 0.6L, respectively.

These effects were observed in the centrifuge tests (Figures 4-7 and 4-8) with various foundation soils' friction angles ϕ and δ (Figure 4-4). For the test where the δ is greater (Figure 4-7), the depth of the rupture surface (approximately 0.5L) is less than that in the test where δ is less (approximately 0.7L) (Figure 4-8). The lateral extents of the rupture surface is clear in Figure 4-7, where it reaches the foundation soil surface at approximately 2 in from the front of the wall (approximately 0.67L). This is less evident in Figure 4-8; however, based on the depth at which the marker lines are displaced and the slight bulging of the lines away from the wall face, the rupture surface appears to have been developed further from the wall face as suggested by Sokolovski (1960).

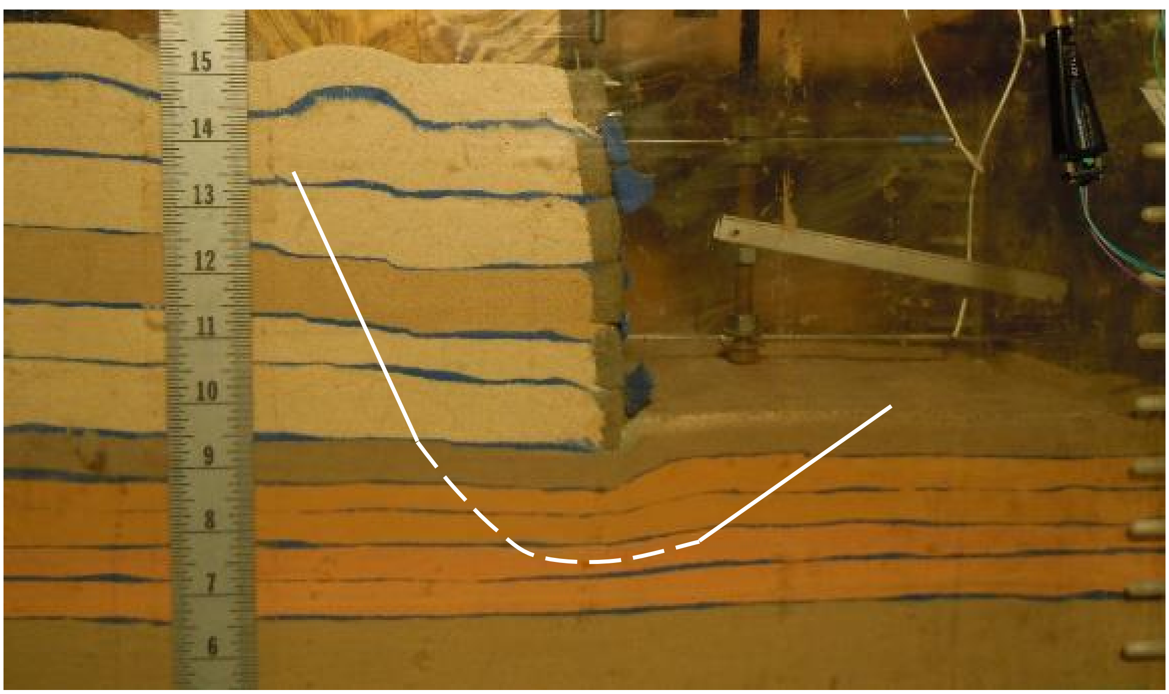

Figure 4-7 Post-test observed rupture surface in Test 15 model (δ = 30° and μ_ϕ = 28°): Dashed line is the estimated surface; Solid line is offset from observed surface

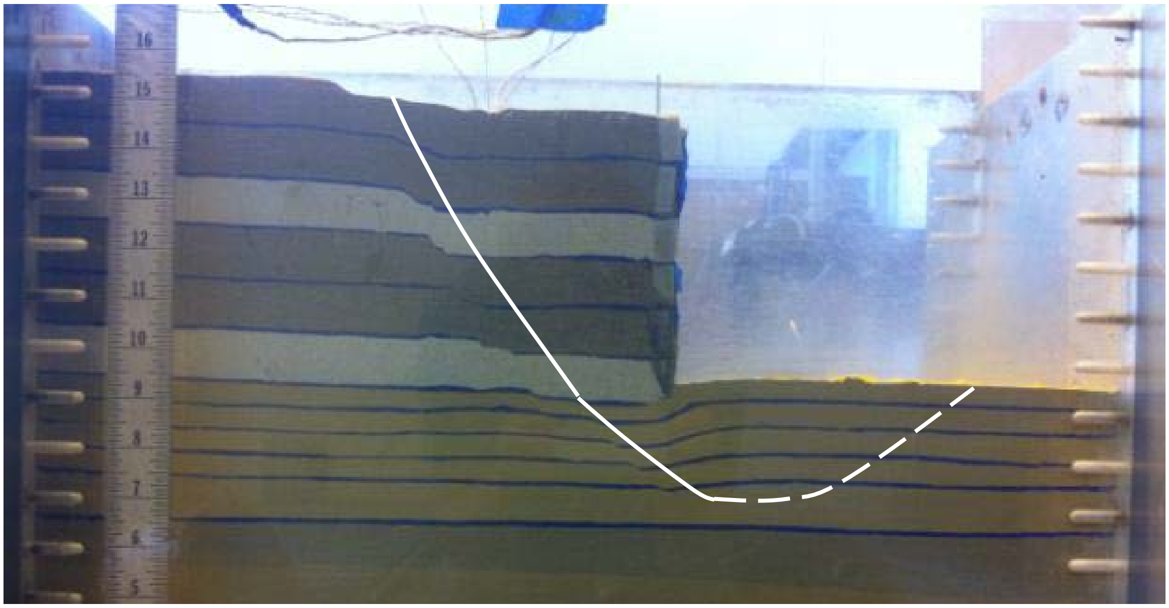

Figure 4-8 Post-test observed rupture surface in Test 42 model (δ = 25° and μ_ϕ = 28°): Dashed line is the estimated surface; Solid line is offset from observed surface

From horizontal force equilibrium of the force polygon acting on the MSE wall and soil wedge (Figure 4-4), an expression for the horizontal load component, S_2, of the total resultant load, T, may be found as a function of $V_{measured}$.

$$S_2 = (W_1 + W_2 + W_3 + Q_S - V_{meas})\tan(\theta - \phi) \qquad \text{Eq. 4-2}$$

This permits an estimation of T and, importantly, δ. Using the $V_{measured}$ (Table 4-2) and MSE wall properties in Table 4-1, S_2 was calculated and then used to back calculate δ (i.e., $\tan^{-1}(S_2/V_{measured})$) from the relationship shown in Figure 4-4. Note, δ may vary from zero (i.e. no horizontal load) to the smaller of the backfill (ϕ_{bf1}) or the foundation (ϕ_{fs1}) soils' angle of internal friction. For this analysis, V is known (integration of vertical stresses from stress gauges) beneath the wall, and δ was back calculated and compared to the friction angles ϕ_{fs1} or ϕ_{bf1}.

Figure 4-9 shows the scatter plot of δ_{calc} versus smaller of ϕ_{fs1} or ϕ_{bf1} for the tests in Table 4-1. The solid line in the plot is the upper bound limit ($\delta = \phi$) of strength, beyond which a δ indicates the shear strength has been exceeded. It is evident that the δ_{calc} values are close to or less than the ϕ_{fs1} or ϕ_{bf1} for the tests. The good agreement between δ and ϕ_{fs1} or ϕ_{bf1}, suggests the force equilibrium model is accurate in predicting δ.

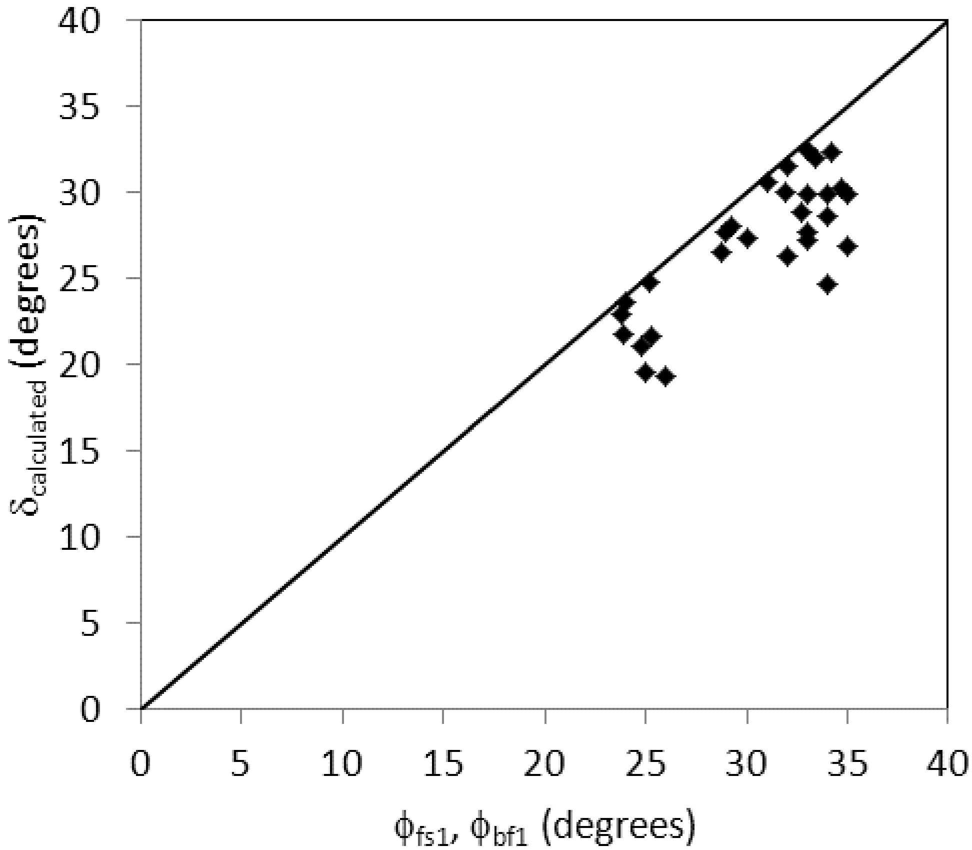

Figure 4-9 δ_{calc} versus ϕ_{fs1}, ϕ_{bf1} for MSE wall tests with upper bound limit

4.4 Vertical Earth Pressure Load Factor

In the centrifuge test process, the model is spun up to the test acceleration level (N_s = 40g), and soil stresses in the reinforced and foundation soil were measured and recorded. Since many tests were performed (>30), a large sample population of measured soil stresses was acquired which may be used to estimate/validate the load factor for vertical earth pressure for reinforced soil.

The load factor can be calculated with the following expression (Nowak, 1995)

$$\gamma = \lambda(1 + nCV) \qquad \text{Eq. 4-3}$$

where γ is the load factor, λ is the load bias (measured/predicted), *n* is a constant and *CV* is for the load bias. The constant, *n*, is chosen such that the probability of exceeding any factored load is always the same. In the development of the load factors recommended in the AASHTO LRFD bridge design code (2012), a value of *n* = 2 was used (Allen et al., 2005).

The vertical dead load in an MSE wall analysis may be a determined from the soil's vertical effective stress, σ_V', at the base elevation under geostatic conditions (i.e. no surcharge). The vertical effective stress, which acts over the reinforcement length, L, (foundation width) is determined as

$$\sigma_V' = \gamma_s' z \qquad \text{Eq. 4-4}$$

where γ_s' is the effective unit weight and *z* is the depth of soil overburden. AASHTO (2012) recommends a load factor of 1.35 for vertical earth pressure that represents the critical load combination for bearing resistance. Generally, this assumption is conservative for the factored load; however, it may not be accurate for MSE walls, which have non-uniform distributions of vertical stress due to the effect of the facing elements and soil reinforcement (Hatami and Bathurst, 2006; Liang and Almoh'd, 2004; Ling et al., 2005; Yoo, 1988).

Figure 4-10 shows the normalized (Eq. 4-4) non-uniform pressures measured at points along the base of the model wall (distance L_{model} = 3 inches) for the tests shown in Table 4-1. There is a significant influence of the interaction between the wall facing elements and backfill, shown from 0 and 0.5 in - left of the figure. However, from 0.5 to

3.0 in the normalized pressures reflect the non-uniform distribution of soil stress due to the reinforcement in the backfill, away from the wall facing. This suggests current load factors (1.35) for vertical earth pressure (uniform) should be recalculated to account for the load uncertainty because of wall and the reinforced soil mass.

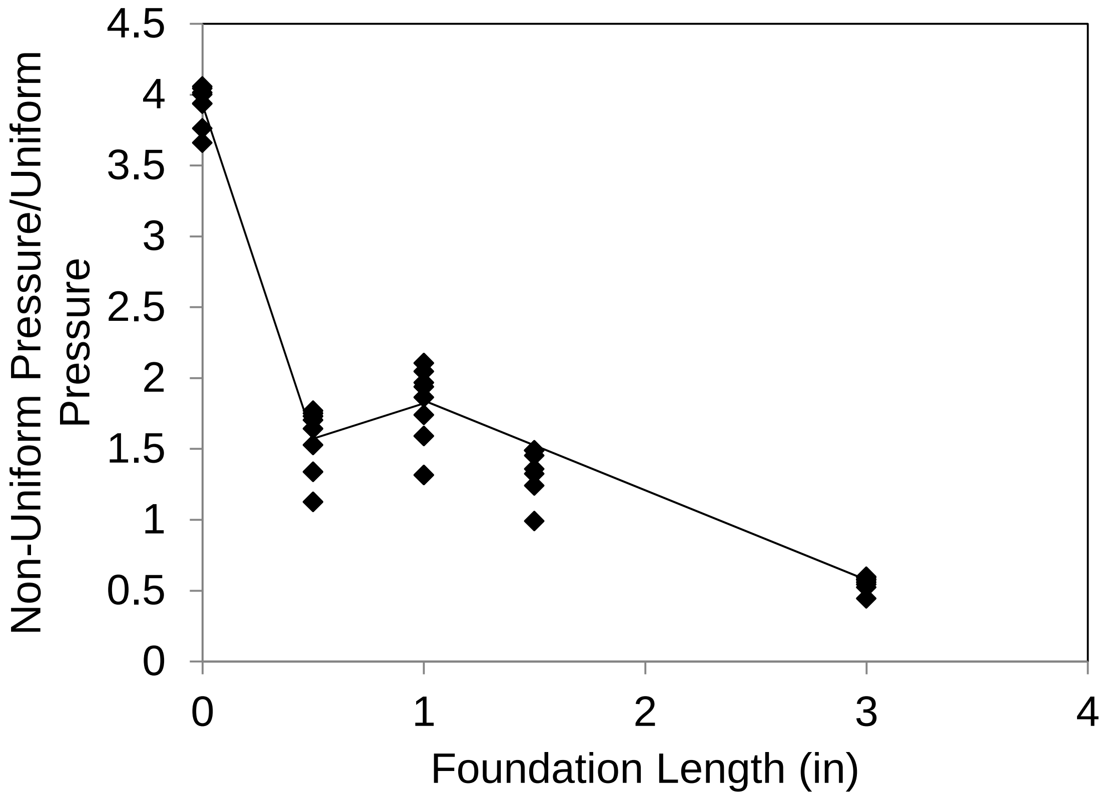

Figure 4-10 Normalized pressure distributions measured from self-weight of MSE wall and piecewise linear approximation

The predicted vertical resultant force due to the non-uniform soil pressure distribution (0.5 – 3 in) was determined using Equation 4-1 where the weight of the wall was not included. The mean load bias was 0.97 and the CV of the load bias was 0.47. Using $n = 2$ in Equation 4-3 (Allen et al., 2005), a new load factor of 1.87 was calculated and its influence on the load is shown in Figure 4-11 where it is applied to the nominal predicted values. Its effect is to bring most of the loads above the 1:1 line, which is the desired result. Bathurst et al. (2008) calculated load factors with n = 2 that ranged from 1.73 to 1.87 from 34 data points taken on 20 instrumented MSE walls with inextensible reinforcement (i.e., bar mat and welded wire). They proposed a load factor of 1.75 for use in determining Φ for MSE wall internal stability design.

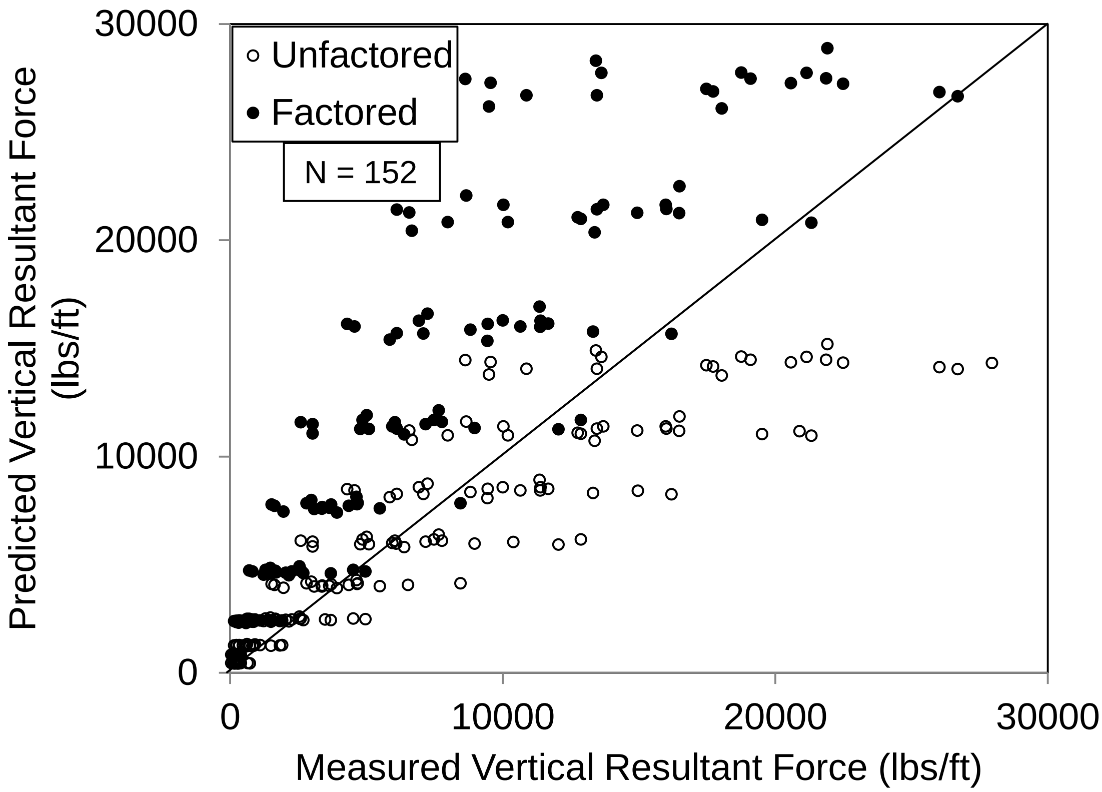

Figure 4-11 Unfactored and factored predicted vertical resultant forces versus measured vertical resultant force

4.5 Methods of Bearing Capacity Estimation

Equation 4-5 is the general equation for bearing capacity of shallow foundations on cohesionless soil, without embedment and with an inclined-eccentric load that was used to estimate the capacity for all tests.

$$q_{u_{pred}} = \frac{1}{2}\gamma L' N_\gamma i_\gamma \qquad \text{Eq. 4-5}$$

where γ is the soil's unit weight, *L'* is the effective foundation width (L-2e), N_γ is the bearing factor, L is length of reinforcement, e is eccentricity of resultant vertical force and i_γ is the load inclination factor. The eccentricity, e, was obtained by summing the moments about the toe of the wall, Figure 4-4.

The influence of the foundation soils was investigated with the following methods for estimating N_γ (bearing capacity factor for self-weight) and i_γ (load inclination factor for a shallow foundation on cohesionless soil) as given in the published literature (Bowles, 1997; Paikowsky et al., 2010).

4.5.1 Soil Self Weight Factors

The factors for self-weight are a function of the factor for overburden given by Prandtl (1920) and Reissner (1924):

$$N_q = e^{\pi \tan\phi} tan^2\left(45° + \frac{\phi}{2}\right) \quad \text{Eq. 4-6}$$

Meyerhof's (1963) empirical bearing capacity factor:

$$N_\gamma = \left(N_q - 1\right)\tan(1.4\phi) \quad \text{Eq. 4-7}$$

Hansen's (1970) empirical bearing capacity factor:

$$N_\gamma = 1.5\left(N_q - 1\right)tan(\phi) \quad \text{Eq. 4-8}$$

Vesic's (1973) analytically derived bearing capacity factor:

$$N_\gamma = 2\left(N_q + 1\right)tan(\phi) \quad \text{Eq. 4-9}$$

Salgado's (2008) bearing capacity factor based on numerical analysis:

$$N_\gamma = \left(N_q + 1\right)tan(1.32\phi) \quad \text{Eq. 4-10}$$

Eurocode (2005) empirical bearing capacity factor based on Muhs and Weiss (1969) and Muhs (1971):

$$N_\gamma = 2\left(N_q - 1\right)tan(\phi) \quad \text{Eq. 4-11}$$

Michalowski (1997) analytically derived bearing capacity factor for a footing with a rough base:

$$N_\gamma = e^{(0.66+1\tan(\phi))} tan(\phi) \qquad \text{Eq. 4-12}$$

Bolton and Lau (1993) bearing capacity factor based on numerical analysis:

$$N_\gamma = (N_q - 1) tan(1.5\phi) \qquad \text{Eq. 4-13}$$

4.5.2 Load Inclination Factors

The evident rupture surfaces in the MSE wall tests (Figures 4-7 and 4-8) coupled with Sokolovski's (1960) analytical work on the inclined load's effect on the rupture surface warrants the assessment of load inclination factors for MSE wall bearing stability. A number of bearing inclination factors have been proposed:

Hansen (1970) load inclination factor:

$$i_\gamma = \left(1 - \frac{0.7S_2}{V}\right)^\eta \qquad \text{Eq. 4-14}$$

$2 \leq \eta \leq 5$ (Bowles, 1997)

Vesic (1975) load inclination factor adjusted for the effective area of the footing:

$$i_\gamma = \left(1 - \frac{S_2}{V}\right)^{m+1} \qquad \text{Eq. 4-15}$$

m = (2+L/B)/(1+L/B) Eq. 4-16

where the ratio of L/B accounts for the footing size effect. L is the foundation width and B is the length of the wall (Figure 4-4). If there is eccentricity in either direction, then the effective dimensions (L' and/or B') should be used in Equation 4-5. For the MSE wall tests, the exponent (m+1) ranges from 2.7 – 2.8.

Muhs and Weiss (1969) load inclination factor:

$$i_\gamma = (1 - \tan(\delta))^\eta \qquad \text{Eq. 4-17}$$

Muhs and Weiss (1969) recommended the exponent (η) for the load inclination factor (Eq. 4-17) be taken as 1 based on field tests of eccentric-inclined loads acting in the direction of the length of a rigid footing underlain by sand. They also suggested that the exponent for loading in direction of the short side of the footing will result in much greater reduction in the capacity (i.e. $\eta > 1$).

Given the similarities between inclination factors (e.g. Muhs et. al and Vesic), it was decided to back calculate the exponent, η, in Equation 4-17 from the experimental data through Equation 4-18, with the predicted ultimate capacity [$V_{qu\ pred} = q_u$ x L' (lbs/ft) –with Bolton's N_γ] without an inclined load (δ= 0 and $i_\gamma = 1$) divided into the measured capacity from each test, V_{meas} (lbs/ft). With the S_2 (horizontal resultant force) values that were calculated for each test, η was solved for tests where $\mu_{\phi fs}$ = 26°-30° and 31°-33°. For 26°-30°, a η of 1.08 was obtained and for 31°-33°, a η of 1.55 was obtained, which are representative of the influence of flexible loads in combination with inclined loads, i.e. in MSE walls. The latter is much smaller than the range of exponents reported in the literature, $1 < \eta < 5$ which has used for both flexible and rigid footings. The new estimation of the load inclination factor specific to MSE walls, Equations 4-19 and 4-20 will be used in conjunction with Muhs, Vesic, and Hansen in estimating LRFD Φ in the next section.

$$\frac{V_{meas}}{V_{qu_{pred}}} = \left(1 - \frac{S_2}{V}\right)^{\eta} \qquad \text{Eq. 4-18}$$

$$i_\gamma = \left(1 - \frac{S_2}{V}\right)^{1.08}, \qquad 26° < \phi_{foundation} < 30° \qquad \text{Eq. 4-19}$$

$$i_\gamma = \left(1 - \frac{S_2}{V}\right)^{1.55}, \qquad 31° < \phi_{foundation} < 33° \qquad \text{Eq. 4-20}$$

4.6 Resistance Factors for Bearing Stability

Equation 4-21 is the form of the LRFD Φ equation (FHWA, 2001) that was used to calculate the Φ's. The CV of the live and dead loads are accounted for with the expression for CV_Q in Equation 4-22 (Styler, 2006).

$$\Phi = \frac{\lambda_R \cdot \sqrt{\frac{(1+CV_Q^2)}{(1+CV_R^2)}} \cdot (\gamma_D \cdot q_D + \gamma_L \cdot q_L)}{(\lambda_D \cdot q_D + \lambda_L \cdot q_L) \cdot e^{\beta_T \sqrt{\ln\left[(1+CV_R^2)(1+CV_Q^2)\right]}}} \qquad \text{Eq. 4-21}$$

$$CV_Q^2 = \frac{q_D^2 \cdot E[\lambda_D]^2 \cdot CV_D^2 + q_L^2 \cdot E[\lambda_L]^2 \cdot CV_L^2}{q_L^2 \left(\frac{q_D^2}{q_L^2} \cdot E[\lambda_D]^2 + 2 \cdot \frac{q_D}{q_L} \cdot E[\lambda_D] \cdot E[\lambda_L] + E[\lambda_L]^2\right)} \qquad \text{Eq. 4-22}$$

The λ_R = mean resistance bias factor and CV_R = coefficient of variation in the resistance are assessed based on the N_γ and i_γ factors selected. The other terms in Equations 21 and 22 are calculated from the test measurements (i.e., mean dead load q_D = 467 kN/m, mean live load q_L = 167 kN/m, dead load factor γ_D = 1.87, mean dead load bias factor λ_D = 0.97, mean live load bias factor λ_L = 1.2, coefficient of variation in the dead load CV_D = 0.47, and coefficient of variation in the live load CV_L = 0.42) and AASHTO (2012) recommendations (i.e., live load factor γ_L = 1.75 and target reliability index β_T = 3.09).

Tables 4-3 through 4-10 show CV_R, λ_R, and estimated Φ values for the prototype MSE walls (H =20 ft and L/H = 0.5) based on the centrifuge tests where $\mu_{\phi fs}$ = 26°-30° and 31°-33°. The estimates are made for each i_γ factor (Eqs. 4-14 through 4-20) in combination with each of the N_γ factors (Eqs. 4-6 through 4-13). The levels of reliability considered were 2.32 and 3.09, which correspond to probabilities of failure, P_f, of 1/100 and 1/1000, respectively.

Evident from Tables 4-4 and 4-8, Vesic's load inclination factor gives the largest bias in resistance, $\lambda_R > 3$, and Φ's >1, for both groups of $\mu_{\phi fs}$. This is a result of the large exponent (m+1 = 2.7 – 2.8) applied in Equation 4-15 which significantly reduces the predicted capacity (Eq. 4-5) for determining λ_R. Muhs's method (Tables 4-5 and 4-9), with $\eta = 1$, results in the smallest λ_R among the methods and gives the most conservative Φ values. Since Φ values ≤ 1 (Allen et al., 2005) and $\beta = 3.09$ ($P_f = 1/1000$) are generally recommended for use in design of retaining walls, Hansen's, Muhs's, and the new method are deemed appropriate.

A comparison between the methods for load inclination factors is made based on Φ/λ_R, an efficiency factor (McVay et al., 2000). It represents the percent of measured resistance (e.g., centrifuge tests) used in design and provides a measure of the relative efficiency of each method, with larger values indicating a more economical solution. Interestingly, for each load inclination factor method, the Φ/λ_R's among the N_γ methods are essentially the same. For example, Hansen's load inclination factor is applied to all $N\gamma$ methods (Table 4-3), Φ/λ_R's ranges from 0.485 to 0.510, for $\beta = 2.32$ ($P_f = 1/100$), and 0.324 to 0.346, for $\beta = 3.09$ ($P_f = 1/1000$). This permits a direct comparison between the $N\gamma$ methods that result in the lowest CV_R (i.e., the largest Φ/λ_R). For $\mu_{\phi fs} = 26°\text{-}30°$, Vesic's method gives the lowest Φ/λ_R's for most of the N_γ methods. For the design recommended $\beta = 3.09$ ($P_f = 1/1000$), the new method (Eq. 4-19) is more efficient (larger Φ/λ_R's) than Hanson's and Muhs's, which are very similar. Combined use of Vesic's N_γ method and the new load inclination factor method (Eq. 4-19), gives the largest Φ/λ_R's and lowest CV_R. For $\mu_{\phi fs} = 31°\text{-}33°$, Muhs's load inclination factor method gives the largest Φ/λ_R's; however, the $\lambda_R < 1$ for all N_γ methods. The methods with $\lambda_R > 1$ are

Vesic's and the new method. Among all these methods, the new method is more efficient (larger Φ/λ_R's) and gives the lowest CV_R. For $\beta = 3.09$ ($P_f = 1/1000$), the calculated Φ factors for the two data sets for $\mu_{\phi fs}$ (26°-30° and 31°-33°) are 0.47 and 0.45, respectively.

Table 4-3 Resistance factors (Φ) for $\mu_{\phi fs}$ = 26° - 30° using Hansen's i_γ

		Meyerhof	Hansen	Vesic	Salgado	Euro7	Michalowski	Bolton
CV_R		0.472	0.464	0.450	0.455	0.464	0.461	0.474
λ_R		1.88	1.93	1.26	1.78	1.44	1.35	1.71
β = 2.32	Φ	0.918	0.954	0.641	0.897	0.715	0.673	0.828
	Φ/λ_R	0.487	0.495	0.510	0.505	0.495	0.498	0.485
β = 3.09	Φ	0.615	0.641	0.434	0.606	0.481	0.453	0.554
	Φ/λ_R	0.326	0.333	0.346	0.341	0.333	0.336	0.324

Table 4-4 Resistance factors (Φ) for $\mu_{\phi fs}$ = 26° - 30° using Vesic's i_γ

		Meyerhof	Hansen	Vesic	Salgado	Euro7	Michalowski	Bolton
CV_R		0.492	0.492	0.492	0.492	0.492	0.492	0.492
λ_R		5.46	5.60	3.67	5.18	4.20	3.93	4.95
β = 2.32	Φ	2.550	2.615	1.714	2.419	1.962	1.835	2.312
	Φ/λ_R	0.467	0.467	0.467	0.467	0.467	0.467	0.467
β = 3.09	Φ	1.688	1.731	1.134	1.601	1.298	1.215	1.530
	Φ/λ_R	0.309	0.309	0.309	0.309	0.309	0.309	0.309

Table 4-5 Resistance factors (Φ) for $\mu_{\phi fs}$ = 26° - 30° using Muhs's i_γ

		Meyerhof	Hansen	Vesic	Salgado	Euro7	Michalowski	Bolton
CV_R		0.477	0.469	0.454	0.460	0.469	0.465	0.479
λ_R		1.60	1.64	1.07	1.51	1.23	1.15	1.45
β = 2.32	Φ	0.771	0.804	0.541	0.754	0.603	0.568	0.696
	Φ/λ_R	0.482	0.490	0.506	0.499	0.490	0.494	0.480
β = 3.09	Φ	0.515	0.539	0.366	0.508	0.404	0.382	0.464
	Φ/λ_R	0.322	0.329	0.342	0.337	0.329	0.332	0.320

Table 4-6 Resistance factors (Φ) for $\mu_{\phi fs}$ = 26° - 30° using the new i_γ (Eq. 19)

		Meyerhof	Hansen	Vesic	Salgado	Euro7	Michalowski	Bolton
CV_R		0.450	0.444	0.433	0.437	0.444	0.441	0.452
λ_R		1.93	1.98	1.29	1.82	1.48	1.39	1.75
β = 2.32	Φ	0.986	1.020	0.682	0.956	0.765	0.721	0.889
	Φ/λ_R	0.510	0.516	0.528	0.524	0.516	0.520	0.508
β = 3.09	Φ	0.668	0.694	0.467	0.652	0.520	0.491	0.602
	Φ/λ_R	0.346	0.351	0.361	0.358	0.351	0.354	0.344

Table 4-7 Resistance factors (Φ) for $\mu_{\phi fs}$ = 31° - 33° using Hansen's i_γ

		Meyerhof	Hansen	Vesic	Salgado	Euro7	Michalowski	Bolton
CV_R		0.436	0.431	0.426	0.429	0.431	0.431	0.437
λ_R		0.87	0.92	0.63	0.87	0.69	0.65	0.78
β = 2.32	Φ	0.457	0.488	0.338	0.463	0.366	0.345	0.409
	Φ/λ_R	0.525	0.530	0.536	0.533	0.530	0.530	0.524
β = 3.09	Φ	0.312	0.334	0.232	0.318	0.251	0.236	0.279
	Φ/λ_R	0.359	0.363	0.368	0.365	0.363	0.363	0.358

Table 4-8 Resistance factors (Φ) for $\mu_{\phi fs}$ = 31° - 33° using Vesic's i_γ

		Meyerhof	Hansen	Vesic	Salgado	Euro7	Michalowski	Bolton
CV_R		0.500	0.495	0.490	0.493	0.495	0.496	0.502
λ_R		3.53	3.72	2.54	3.51	2.79	2.63	3.17
β = 2.32	Φ	1.621	1.726	1.191	1.636	1.295	1.218	1.450
	Φ/λ_R	0.459	0.464	0.469	0.466	0.464	0.463	0.457
β = 3.09	Φ	1.068	1.141	0.789	1.082	0.856	0.804	0.954
	Φ/λ_R	0.303	0.307	0.311	0.308	0.307	0.306	0.301

Table 4-9 Resistance factors (Φ) for $\mu_{\phi fs}$ = 31° - 33° using Muhs's i_{γ}

		Meyerhof	Hansen	Vesic	Salgado	Euro7	Michalowski	Bolton
CV_R		0.435	0.430	0.425	0.428	0.430	0.430	0.436
λ_R		0.73	0.77	0.53	0.73	0.58	0.55	0.66
β = 2.32	Φ	0.384	0.409	0.285	0.390	0.308	0.292	0.347
	Φ/λ_R	0.526	0.532	0.537	0.534	0.532	0.532	0.525
β = 3.09	Φ	0.262	0.281	0.196	0.267	0.211	0.200	0.237
	Φ/λ_R	0.360	0.364	0.369	0.366	0.364	0.364	0.359

Table 4-10 Resistance factors (Φ) for $\mu_{\phi fs}$ = 31° - 33° using the new i_{γ} (Eq. 20)

		Meyerhof	Hansen	Vesic	Salgado	Euro7	Michalowski	Bolton
CV_R		0.440	0.436	0.431	0.434	0.436	0.436	0.442
λ_R		1.71	1.80	1.23	1.70	1.35	1.27	1.53
β = 2.32	Φ	0.890	0.945	0.652	0.896	0.709	0.667	0.793
	Φ/λ_R	0.521	0.525	0.530	0.527	0.525	0.525	0.519
β = 3.09	Φ	0.607	0.645	0.447	0.613	0.484	0.455	0.540
	Φ/λ_R	0.355	0.359	0.363	0.360	0.359	0.359	0.353

4.7 Observations and Findings of MSE Bearing Analysis

A centrifuge test program to determine the influence of soil variability in the bearing capacity of MSE walls and development of Φ's was reported. A total of 29 tests were performed on a model wall 1/40th the scale of the prototype (H = 20 ft) and with L/H = 0.5. Soil variability in the foundation soils and wall backfill was modeled in each test and are described by their statistical descriptors (μ_ϕ, μ_γ, CV_ϕ, and CV_γ). Measurements of vertical bearing stress under the footprint on the MSE wall permitted observations of non-uniform soil stress distributions during external surcharge loading. Vertical resultant forces at bearing failure were compared with predictions using conventional methods used in design. Effects of load inclination were discussed and resistance factors are calculated using the FHWA expression for Φ. A comparison of the different load inclination factors is made with Φ/λ_R for two ranges of μ_ϕ of the foundation soils. The following conclusions from the research are noted:

- Low profile, miniature soil stress sensors were successfully used in centrifuge model tests following calibration. The calibration involved embedding the sensors in uniform density soil and using the centrifuge's increased acceleration field, g, and its effect on the body weight of the soil to create increased overburden pressures. The sensors small diameters (6 mm) permitted the use of 4-5 units in the footprint of MSE wall model, which resulted in good measurements of non-uniform soil stress distributions.
- The measured soil stress distributions were integrated over the footprint of the MSE wall (reinforcement length = L) and plotted against the vertical displacement of the wall to obtain load displacement curves. From the load

displacement curves the capacity was determined where the slope of the curve reached a steady or maximum value.

- The measured results were validated with a MSE wall/soil wedge model. Vertical and horizontal force equilibrium of a MSE wall/soil wedge provided an $R^2 = 0.85$.
- Observations of the models post-test indicated bearing rupture surfaces that occurred at shallower depths where the foundation soil's friction angle was greater. This suggested the influence of inclined resultant load acting on the foundation soil's surface.
- Measured soil stresses during the spin up part of all the centrifuge tests resulted in 152 measurements of vertical dead load due to the reinforced soil and a load factor, $\gamma_D = 1.87$, was calculated. AASHTO (2012) recommends γ_D for vertical earth pressure = 1.35, while Bathurst et al. (2008) proposed $\gamma_D = 1.75$ calibrated from measurements on non-extensible reinforcements in full scale MSE wall tests. The γ_D calculated herein was used in the determination of the Φ for bearing capacity of MSE walls.
- Different methods to predict the influence of load inclination and the self-weight of the foundation soil through the terms i_γ and N_γ in the general bearing capacity equation were used to calculate the respective Φ. The relative efficiency of the methods for i_γ was shown based on Φ/λ_R. The results indicate that Vesic's N_γ and a new method for i_γ are the most appropriate for the bearing capacity of MSE walls. Furthermore, the Φ at $\beta = 3.09$ for the foundation soil's $\mu_\phi = 26°\text{-}30°$ and $31°\text{-}33°$ are 0.47 and 0.45, respectively. For $\beta = 2.32$, Φ for the proposed method range from 0.65 to 0.68.

- Current practice of MSE wall design for bearing capacity uses $\Phi = 0.65$ as recommended by AASHTO (2012). This implicitly encompasses all soil strengths and uncertainty arising from soil variability (i.e., μ and CV). The Φ's reported herein explicitly account for soil variability of known μ and CV through the influence on the load and resistance (i.e., CV_Q and CV_R).

CHAPTER 5
BEARING STABILITY OF MSE WALLS ON EMBANKMENTS

5.1 Introduction

Recently, it has been identified in congested urban areas (i.e., multiple highway interchange overpasses or supplement natural grade to achieve roadway elevation) that MSE walls sit atop a sloped soil embankment, set back from the embankment edge. For such cases, the FDOT has identified that bearing capacity prediction methods for walls don't agree very well, as well as have conservative assumptions.

Figure 5-1 illustrates the two cases of footings on or near a slope. It is generally believed that the reduced soil mass in the passive and radial zones results in a reduced length of the shear surface along these zones (dashed lines). Bowles (1997) proposed a method to adjust the general bearing capacity equation (Eq. 5-1) for the case of a cohesionless material (c=0) and a footing (MSE wall) at some distance (b) from the edge of the slope through the N'_γ term (weight influence factor) according to Eq. 5-2.

$$q_u = c\mathrm{N}_c + \gamma_s D_f N_q C_q + 0.5\gamma_s L N_\gamma C_\gamma \qquad \text{Eq. 5-1}$$

where c =cohesion, γ = total unit weight, D_f = footing embedment depth, C_q, C_γ = correction factors, L =footing width, N_c, N_q, N_γ are the cohesion, surcharge and soil self-weight bearing capacity factors.

$$N'_\gamma = \frac{N_\gamma}{2} + \frac{N_\gamma}{2}\left[R + \frac{b}{2L}(1-R)\right] \qquad \text{Eq. 5-2}$$

where N_γ = soil self-weight bearing capacity factor, R = Ratio of minimum to maximum K_p, b = distance of footing from edge of slope, L = footing width.

However, other methods have been proposed (Meyerhof, Hansen, Vesic), for the bearing capacity factors near slopes. FDOT engineers have shown comparison of bearing capacity results using Bowles and other non-adjusted factors (Figure 5-2). The figure identifies the influence of distance to the slope crest on the bearing capacity ratio using Bowles as well as Meyerhof, Hansen, and Deschenes. Evident from Figure 5-2, there is a factor of 3 differences between the smallest and largest values.

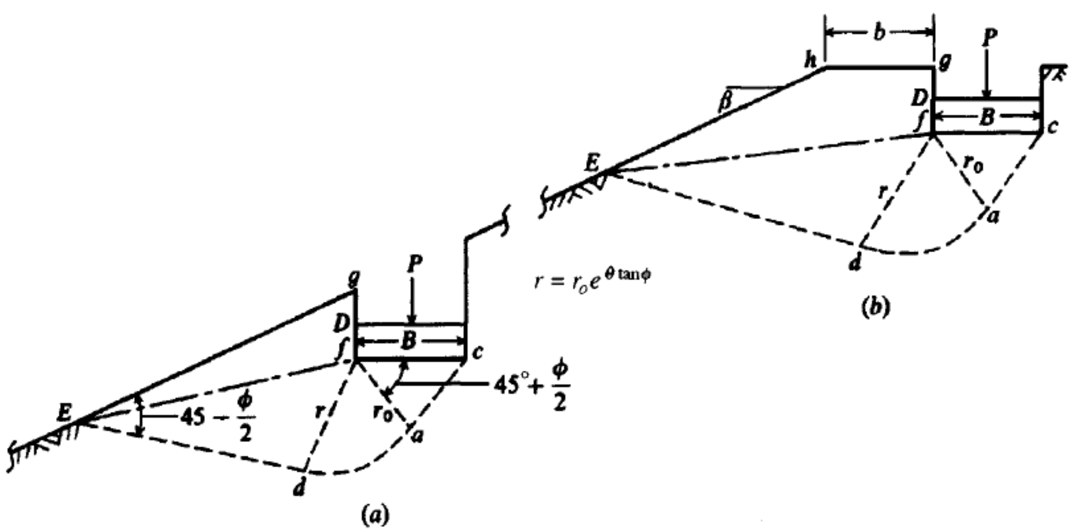

Figure 5-1 Footing (a) on slope and (b) near slope (Bowles, 1997)

Interestingly, AASHTO recommends Φ's of 0.65 for all bearing capacity (e.g. MSE) including foundations near slopes. Based on Figure 5-2, the latter values are highly un-conservative (factor of 3 difference).

To investigate MSE walls near slopes, FDOT's worst case scenario, i.e. walls abutting slopes with inclinations of 26°, were investigated in the centrifuge. The walls were designed with L/H=0.5, with slope (foundation) soil with angles of internal friction of 26° and both deformation and stresses were monitored on the wall. The results were compared initially to prediction methods (Bowles, Meyerhof, etc.) near slopes as well as flat ground results (chapter 4). It was discovered that the results were quite different (> > predictions). Further investigation revealed that traditional bearing capacity, i.e. passive stress states were not appropriate for this case (i.e. failure surface was not at 45°-ϕ/2), suggesting that slope stability analysis was more appropriate. A detailed discussion of the experiments, results, and analysis follows.

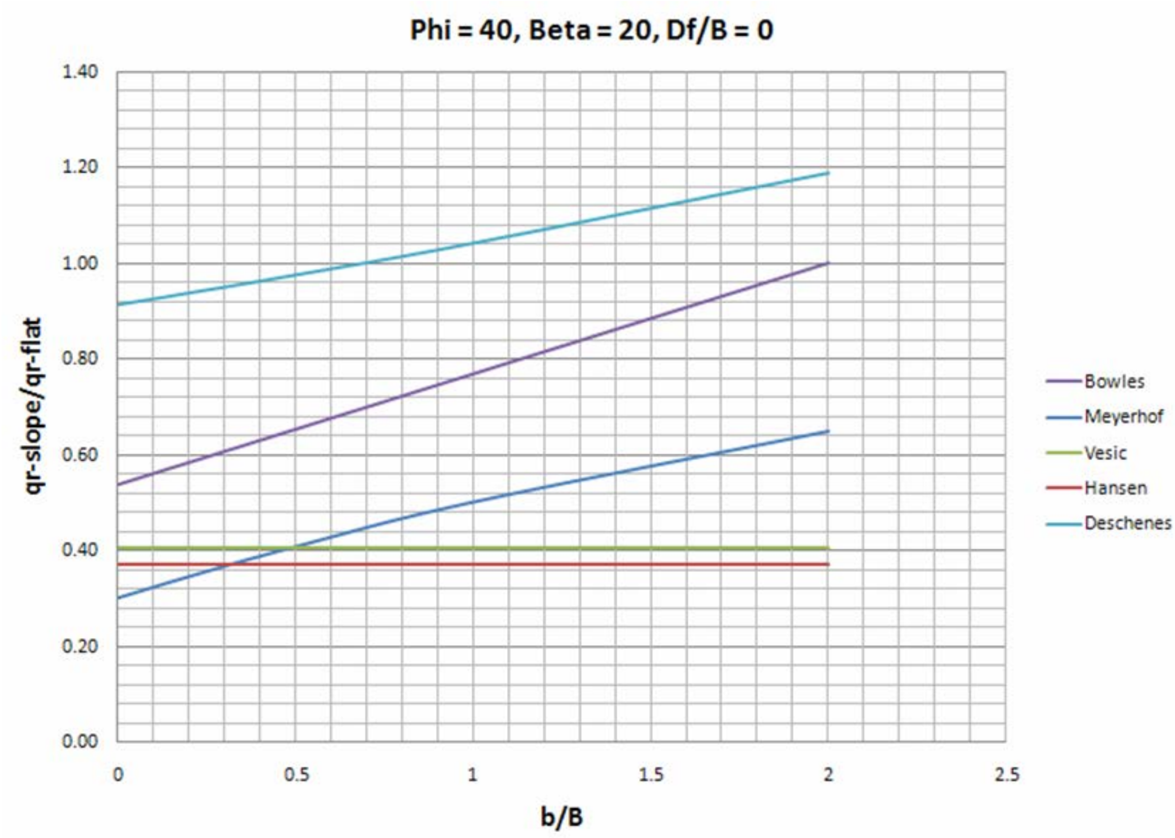

Figure 5-2 Comparison of methods for ratio of bearing capacity to influence of distance to slope, for a beta of 20°

5.2 MSE Wall Models for Bearing Stability on Embankment Experiments

Figure 5-3 shows the model wall that was used in the embankment tests and is the same one used in the tests discussed in Chapter 4. The internal stability analysis of the wall is described in Chapter 4.

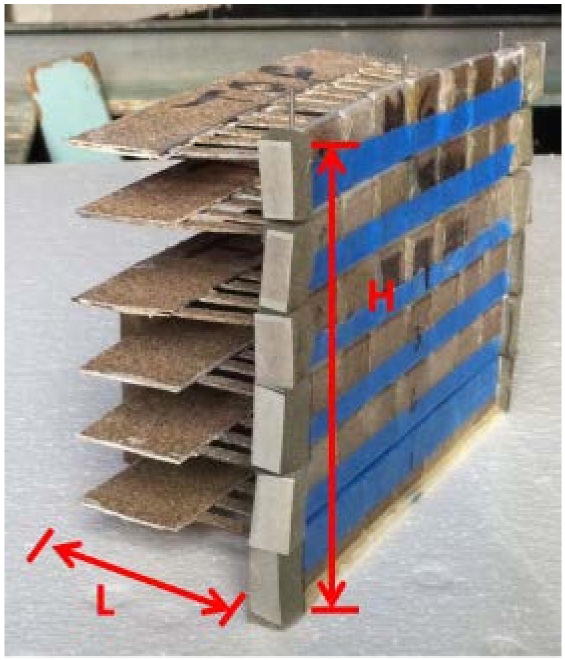

Figure 5-3 MSE wall model for embankment bearing tests

5.3 Centrifuge Tests on MSE Walls on Embankments

5.3.1 Results and Analysis

To investigate the actual bearing capacity for the case of an MSE retaining wall near embankments, centrifuge models were tested for slopes of 2:1 (β=26°), with variable embankment soil and backfill (μ_ϕ, μ_γ, CV_ϕ, CV_γ), and d/L= 0 (d=offset distance, Figure 5-1b, and L=foundation width). The retaining wall models are 1/40th of the prototype (H= 20 ft), with L/H = 0.5 and tested at 40-g acceleration.

Figure 5-4 shows a model MSE wall and embankment model in a test container completely assembled with the support frames for LVDT's and load reaction. To create a uniform surcharge, q_s, a Bimba air piston was used to apply load to a ½ inch thick aluminum surcharge plate with a compressible layer of Styrofoam attached to the bottom. The plate is free to rotate under the piston load during contact and LVDT's are placed on the top of the plate at the front and back to measure vertical movements of the wall. Two LVDT's are oriented laterally and placed on the front face of the wall to

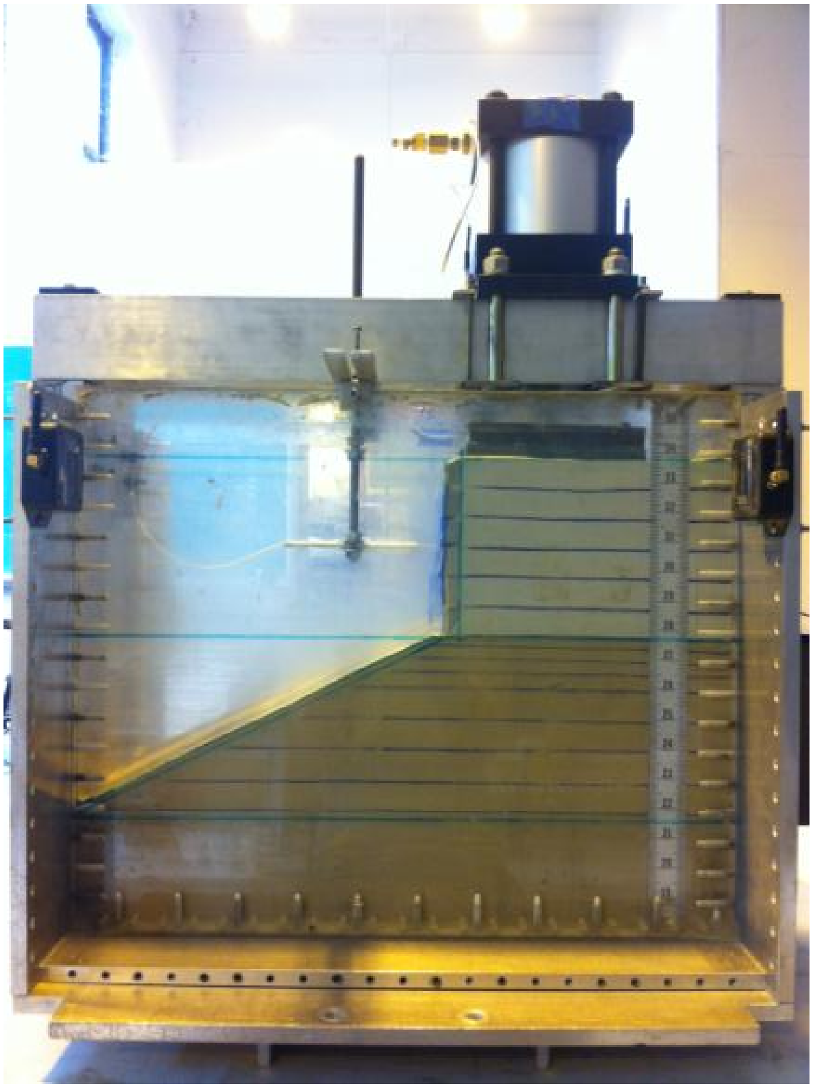

Figure 5-4 Model MSE wall on embankment with blue marker lines and surcharge piston measure lateral movements. Note, blue marker lines are placed in the backfill and the embankment (slope) to permit observations of shear failure (i.e. depth and length of the rupture). The marker lines are blue fine sand, placed only at the boundary of the model, in thin (1/8 inch) lines, so that there is minimal influence on the model behavior.

A total of 19 tests were completed for MSE near slopes and they are summarized in Table 5-1. The embankments of the initial models (Tests 1-3) were built with A-1-b soil (AASHTO) having 4% fines and compacted with 5% water content. At the time, it was decided to use moisture in the soil to facilitate a cut embankment with $\beta = 26°$. Due

Table 5-1 Statistical descriptors of soil properties for tests of MSE wall on embankment

Test	Backfill				Embankment (Foundation Soil)			
	Unit Weight (pcf) $(\mu)_\gamma$	Unit Weight CV_γ (%)	Friction Angle (°) $(\mu)_\phi$	Friction Angle CV_ϕ (%)	Unit Weight (pcf) $(\mu)_\gamma$	Unit Weight CV_γ (%)	Friction Angle (°) $(\mu)_\phi$	Friction Angle CV_ϕ (%)
1	95	7	30	7	100	5	32	5
2	94	8	28	12	105	5	34	5
3	103	6	36	5	105	5	33	5
4	98	1	37	2	107	2	34	2
5	97	1	37	2	107	2	34	2
6	98	2	38	5	86	1	26	1
7	99	13	38	2	90	5	27	4
8	98	1	38	2	86	3	26	2
9	98	1	38	2	85	2	26	2
10	97	1	37	3	82	2	26	2
11	97	1	37	2	90	2	27	2
12	97	1	37	3	82	2	26	2
13	98	1	38	3	85	1	26	1
14	95	1	35	1	83	3	26	2
15	95	1	35	1	83	2	26	2
16	96	1	36	4	84	10	26	3
17	97	2	37	4	82	2	26	2
18	98	4	38	9	82	4	26	4
19	97	2	37	4	85	3	26	2

to the possible influence from capillary tension on strength, it was decided to build the ensuing embankments with only dry soil. Test 4 and 5 were dry A-1-b soil from Florida. Tests 6-19 used dry Vicksburg silt as the embankment material which has lower ϕ's (20° -32°) and resulted in observed bearing capacity failures in the slope.

The tests employed the same testing procedure for MSE retaining walls constructed on flat ground and utilized the same instrumentation to measure the wall movements and soil stresses (i.e., vertical and horizontal LVDTs and miniature soil stress sensors). Shown in Figure 5-5 is the distribution of bearing pressure developed beneath the MSE wall in response to a surcharge load, q_s, applied on top of the wall over a distance of H (20 ft) from the wall facing.

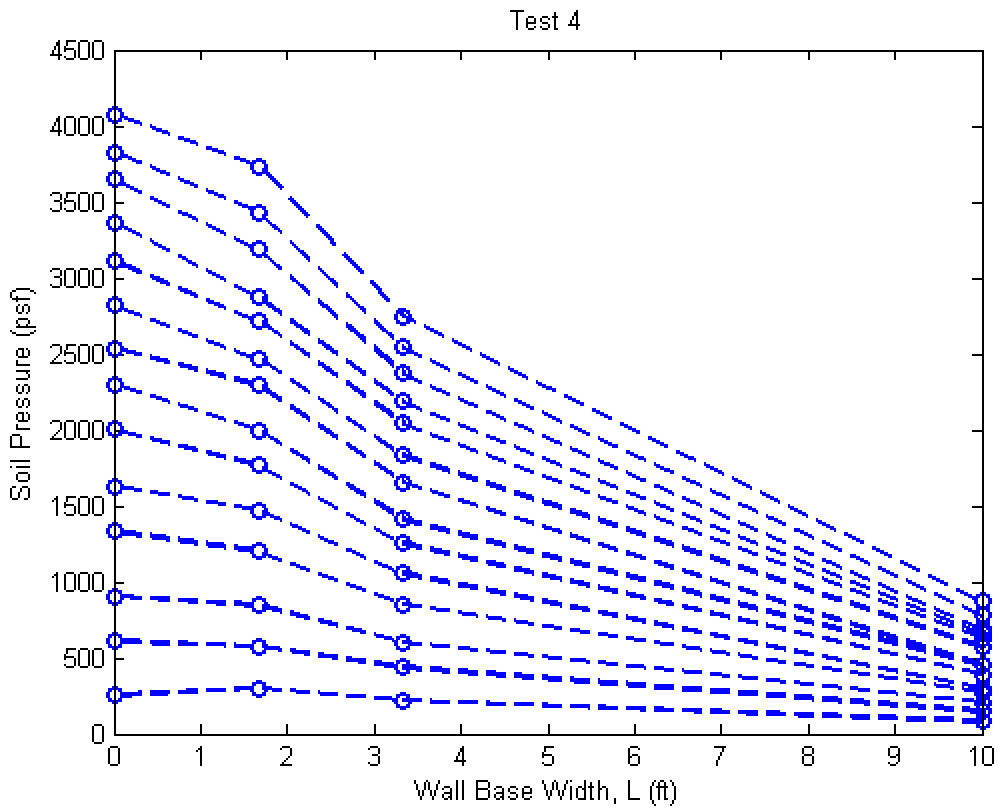

Figure 5-5 Distributions of soil pressure beneath MSE wall in Test 4 for increasing surcharge

Figure 5-6 shows the measured load ($V_{measured}$) settlement curves for Tests 1 and 2 where the embankment was prepared with 4% - 6% moisture content, with 100 pcf and 105 pcf dry unit weights (γ_d), respectively. The effective internal friction angles for the embankments were 33° and 34°, respectively. Evident is the apparent maximum resistance at small vertical movements (≈ 0.85 inch and 0.5 inch). Test 2 had γ_d = 105 pcf and ϕ = 34° and exhibited greater measured capacity at a less vertical movement (18,000 lbs/ft and 0.5 inch). Test 1 had γ_d = 100 pcf and ϕ = 33° and exhibited less

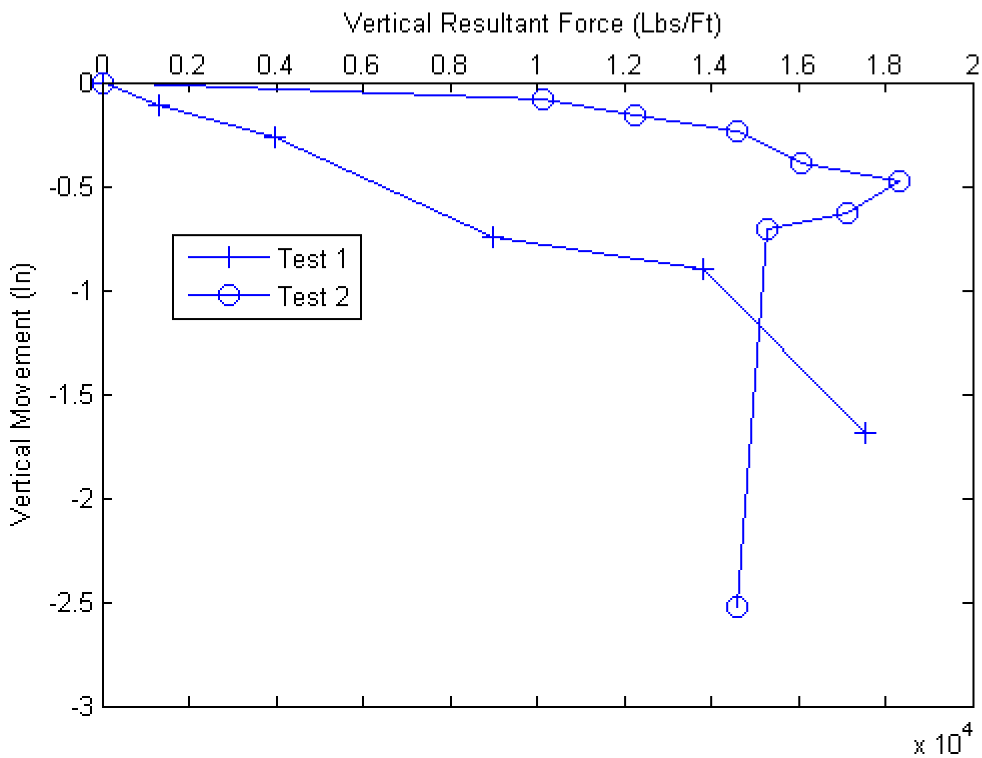

Figure 5-6 Load settlement curves for MSE walls on embankments for Tests 1 and 2

measured resistance at a greater vertical movement (13,830 lbs/ft at 0.85 inch).

Figure 5-7 shows the measured load ($V_{measured}$) settlement curves for Tests 4 and 5 where the embankment was prepared dry and had γ = 107 pcf and ϕ = 34°. It is evident there was not any ultimate capacity developed and, based on post test observations (Figure 5-18), no failure rupture surfaces developed in the embankment. Consequently, it was decided to lower the strength of foundation soil to observe rupture failure in the slope.

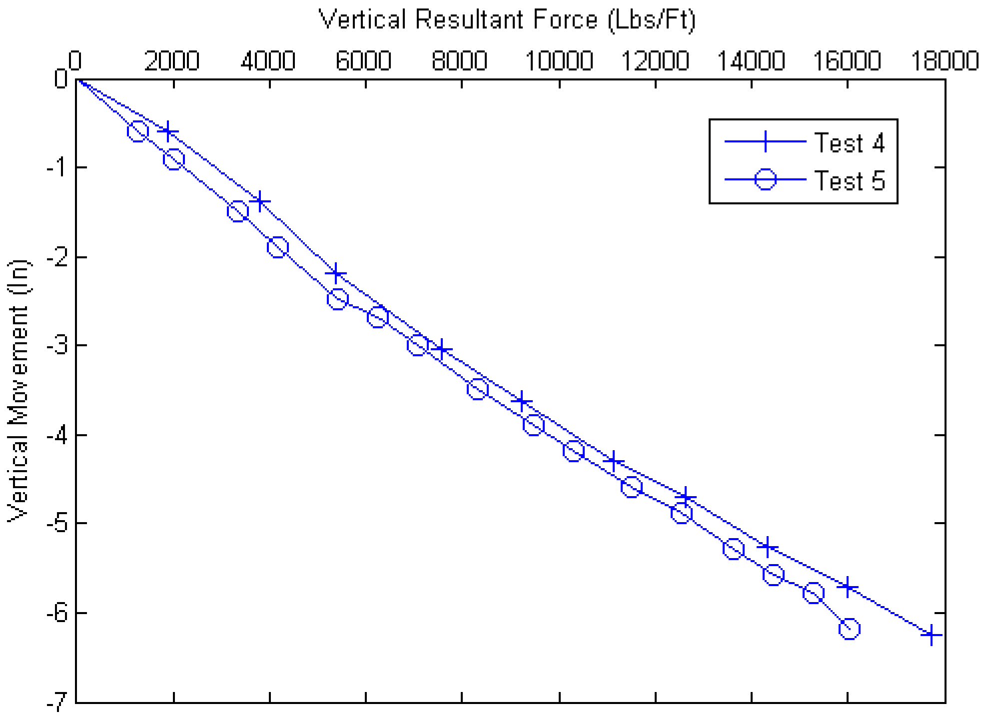

Figure 5-7 Load settlement curves for MSE walls on embankments for Tests 4 and 5

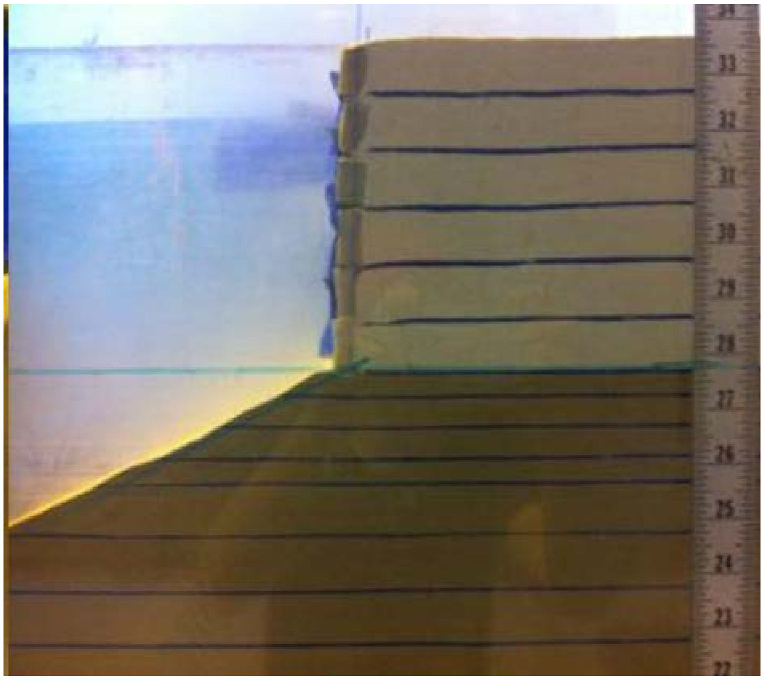

Figure 5-8 Post-test observation of Test 4 model

Figure 5-9 shows the measured load ($V_{measured}$) settlement curves for Tests 6-10 (silt slopes) where γ varied from 82 pcf – 90 pcf and ϕ varied from 26°-27°. The measured failure occurred at higher loads than the first set of tests (ϕ = 33° and 34°), but at larger vertical movements. The average relative density of the embankment was 75% and constructed from silt in order to attain $\phi < 30°$. The capacities suggested by the measured curves are approximately 26,000 lbs/ft – 35,000 lbs/ft. Observations of the failure surfaces (for example Figures 5-10 and 5-11) showed ruptures surfaces within the embankment that were deeper (3 inches – 4.5 inches) than those observed with higher ϕ (0.5 inch – 1.5 inches, Tests 1 and 2). Figure 5-12 shows the rupture surface in test 10 with the failure surface exiting at a distance of 8.5 inches from the face of the MSE wall. Again these observations support the influence of the inclined resultant load on the developed rupture surface. For lower ϕ soil, a smaller the inclination of the resultant load develops on the ground surface (i.e., top of embankment) and a deeper and wider rupture surface occurs beneath the foundation (i.e., MSE wall).

The results of the model tests show: a) reproducibility; b) influence of embankments with lower ϕ and without moisture content; and c) support previous observations of higher capacities with lower ϕ soil (reduction in the vertical component of the inclined resultant load acting on the ground surface). The next section will compare the measured capacities ($V_{measured}$) with the predicted results.

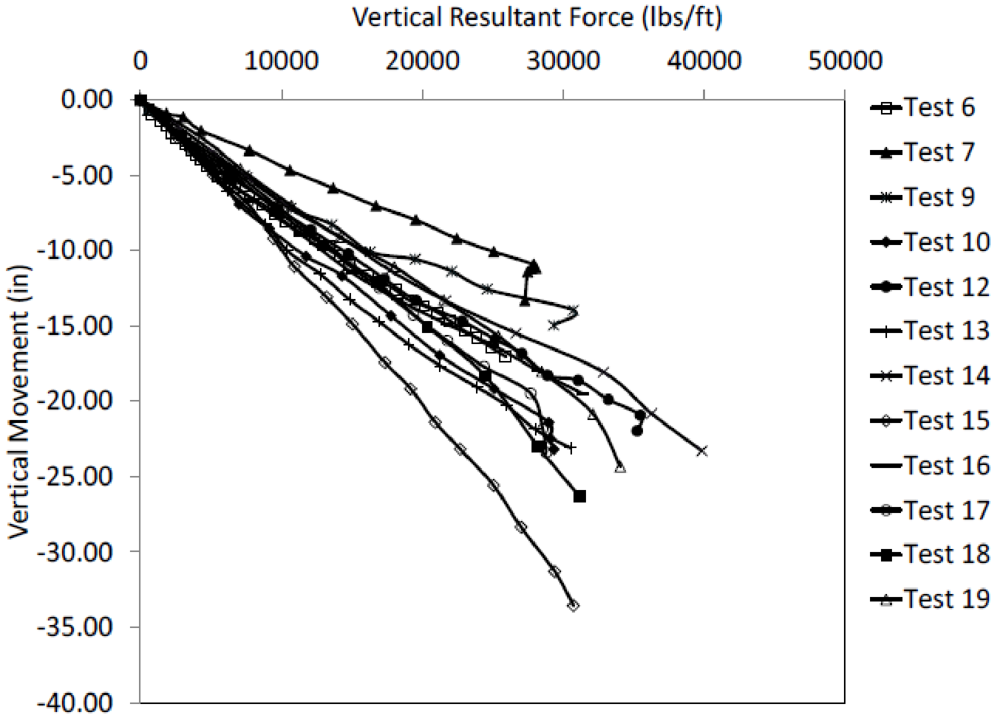

Figure 5-9 Load settlement curves for MSE walls on embankments for Tests 6-19

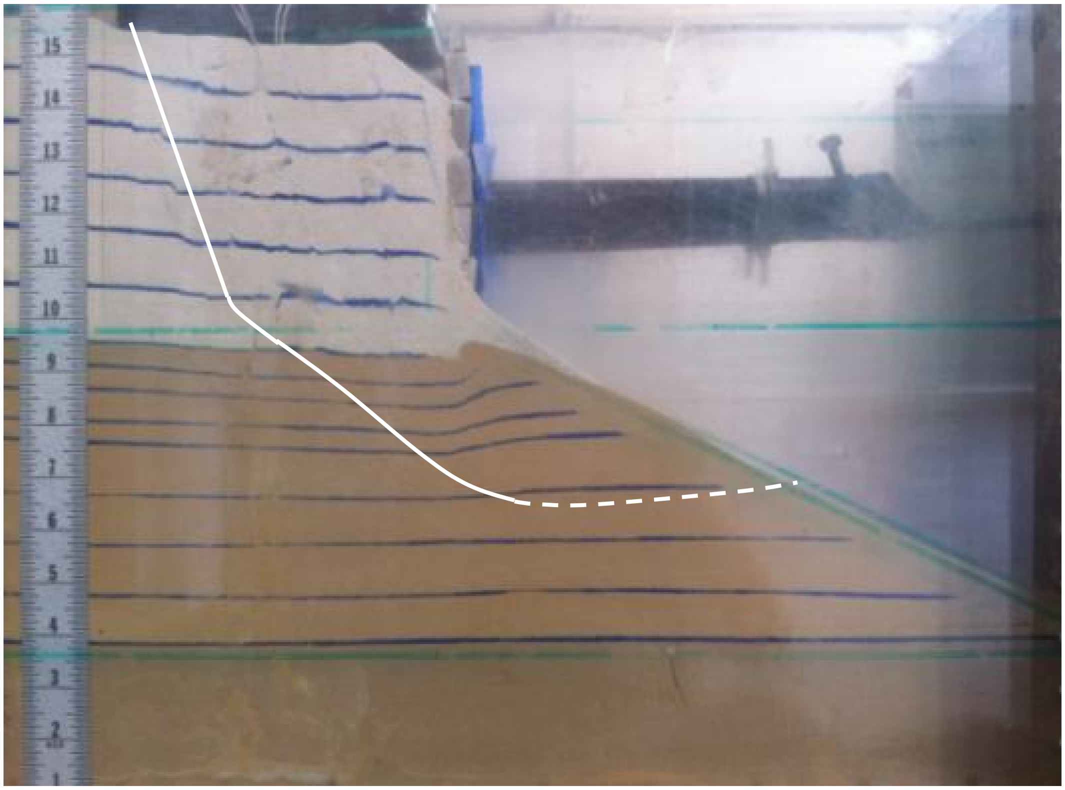

Figure 5-10 Post-test observed rupture surface (solid line) and estimated rupture surface (dashed line) in Test 7 model

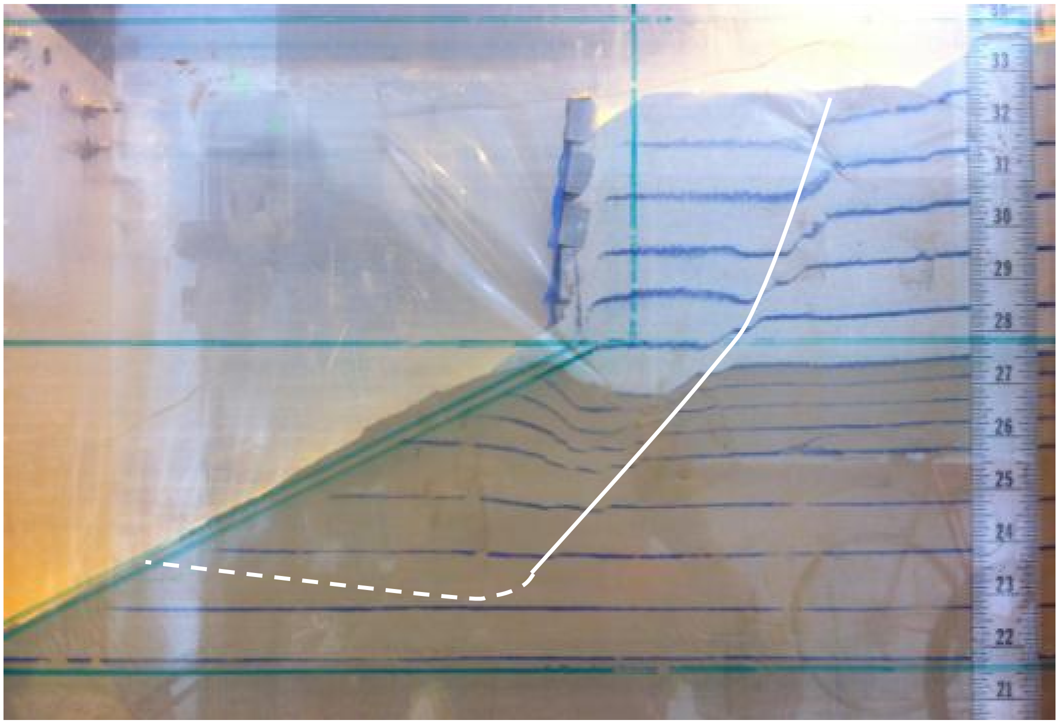

Figure 5-11 Post-test observed rupture surface (solid line) and estimated rupture surface (dashed line) in Test 10 model

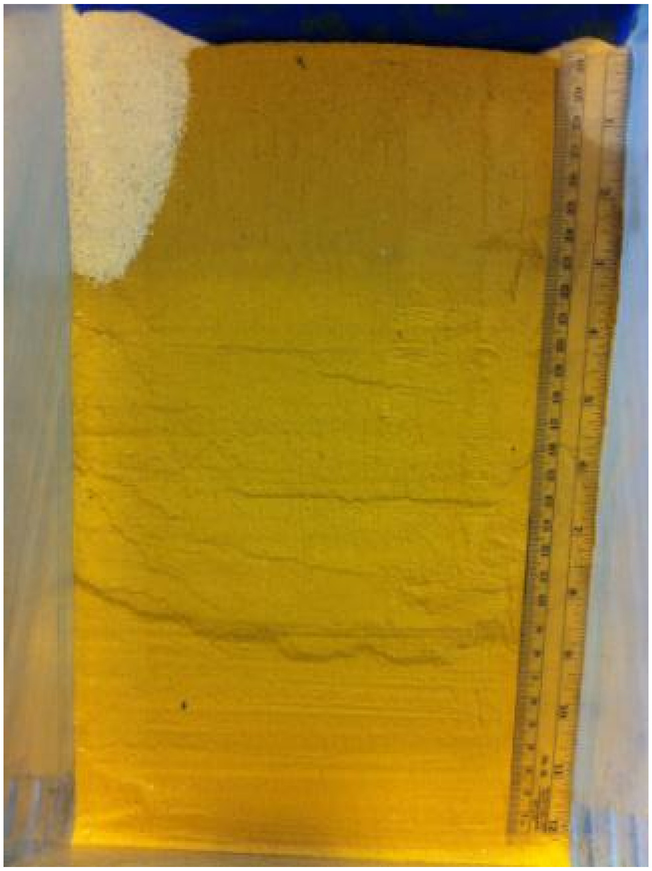
Figure 5-12 Post-test observed rupture on surface of embankment in Test 12 model

5.3.2 Force Equilibrium

The resultant measured forces ($V_{measured}$) were obtained by integrating the observed vertical stresses from Figure 5-5. Subsequently, the predicted vertical force, $V_{calculated}$ was obtained from the same force polygon as that presented in Chapter 4 and described by Equation 4-1 using soil properties (i.e. weights) from Table 5-1. The same equations of equilibrium for the MSE wall on level ground apply to the MSE wall near an embankment (i.e., the slope does not affect equilibrium of the wall). Figure 5-13 shows a scatter plot of $V_{calculated}$ versus $V_{measured}$ for tests in Table 5-2 where the embankment soil had μ_ϕ = 26° - 34°. It is evident that good correlation exists ($R^2 = 0.725$) suggesting confidence in the $V_{measured}$ and $V_{calculated}$ (the latter a function of the soil properties).

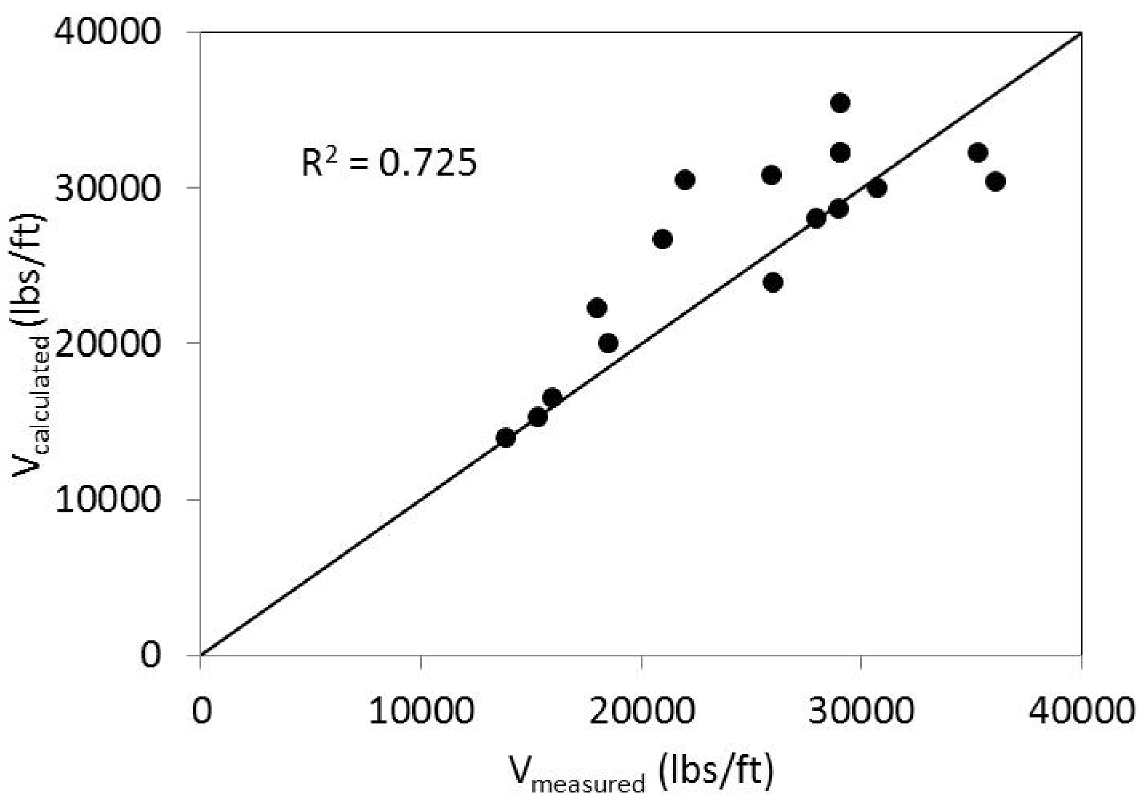

Figure 5-13 $V_{calculated}$ versus $V_{measured}$ for all MSE wall near embankment tests

5.4 Methods of Bearing Capacity Estimation

The bearing capacity of MSE walls resting on top of a sloped embankment and located a distance (d) from the crest (Figure 5-14) suggests a reduced soil weight in the counter passive soil resistance, which results in a reduction of bearing capacity. Further, as was shown in the case of an MSE wall on level ground, the resultant load (T in Figure 4-5) is inclined, i.e. including vertical and horizontal components of the load which influence the depth of the rupture surface and the magnitude of bearing capacity.

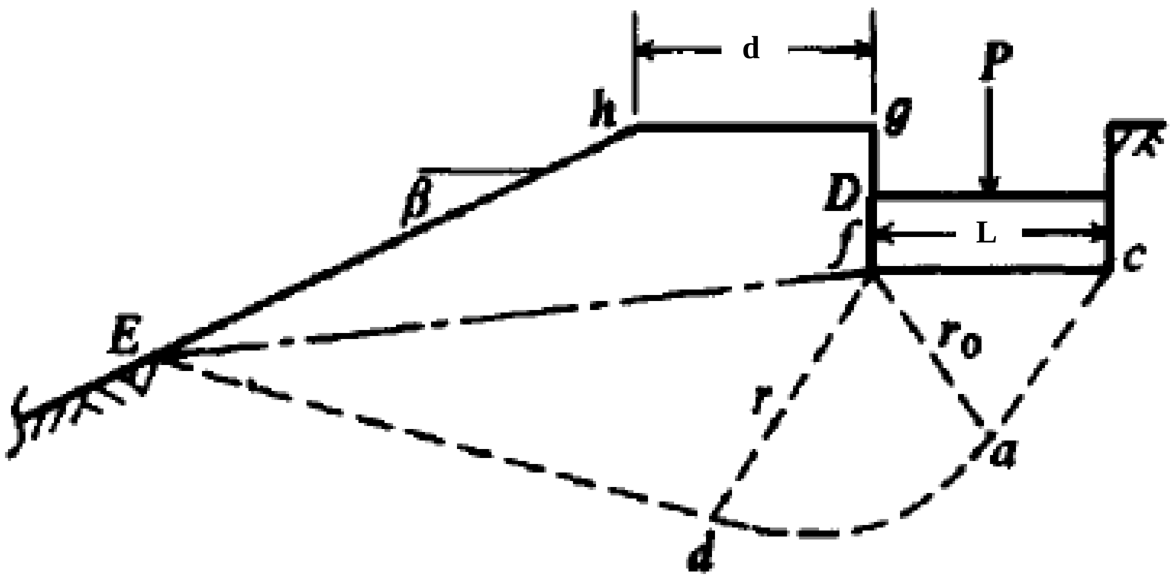

Figure 5-14 Shallow footing with concentric load and near an embankment (Bowles, 1997)

Existing methods to account for MSE walls on slopes include the work of Hansen, Vesic and Bowles. Each attempts to account for the reduced rupture surface (cadE in Figure 5-16) when computing the bearing capacity. Generally, the methods include ground inclination factors (Hansen and Vesic) and a modified N_{γ}' (Bowles) discussed below. Note, the methods for load inclination factor that were discussed in the previous sections were used to account for the inclined resultant load's influence on the rupture surface. MSE wall and embankment properties that were used in predicting the capacities of 20-ft-tall walls with L/H = 0.5 on an embankment with $\beta = 26°$ are given in Table 5-1.

Bowles (1997) suggested calculating a modified N'_γ using Equation 5-2 and estimating the q_u for footing near an embankment using Equation 5-1.

The R term in Eq. 5-2 is obtained from Figure 5-15, Bowles (1997), is obtained from Coulomb passive earth pressure wedge acting on positive and negative backfill slope or $K_p(-\beta)/K_p(+\beta)$ where β is the angle of the slope measured from the horizontal. Equation 5-3 is Coulomb's expression for the coefficient of passive earth pressure based on the parameters shown in Figure 5-15. The MSE wall can be taken as the gravity wall meaning that δ in Figure 5-15 (angle that the resultant passive force acts) is the ϕ of the backfill and α = 90°. Equation 5-3 has been modified for use in MSE walls analyzed in this study.

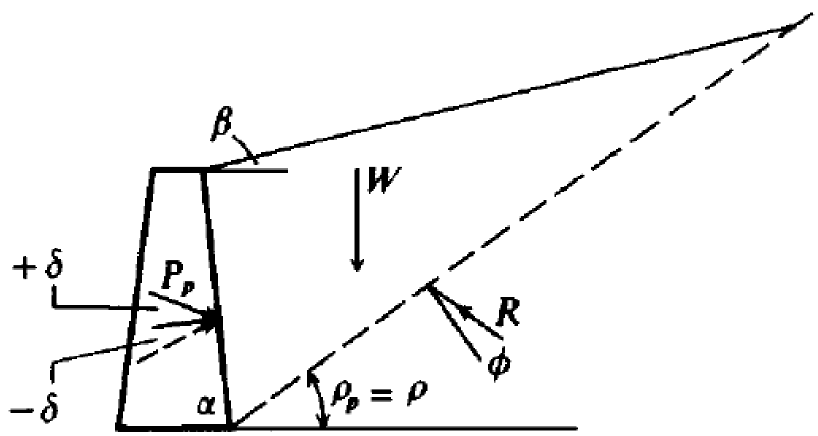

Figure 5-15 Failure wedge and forces acting on gravity retaining wall for passive earth pressure (Bowles, 1997)

$$K_p = \frac{\sin^2(\alpha - \phi)}{\sin^2(\alpha)\sin(\alpha + \phi)\left[1 - \sqrt{\frac{\sin(\phi + \phi)\sin(\phi + \beta)}{\sin(\alpha + \phi)\sin(\alpha + \beta)}}\right]^2} \qquad \text{Eq. 5-3}$$

Hansen and Vesic recommended ground inclination factors (g_γ) that account for a slope's effect on the N_γ term in Equation 5-4.

$$q_{u_{pred}} = \frac{1}{2}\gamma L' N_\gamma i_\gamma g_\gamma \qquad \text{Eq. 5-4}$$

Hansen (1970) suggested a ground inclination factor that is a function of the slope angle (β) and is expressed as

$$g_\gamma = (1 - 0.5\tan\beta)^5 \qquad \text{Eq. 5-5}$$

Vesic (1975) suggested a ground inclination factor that is similarly a function of β and is expressed as

$$g_\gamma = (1 - \tan\beta)^2 \qquad \text{Eq. 5-6}$$

Where β is the angle of the sloped embankment.

To illustrate the differences between the N'_γ for the methods discussed, Figure 5-16 shows their values for the embankment μ_ϕ from Table 5-1. Note, g_γ for Hansen and Vesic are only a function of the slope angle (β) of the embankment, while Bowles accounts for the influence of the ground inclination using β and μ_ϕ. The β for all of the tests were 26° with Hansen's $g_\gamma = 0.247$ and Vesic's $g_\gamma = 0.262$. It is evident that Bowles N'_γ always gives the largest factor (smallest reduction) and has less of an influence as the μ_ϕ increases from 26°-34°.

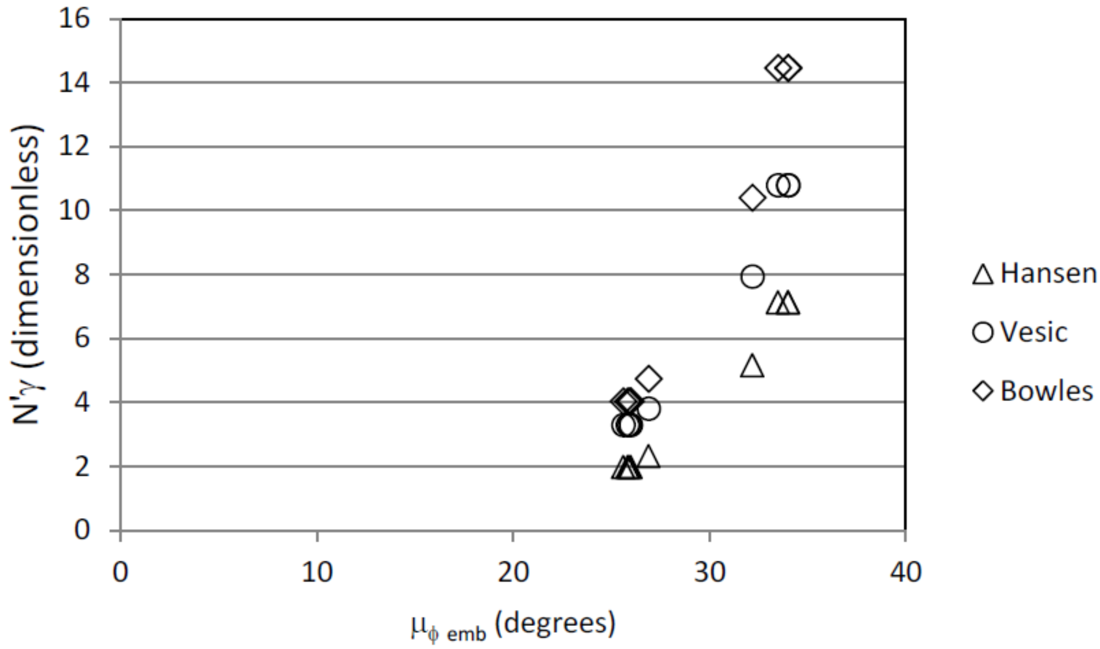

Figure 5-16 N'_{γ} values from Hansen's, Vesic's and Bowles' methods for the model tests

5.5 Comparison of Measured and Predicted Bearing Capacity

Table 5-2 shows the predicted (Eq. 5-4) and measured bearing capacities for all MSE walls near slopes that were tested. The predicted capacity based on Bowles method used Hansen's recommended $N\gamma$ in Equation 5-5 (as suggested by Bowles, 1997) and for Hansen's load inclination factor, i_{γ} (Eq. 4-14), $\eta = 2$ was selected.

Evident from Table 5-2, test results 6-19, $V_{u\ Bowles}$ gives the greatest estimate among the methods, however, the average bias =3.4 (measured/predicted). Hansen's method gives an average bias of 7.2 and Vesic's gives 4.3. Further review of the literature has only identified the discussed methods and a graphical method by Meyerhof, i.e. charts. Presently, Meyerhof's charts results in smaller predicted values for the case considered (setback = 0).

Table 5-2 Predicted and measured bearing capacities (kips/ft) for MSE wall near embankment model tests

Test	μ_γ (lbs/ft^2)	μ_ϕ (degree)	$V_{u\ Hansen}$ (kips/ft)	$V_{u\ Vesic}$ (kips/ft)	$V_{u\ Bowles}$ (kips/ft)	V_{meas} (kips/ft)
1	100	32	3.8	1.2	7.7	13.8
2	105	34	5.6	2.7	11.3	18.5
4	107	34	10.5	2.7	21.3	16.0
5	107	34	9.2	2.3	18.7	15.3
6	86	26	3.7	2.3	7.5	25.9
7	90	27	4.5	2.8	9.2	27.9
9	86	26	3.5	2.0	7.2	30.7
10	85	26	3.6	2.3	7.4	29.0
11	90	27	3.5	5.8	9.0	29.0
12	82	26	3.5	2.2	7.2	28.5
13	85	26	3.6	2.3	7.4	28.2
14	83	26	3.4	5.7	7.0	32.9
15	83	26	3.4	5.7	7.0	24.5
16	84	26	3.3	5.5	6.8	18.0
17	82	26	3.4	5.7	6.9	28.0
18	82	26	2.9	5.0	5.6	25.0
19	85	26	4.1	6.8	8.3	32.0

Given the observed biases (3.4 Bowles, 7.2 Hansen, and 4.3 Vesic), it was proposed that the failure was not bearing but a slope stability issue. This was verified through the observed rupture surfaces (e.g. Figure 5-12 and 5-13) which do not exhibit the classical passive failure plane (i.e. 45-ϕ/2), (e.g. Figure 5-1) which is the basis of the resistance.

Based on the observed rupture surfaces, as well the measured failure resistance loads (V_{meas}), it was decided to perform a finite element analysis, i.e. Plaxis, of both the MSE wall, backfill and underlying foundation soil with slope. Figure 5-17 shows the Plaxis model with soil properties and embankment and wall geometries similar to Tests 6-19. The rupture surfaces from the flat ground tests (Ch. 4) as well as predicted (Plaxis

– deeper) for the same soil properties and slope are shown in the model. Points along the flat ground rupture vs. slope (deeper rupture) were selected to show the Mohr's circles and identify if failure was occurring on the shallower (i.e. flat ground) rupture surface. Figure 5-18 shows the Mohr's circles for points a and b and Figure 5-19 shows the Mohr circle stress state for points c and d, which occur for the deeper observed (centrifuge) rupture surface. Evident from Figure 18, the Mohr's circles for points a and b do not touch the Mohr-Coulomb strength envelope, suggesting that traditional bearing resistance, i.e. development of passive wedge does not occur in MSE walls on slopes. However, the Mohr circles for points c and d (deeper rupture observed in embankment tests) do reach the failure envelope, suggesting a slope limit state. However, since the latter limit state is not of a passive nature, the stability analysis requires a traditional slope stability analysis, i.e. breaking up the mass into slices and solving the resistance along the

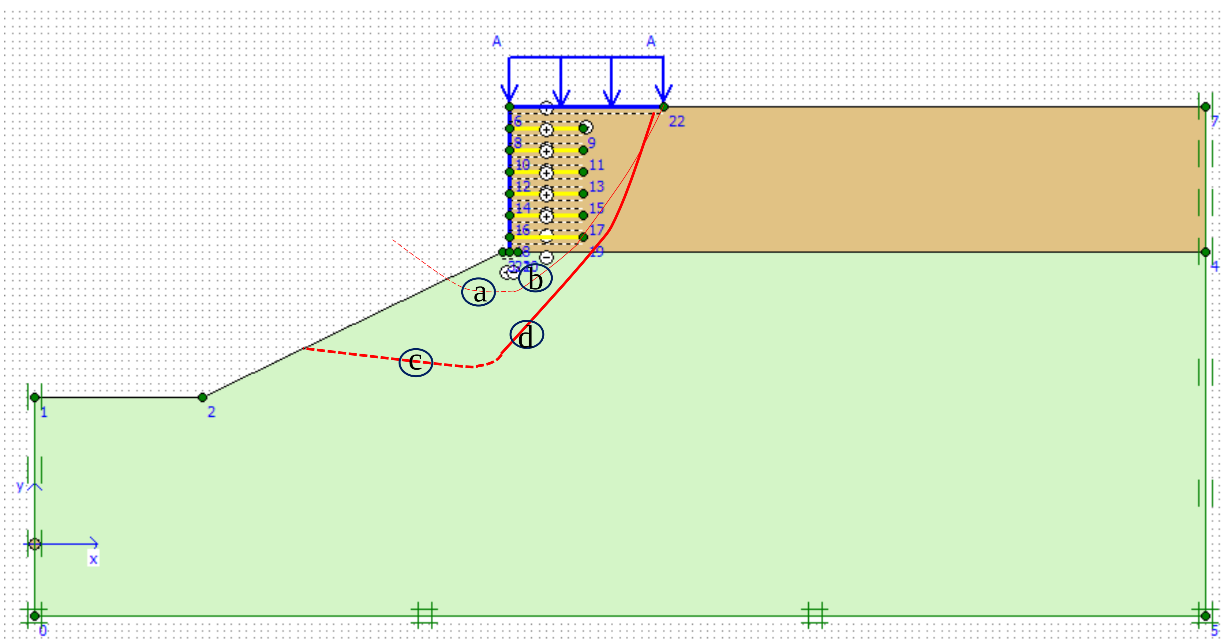

Figure 5-17 Rupture surfaces for bearing failure (points a and b) and slope failure (points c and d) superimposed to Plaxis model

bottom with subsequent driving vs. resistance moments (i.e. slope stability methods - modified Bishop, simplified Janbu, etc.) to assess failure.

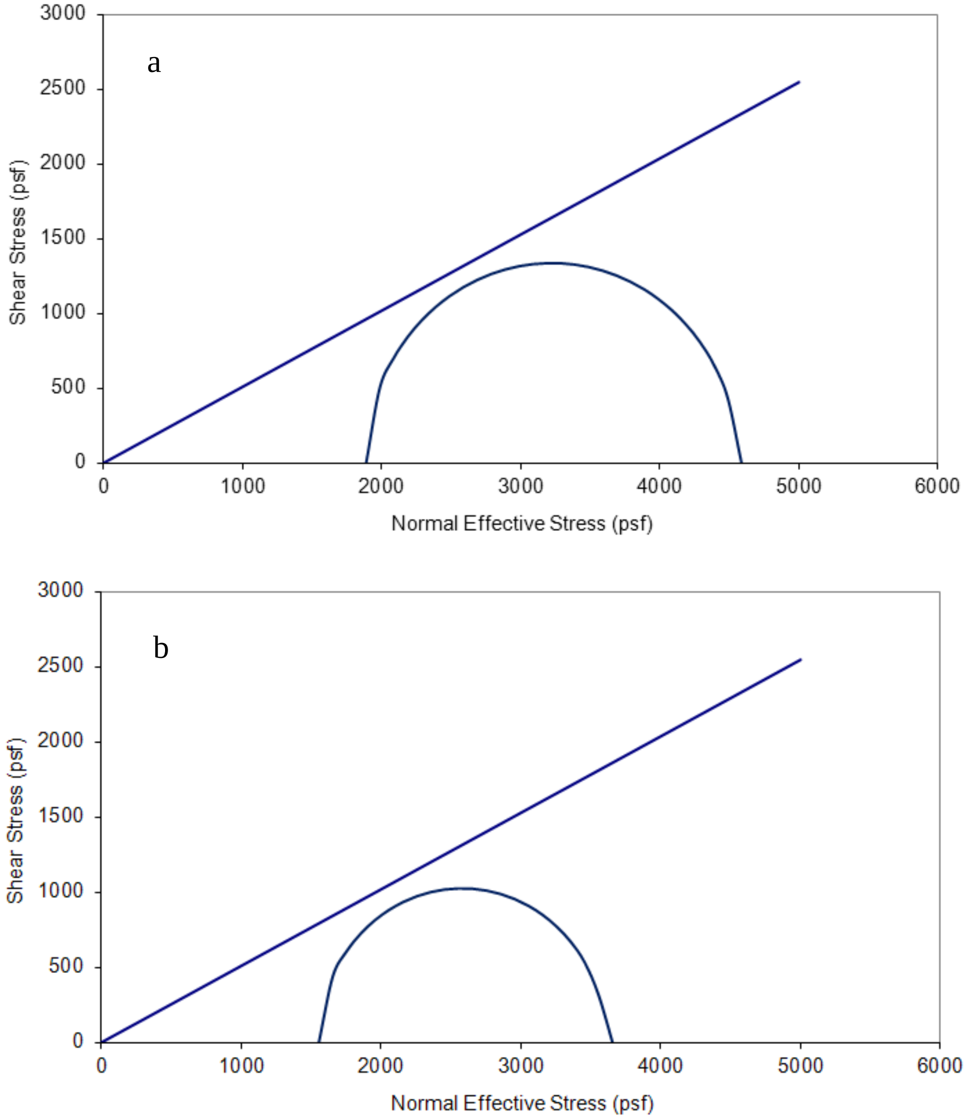

Figure 5-18 Mohr circles for points a and b on the bearing rupture surface

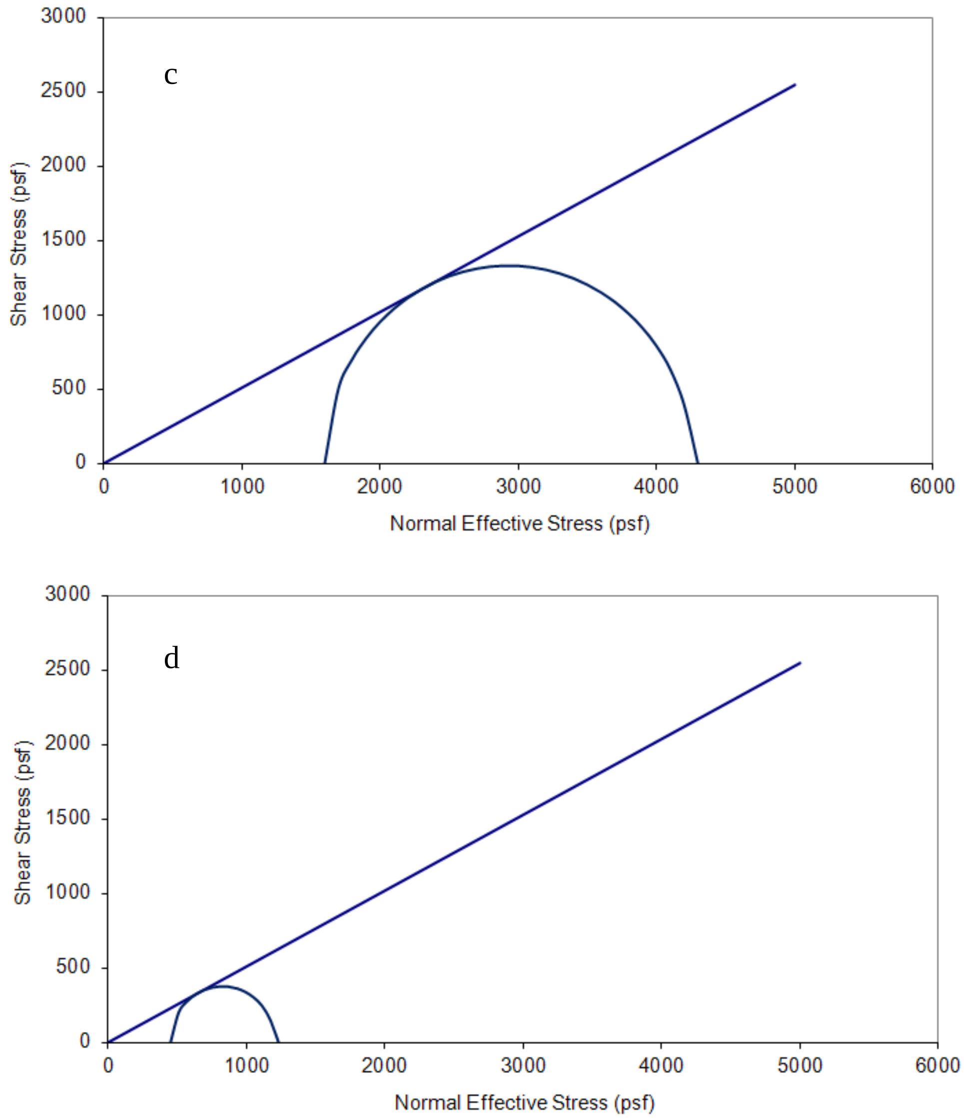

Figure 5-19 Mohr circles for points c and d on the slope rupture surface

5.6 Observations and Findings of MSE Wall on Embankment Bearing Analysis

The primary goal of the study presented in this chapter was to assess the stability method which most accurately predicts the limit state of MSE walls on embankments.

Initially, a bearing analysis using three methods (Hansen, Vesic and Bowles) were compared to measured results. Evident in Table 5-2, the Bowles method predicts the greatest capacity of the methods considered. Vesic's predicted capacity is the lowest values for all tests. Hansen's predicted capacity is based on its own ground inclination factor (Eq. 5-5), load inclination factor (Eq. 4-15) with $\eta = 2$ results in values between Bowles and Vesic. However, the average bias (measured/predicted) varied from 3.4 (Bowles) to 4.3 (Vesic) and 7.2 (Hansen).

Further analysis of the MSE wall failure on slopes through both the experimental and Finite Element Analysis revealed that the failure limit state was not bearing (i.e. passive earth pressure: 45- $\phi/2$), but a general limit state observed in slope stability. The latter requires that the soil mass (MSE wall, slope, etc.) be divided into slices to solve for resistance on the bottom surface; with likelihood of a rupture to be computed from a comparison of the driving moments vs. the resisting moments.

CHAPTER 6
ANALYTICAL LRFD RESISTANCE FACTORS FOR EXTERNAL STABILITY

6.1 Introduction

The external stability of MSE walls is a function of the earth pressures applied to the stabilized earth and the pressures it applies to the underlying foundation. For example, the unit weight of the MSE wall backfill is placed in lifts and then compacted. The placement and compaction process introduces some variability in the unit weight, and the lifts (layers) introduce variability in stresses. Specifically, variability in unit weight and friction angle influences the horizontal stress distribution on the vertical plane at the back of the stabilized earth, which contributes to the total driving force. In general, the driving force is most significantly influenced by the soil strength, cohesion, c, and angle of internal friction, ϕ. Since retaining walls are designed and constructed with fines content less than 15% to control drainage of water and pore pressures, cohesionless soils are frequently utilized and thus ϕ is the only soil strength parameter considered in this analysis.

The variability of the vertical earth pressures is only due to the variability of unit weights, which are represented by their mean. The plane at the base of the wall is a “line of action” for sliding failure and is where the shear resistance is mobilized. The shear strength (resistance) is a function of the vertical earth pressure and the soil’s strength (c and ϕ). The smallest soil strength parameter will dictate the shear strength available on the plane.

For external stability analysis of a retaining wall, stability must be satisfied for sliding, bearing, overturning and overall. Each case is a function of the factored resistance (i.e., shear, bearing, etc.) and factored earth pressure loads. The resistance factor, as explained by Withiam et al. (1997), accounts for all of the following:

- Variability of the soil and rock properties
- Reliability of the equations used for predicting resistance
- Construction QC
- Extent of subsurface soil knowledge
- Consequences of failure

The goal of the work proposed in this chapter is to develop the framework to study these components influence on MSE LRFD Φ for external stability. Analytical expressions of CV for the loads and resistance (CV_{DL}, CV_{LS} and CV_R) are developed along with expressions for mean dead and live loads for use in the LRFD Φ equations (e.g. Eq. 4-21). Each expression is in terms of the soil's statistical descriptors and was validated using Monte Carlo analysis assuming lognormal distributions. A discussion of each follows.

6.2 Analytical Expressions for Coefficient of Variation of Sliding Stability

The form of the LRFD equation describing the required stability against sliding is

$$\varphi(\alpha_{EV} P_{EV} \tan\phi) = \eta(\alpha_{EH} P_{EH} + \alpha_{LS} P_{LS}) \qquad \text{Eq. 6-1}$$

where subscripts *EV*, *EH* and *LS* represent the vertical and horizontal earth pressure and the load surcharge. Note the vertical earth pressure (P_{EV}) acts on the resistance side of the inequality and is modified by it respective load factor, α_{EV}. The loads are defined as follows

$$P_{EV} = \gamma_{rs} H L \qquad \text{Eq. 6-2}$$

$$P_{EH} = \frac{1}{2} \gamma_{bf} H^2 K_a \qquad \text{Eq. 6-3}$$

$$P_{LS} = q_s H K_a \quad \text{Eq. 6-4}$$

The CV_R, the dead load, CV_D, and the live load, CV_L, describe the distribution of the soil pressures (horizontal driving force and vertical normal force) and static friction (Tanϕ) in the sliding stability case. Since the soil unit weight, γ, and angle of internal friction, ϕ, may be correlated, the analytical expression of CV for both distributions should include the effect of correlation.

6.2.1 Load

The following is the CV_{EH} and the derivation is presented in Appendix A.

$$CV_{EH}^2 = \frac{\rho_{\gamma K_a}^2 \cdot CV_\gamma^2 \cdot CV_{K_a}^2 + 2 \cdot \rho_{\gamma K_a} \cdot CV_\gamma \cdot CV_{K_a} + CV_\gamma^2 + CV_{K_a}^2 + CV_\gamma^2 \cdot CV_{K_a}^2}{CV_\gamma^2 \cdot CV_{K_a}^2 \cdot \rho_{\gamma K_a}^2 + 2 \cdot \rho_{\gamma K_a} \cdot CV_\gamma \cdot CV_{K_a} + 1} \quad \text{Eq. 6-5}$$

The CV_{LS} is a function of the product of two random variables, qs and Ka. There is no dependency assumed between these parameters (ρ = 0) and the resulting form of CV_{LS} is shown in Equation 6-6 and derived in Appendix A.

$$CV_{LS}^2 = \frac{E[q_s]^2 \cdot var[K_a] + E[K_a]^2 \cdot var[q_s] + var[K_a] \cdot var[q_s]}{E[K_a]^2 \cdot E[q_s]^2} \quad \text{Eq. 6-6}$$

6.2.2 Resistance

The following is the CV_R and its derivation is presented in Appendix A.

$$CV_R^2 = \frac{E[\tan\phi]^2 \cdot var[\gamma] + E[\gamma]^2 \cdot var[\tan\phi] + var[\gamma] \cdot var[\tan\phi]}{E[\gamma]^2 \cdot E[tan\phi]^2} \quad \text{Eq. 6-7}$$

6.3 Analytical Expressions for Coefficient of Variation of Bearing Stability

The form of the LRFD equation (Eq. 6-8) describing the required stability against bearing failure is

$$\Phi\left(\frac{1}{2}\gamma_{bf} L N_\gamma\right) = \eta(\alpha_{EH} P_{EV} + \alpha_{LS} P_{LS}) \quad \text{Eq. 6-8}$$

where subscripts *EV* and *LS* represent the vertical earth pressure and the load surcharge, respectively.

For expression of the bearing capacity Φ, dead and live loads and the CV of load and resistance need be expressed in terms of their components. The components in the case of an MSE wall are the soil properties and the external surcharge loads. The following sections on loads and resistance for sliding stability describe the CV_{EV}, CV_{LS} and CV_R as a function of the statistical descriptors soil properties.

6.3.1 Load

The stability of an MSE wall for reliability against bearing failure is dependent on loads developed on the horizontal plane at the base of the wall which is defined by the reinforcement length (L). The loads (pressures due to the reinforced soil and backfill) are influenced by the unit weight and friction angle, ϕ. When present, a surcharge due to live loads is considered to act over a distance of 2L and would cause an increase in the subsurface stresses throughout the reinforced soil zone and at the base of the wall.

Next, force equilibrium the soil wedge shown in Figure 6-1 (failed MSE wall and soil wedge in the test model) was considered to estimate e and V. Figure 6-1 shows all of the body forces and resultant forces, and orientations considered in the analysis. A Coulomb case is considered as the active failure plane which passes through the toe of the backfill and Q_s is the force per unit length of the wall. Figure 6-2 shows the force polygon for Figure 6-1 from which the vertical resultant force, V, can be determined with known soil and wall weights.

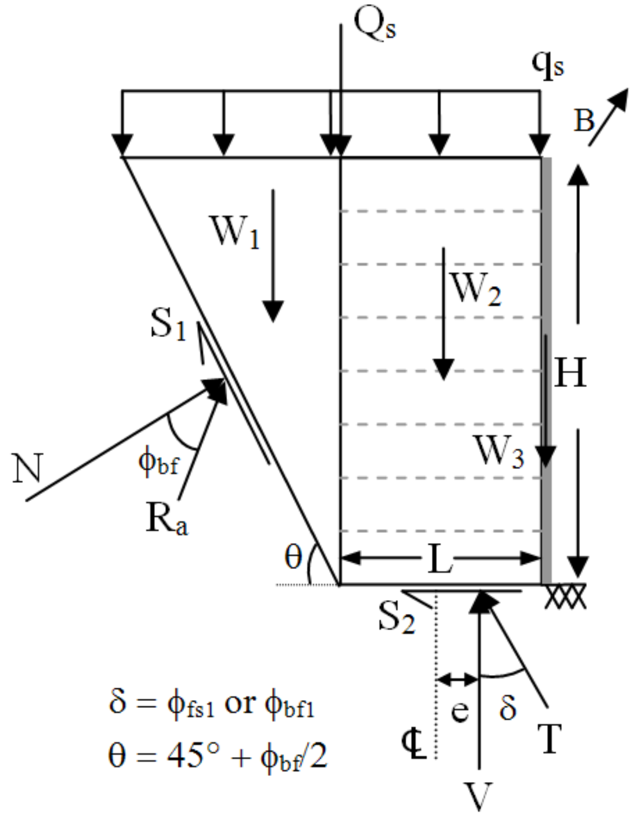

Figure 6-1 Force diagram for MSE wall and soil wedge

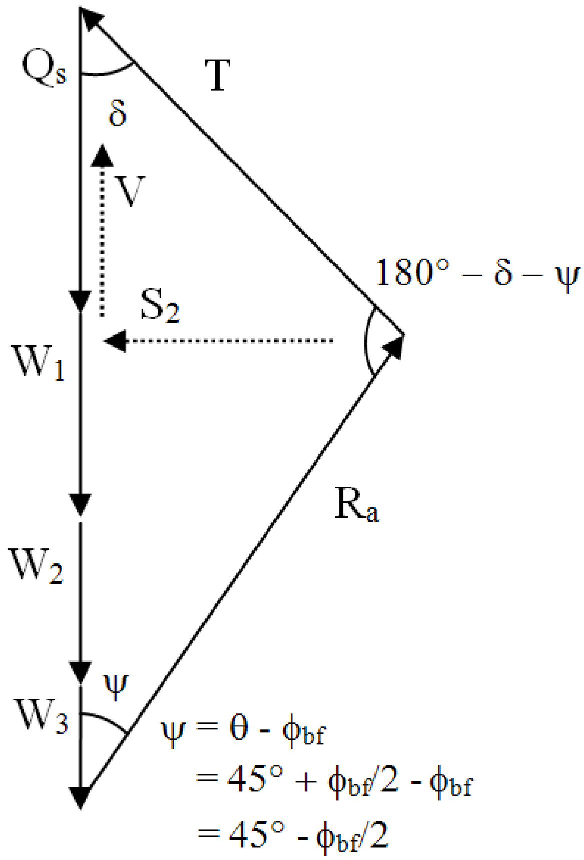

Figure 6-2 Force polygon for MSE wall and soil wedge

The vertical resultant force (V) per unit length of the wall can be calculated based on equilibrium of forces (Equations 6-8 and 6-9) acting on the body of soil (MSE and soil wedge) shown in Figure 6-1. Equation 6-11 is the total resultant force (T) acting on the interface or plane between the MSE wall and the bearing soils and acts at δ from the horizontal.

$$\sum F_y = Q_s + W_1 + W_2 + W_3 - T\cos(\delta) - R_a\cos(\psi) = 0 \qquad \text{Eq. 6-9}$$

$$\sum F_x = R_a\sin(\psi) - T\sin(\delta) = 0 \qquad \text{Eq. 6-10}$$

$$R_a = T\frac{\sin(\delta)}{\sin(\psi)}$$

$$Q_s + W_1 + W_2 + W_3 = T\cos(\delta) + T\frac{\sin(\delta)}{\sin(\psi)}\cos(\psi)$$

$$T = \frac{Q_S + W_1 + W_2 + W_3}{\cos(\delta) + \frac{\sin(\delta)}{\sin(\psi)}\cos(\psi)}$$ Eq. 6-11

Equation 6-12 is V as a function of the total resultant, T, and δ (angle of load inclination). Accounting for the other terms in the polygon results in Equation 6-13.

$$V = T\cos(\delta)$$ Eq. 6-12

$$V = \frac{Q_S + W_1 + W_2 + W_3}{\cos(\delta) + \frac{\sin(\delta)}{\tan(\psi)}}[\cos(\delta)]$$ Eq. 6-13

With Equation 6-13, the applied load acting on the foundation soil can be calculated for any level of surcharge. Note, the expression includes both the dead load (EV) and the surcharge load (LS). Furthermore, the weights due to surcharge, soil and wall are multiplied by

$$M = \frac{\cos(\delta)}{\cos(\delta) + \frac{\sin(\delta)}{\tan(\psi)}}$$ Eq. 6-14

where the δ is a constant and $\psi = \theta - \phi_{bf}$, which varies due to the variable backfill. Thus, Equation 6-14 needs to be expanded in the determination of CV for the dead and live load. Equations 6-15 and 6-16 give the mean and CV of M.

$$E[M]^2 = \frac{\cos(\delta)^2}{\cos(\delta)^2 + \frac{\sin(\delta)^2}{\tan\left(45° - \frac{\mu_{\phi_{bf}}}{2}\right)^2}}$$ Eq. 6-15

$$var[M] = \left[\frac{\cos(\delta)\sin(\delta)\csc\left(45° - \frac{\mu_{\phi_{bf}}}{2}\right)\left(\frac{1}{2}\right)}{\left(\cos(\delta) + \sin(\delta)\cot\left(45° - \frac{\mu_{\phi_{bf}}}{2}\right)\right)^2}\right]^2 var_{\phi_{bf}}$$ Eq. 6-16

The CV of the dead load (EV) is derived in the same manner as previous CV's; however, the expression is based on Figure 6-1.

$$CV_{DL}^2 = \frac{\sigma_{DL}^2}{E[DL]^2} = \frac{var_{DL}}{E[DL]^2} = \frac{var_{EV}}{E[EV]^2}$$ Eq. 6-17

First, the CV will be expanded for the weights and the M term (Equations 6-15 and 6-16) will be included.

$$P_{EV} = \left(\alpha \frac{1}{2}\gamma_{bf}HL + \alpha\gamma_{bf}HL + \alpha\gamma_c HB\right)M$$

Note, the unit weight of the backfill, γ_{bf}, will be expressed as γ

$$E[EV]^2 = \left(\alpha^2 \left(\frac{1}{2}\right)^2 H^2L^2E[\gamma]^2 + \alpha^2H^2L^2E[\gamma]^2 + \alpha^2H^2B^2E[\gamma_c]^2\right)E[M]^2$$

$$var[EV] = \alpha^2 \left(\frac{1}{2}\right)^2 H^2L^2var[\gamma M] + \alpha^2H^2L^2var[\gamma M] + \alpha^2H^2B^2var[\gamma_c M]$$

$$var[\gamma M] = E[\gamma]^2 \cdot var[M] + E[M]^2 \cdot var[\gamma] + var[M] \cdot var[\gamma]$$

$$var[\gamma_c M] = E[\gamma_c]^2 \cdot var[M] + E[M]^2 \cdot var[\gamma_c] + var[M] \cdot var[\gamma_c]$$

$$CV_\gamma^2 = \frac{\alpha^2\left(\frac{1}{2}\right)^2 H^2L^2\left[E[\gamma]^2 \cdot var[M] + E[M]^2 \cdot var[\gamma] + var[M] \cdot var[\gamma]\right]}{\alpha^2\left(\frac{1}{2}\right)^2 H^2L^2E[\gamma]^2 \cdot E[M]^2} \quad \text{Eq. 6-18}$$

$$CV_\gamma^2 = \frac{E[\gamma]^2 \cdot var[M] + E[M]^2 \cdot var[\gamma] + var[M] \cdot var[\gamma]}{E[\gamma]^2 \cdot E[M]^2} \quad \text{Eq. 6-19}$$

$$CV_\gamma^2 = CV_\gamma^2 + CV_M^2 + CV_\gamma^2 \cdot CV_M^2$$

$$CV_{\gamma_c}^2 = CV_{\gamma_c}^2 + CV_M^2 + CV_{\gamma_c}^2 \cdot CV_M^2$$

Combining all CV terms of the components gives the expression for CV of the dead load (EV) (Equation 6-20).

$$CV_{EV}^2 = 2{CV_\gamma}^2 + {CV_{\gamma_c}}^2 + 3{\mathrm{CV}_M}^2 + {\mathrm{CV}_M}^2 \cdot \left(2{CV_\gamma}^2 + {CV_{\gamma_c}}^2\right) \quad \text{Eq. 6-20}$$

The load surcharge (live load) is expressed as

$$P_{LS} = \alpha q_s H$$

The CV_{LS} is a function of the product of two random variables, q_s and M. There is no dependency assumed between these parameters ($\rho = 0$) and the resulting form of CV_{LS} is shown in Equation 6-21 and derived in Appendix A.

$$CV_{LS}^2 = \frac{E[q_s]^2 \cdot var[M] + E[M]^2 \cdot var[q_s] + var[M] \cdot var[q_s]}{E[M]^2 \cdot E[q_s]^2} \qquad \text{Eq. 6-21}$$

6.3.2 Resistance

The equations governing the bearing capacity of spread footings are applied to MSE walls for the case of zero embedment and resting on cohesionless soil. Equation 7-22 is the predicted force/unit length capacity for bearing.

$$R_{Bearing} = \frac{1}{2}\gamma L'^2 N_\gamma i_\gamma \qquad \text{Eq. 6-22}$$

where γ' is the foundation soil's unit weight, L' is the effective foundation width, N_γ is the factor due to self-weight (function of ϕ) and i_γ is the load inclination factor.

The CV_R can be developed as follows

$$CV_R^2 = \frac{\sigma_R^2}{E[R]^2} = \frac{var_R}{E[R]^2} \qquad \text{Eq. 6-23}$$

The squared mean of R is expressed as

$$E[R]^2 = E\left[\frac{1}{2}\gamma L'^2 N_\gamma i_\gamma\right]^2$$

$$E[R]^2 = \left(\frac{1}{2}\right)^2 E\left[\frac{1}{2}\gamma L'^2 N_\gamma i_\gamma\right]^2 \qquad \text{Eq. 6-24}$$

$$E[R]^2 = \left(\frac{1}{2}\right)^2 E\left[L'^2\right]^2 E\left[\gamma N_\gamma\right]^2 E\left[i_\gamma\right]^2 \qquad \text{Eq. 6-25}$$

The expected value of dependent (correlated) random variables (γ and N_γ) can be determined from the covariance, COV, of two random variables

$$COV\left[\gamma, N_\gamma\right] = E\left[\gamma N_\gamma\right] - E[\gamma] \cdot E\left[N_\gamma\right]$$

$E[\gamma N_\gamma] = COV[\gamma, N_\gamma] + E[\gamma] \cdot E[N_\gamma]$

Thus

$E[\gamma N_\gamma]^2 = COV[\gamma, N_\gamma]^2 + 2 \cdot COV[\gamma, N_\gamma] \cdot E[\gamma] \cdot E[N_\gamma] + E[\gamma]^2 \cdot E[N_\gamma]^2$

And Eq. 6-25 becomes

$$E[R]^2 = \left(\frac{1}{2}\right)^2 E[i_\gamma]^2 E[L'^2]^2 \left(COV[\gamma, N_\gamma]^2 + 2 \cdot COV[\gamma, N_\gamma] \cdot E[\gamma] \cdot E[N_\gamma] + E[\gamma]^2 \cdot E[N_\gamma]^2\right) \quad \text{Eq. 6-26}$$

The COV can be represented in terms of the correlation coefficient, ρ, which is

$$\rho_{\gamma N_\gamma} = \frac{COV[\gamma, N_\gamma]}{\sigma_\gamma \cdot \sigma_{N_\gamma}} \quad \text{Eq. 6-27}$$

Squaring the terms of Equation 6-27 and substituting into Equation 6-26 results in

$$E[R]^2 = \left(\frac{1}{2}\right)^2 E[i_\gamma]^2 E[L'^2]^2 \left(var[\gamma] \cdot var[N_\gamma] \cdot {\rho_{\gamma N_\gamma}}^2 + 2 \cdot \sqrt{(var[\gamma] \cdot var[N_\gamma])} \cdot \rho_{\gamma N_\gamma} \cdot E[\gamma] \cdot E[N_\gamma] + E[\gamma]^2 \cdot E[N_\gamma]^2\right) \quad \text{Eq. 6-28}$$

The variance of R is expressed as

$$var[R] = E[(R - E[R])^2]$$

$$var[R] = E\left[\left(\frac{1}{2}\gamma L'^2 N_\gamma i_\gamma - E\left[\frac{1}{2}\gamma L'^2 N_\gamma i_\gamma\right]\right)^2\right]$$

$$var[R] = \left(\frac{1}{2}\right)^2 E\left[\left(\gamma L'^2 N_\gamma i_\gamma - E[\gamma L'^2 N_\gamma i_\gamma]\right)^2\right]$$

$$var[R] = \left(\frac{1}{2}\right)^2 var[\gamma L'^2 N_\gamma i_\gamma] \quad \text{Eq. 6-29}$$

The variables, γ and N_γ may be correlated, so the variance of the product of two dependent variables is expressed as

$$var[\gamma N_\gamma] = COV[\gamma, N_\gamma]^2 + 2 \cdot COV[\gamma, N_\gamma] \cdot E[\gamma] \cdot E[N_\gamma] + E[N_\gamma]^2 \cdot var[\gamma] + E[\gamma]^2 \cdot var[N_\gamma] + var[\gamma] \cdot var[N_\gamma] \quad \text{Eq. 6-30}$$

Obtaining the variance in terms of the correlation coefficient (Equation 6-27) gives

$$var[\gamma N_\gamma] = {\rho_{\gamma N_\gamma}}^2 \cdot var[\gamma] \cdot var[N_\gamma] + \ldots$$
$$2 \cdot \rho_{\gamma N_\gamma}\sqrt{(var[\gamma] \cdot var[N_\gamma])} \cdot E[\gamma] \cdot E[N_\gamma] + \ldots$$
$$E[N_\gamma]^2 \cdot var[\gamma] + E[\gamma]^2 \cdot var[N_\gamma] + var[\gamma] \cdot var[N_\gamma] \qquad \text{Eq. 6-31}$$

If γN_γ is set equal to A, the variance of the product of $L'^2 \gamma N_\gamma i_\gamma$ can be expressed

$$var[L'^2 A i_\gamma] = \left(E[L'^2] \cdot E[A] \cdot E[i_\gamma]\right)^2 \left(CV^2_{L'^2} + CV^2_A + CV^2_{i_\gamma}\right) \qquad \text{Eq. 6-32}$$

where $var[A] = var[\gamma N_\gamma]$ and $E[A] = E[\gamma N_\gamma]$.

With Equations 6-31 and 6-32 the full expression for variance of resistance can be expressed (Equation 6-29).

The terms for L' and i_γ are not correlated to other terms in Equation 6-22, however are functions of soil properties. The effective foundation width, L', ($L - 2e$) can be derived from moments and the vertical resultant force, V. The eccentricity, e, is

$$e = \frac{M_R - M_o}{V} \qquad \text{Eq. 6-33}$$

where M_R is the resisting moment, M_o is the overturning moment and V is the vertical resultant force.

The CV's of the components of e are

$$CV^2_{M_R} = CV^2_{\gamma_{bf}} + CV^2_{q_s}$$

$$CV^2_{M_o} = \frac{\rho^2_{\gamma_{bf}K_a} \cdot CV^2_{\gamma_{bf}} \cdot CV^2_{K_a} + 2 \cdot \rho_{\gamma_{bf}K_a} \cdot CV_{\gamma_{bf}} \cdot CV_{K_a} + CV^2_{\gamma_{bf}} + CV^2_{K_a} + CV^2_{\gamma_{bf}} \cdot CV^2_{K_a}}{CV^2_{\gamma_{bf}} \cdot CV^2_{K_a} \cdot \rho^2_{\gamma_{bf}K_a} + 2 \cdot \rho_{\gamma_{bf}K_a} \cdot CV_{\gamma_{bf}} \cdot CV_{K_a} + 1 + CV^2_{q_s} + CV^2_{K_a} + CV^2_{q_s} \cdot CV^2_{K_a}}$$

Note, the CV of Ka is derived in the development of loads for sliding stability.

And the CV of the vertical resultant force, which its components are expressed under the following section on loads.

$$CV_V^2 = CV_{EV}^2 + CV_{LS}^2$$

With all other terms in Equation 6-33 being constant, the CV for L' is

$$CV_{L'}^2 = \frac{CV_{M_R}^2 - CV_{M_O}^2}{CV_V^2} \qquad \text{Eq. 6-34}$$

The mean and variance of Hansen's load inclination factor, i_γ, can be expressed as

$$E[i_\gamma] = (1 - 0.7\tan(\mu_\delta))^2$$

$$var[i_\gamma] = \sigma_\delta^2 \left[\frac{di_\gamma}{d\delta}\right]_{\mu_\delta} = \sigma_\delta^2[2 \cdot (1 - 0.7\tan(\mu_\delta)) \cdot \sec(\mu_\delta)^2]^2$$

And

$$CV_{i_\gamma}^2 = \frac{var[i_\gamma]}{E[i_\gamma]^2} \qquad \text{Eq. 6-35}$$

With the full expressions of Equations 6-29 and 6-25 the CV_R (Eq. 6-23) with correlated random variables can be expressed.

$$CV_R^2 = \frac{var[\gamma L'^2 N_\gamma i_\gamma]}{E[L'^2]^2 E[\gamma N_\gamma]^2 E[i_\gamma]^2} \qquad \text{Eq. 6-36}$$

If correlation doesn't exist (i.e., ρ = 0) between γ and N_γ, CV_R^2 becomes

$$CV_R^2 = CV_{L'^2}^2 + CV_\gamma^2 + CV_{N_\gamma}^2 + CV_{i_\gamma}^2 + CV_{L'^2}^2 \cdot CV_\gamma^2 \cdot CV_{N_\gamma}^2 \cdot CV_{i_\gamma}^2 \qquad \text{Eq. 6-37}$$

6.4 Comparison of Predicted vs. Measured LRFD Φ for MSE Bearing Capacity

A comparison between the results of predicting a Φ with the derived expressions and the observed Φ from the tests is warranted. The usefulness of the analytical expressions in a value at risk model hinges on their ability to explain the variability in load and resistance (CV_Q and CV_R) and predict a Φ for a desired level of reliability, β.

The measurements of soil variability (unit weight and friction angle) from the two sets of results analyzed in Chapter 4 (bearing stability on flat ground) are used here. These are grouped for $\mu_{\phi fs}$ = 26°-30° and $\mu_{\phi fs}$ = 31°-33°. The first set ($\mu_{\phi fs}$ = 26°-30°) had 17 values and the following descriptors of the soil: $\mu_{\phi bf}$ = 34° $\mu_{\gamma bf}$ = 98 pcf, $\mu_{\gamma fs}$ = 96 pcf, μ_{δ} = 28°, $CV_{\phi bf}$ = 0.10, $CV_{\gamma bf}$ = 0.035, $CV_{\gamma fs}$ = 0.05, CV_{δ} = 0.13 with the median of the set's $\mu_{\phi fs}$ as 28°. The other required terms for calculating are: mean dead load q_D = 32,314 lbs/ft, mean live load q_L = 11,440 lbs/ft, dead load factor γ_D = 1.80, mean dead load bias factor λ_D = 0.96, mean live load bias factor λ_L = 1.2, CV_{DL} = 0.42, and CV_{LS} = 0.42. The CV_R for the set (determined using Equation 6-37 – case of zero correlation between unit weight (γ) and N_γ) calculated to be 0.30 and the Φ calculates to be 0.70. This is compared to the results in Table 4-6 for the new method of i_γ and Vesic's N_γ where the CV_R = 0.43 and the Φ = 0.47 (P_f = 0.1%). Note, if correlation between the unit weight and the N_γ factor is assumed to be 0.8, the CV_R increases by about 10%, which decreases the Φ. The difference in CV may be due to the analytical expression's lack in accounting for other sources of variability, such as soil spatial variability (e.g., quantified correlated structure of unit weight and friction angle which can be represented with its own CV) or method error (McVay et. al., 2012). The bias in resistance (λ_R = measured/predicted) results in 1.10 compared to the bias in Table 4-6. There is good agreement between the mean (bias) however, suggesting that the analytical expression of CV lacks in accounting for all variability.

In conclusion, the analytical expressions were validated through Monte Carlo analyses assuming a lognormal distribution for each variable. For bearing stability, the expressions were compared to the CV_R and Φ observed from the centrifuge test results where $\mu_{\phi fs}$ = 26°-30° and for the new method of i_γ and Vesic's N_γ. The comparison shows the predicted CV_R to be less than the observed (0.30 vs. 0.43), suggesting the need for further investigation into analytically quantification of other sources of variability which contribute to the CV_R.

CHAPTER 7
SUMMARY, CONCLUSIONS, AND RECOMMENDATIONS

7.1 Background

The Florida Department of Transportation (FDOT) has adopted the Load and Resistance Factor Design (LRFD) design approach for retaining walls and is using AASHTO's recommended LRFD resistance factors, Φ, for external wall stability assessment. Current (2012) AASHTO LRFD Φ factors are 0.9 -1.0 for sliding stability and 0.65 for bearing stability, while there isn't a recommended value for overturning. These values were obtained by back fitting to Allowable Stress Design (ASD) Factors of Safety (FS). Unfortunately, AASHTO fails to account for any soil variability (e.g. Coefficient of Variation, CV of soil properties), and any method error.

Also, predictions of the bearing capacity of MSE walls on slopes have revealed that conventional methods don't agree which have resulted in conservative assumptions. Generally, the methods (Bowles, Meyerhof, Hansen, and Vesic) suggest a reduction in either the N_γ term (self-weight) or a slope factor to reduce the traditional bearing capacity equation. Note, in all cases, it is assumed the reduced soil mass results in reduced passive and radial zones, which reduces the length of the shear surface and limit (bearing) resistance.

7.2 Investigation of MSE Wall Sliding and Bearing Stability

A study of sliding and bearing stability to assess the load and resistance factors for MSE walls was performed using both numerical and centrifuge modeling. Variable soil conditions found in the field were characterized with lognormal representation in the both numerical work and by placement in the centrifuge models at representative CV's of the friction angle and unit weight. The numerical work identified the soil parameters of significant influence on the reliability of MSE walls. The centrifuge tests focused on varying these parameters and testing model walls to attain failure. Measurements with miniature soil stress sensors and LVDTs resulted in good assessments of MSE wall behavior under loading for sliding and bearing. The findings of the work on the sliding stability were that the resistance factors based on Coulomb loading are more conservative than that of Rankine and are less than the current recommended resistance factor (i.e., 0.6 versus 1.0). For the bearing stability, the resistance factors determined from the centrifuge tests were also less than the current recommended AASHTO values (0.65) and they varied for the foundation soil's friction angle. Specifically, the higher friction angle soils had smaller resistance factors. In addition, the centrifuge tests provided valuable measurements for estimating the load factors in case of reinforced soil, i.e. MSE walls.

7.2.1 Observations and Findings of MSE Wall Sliding Stability Analysis

- Load factors for horizontal earth pressure based on Rankine's and Coulomb's method of determining lateral resultant load were determined to be 1.52 and 1.63, respectively. Currently, AASHTO (2012) recommends a load factor of 1.5 for all predictions of lateral resultant load in MSE walls.
- Based on the results, LRFD Φ values were calculated to be 0.74 to 0.94 for the Rankine load case, and 0.63 to 0.68 for the Coulomb load case. The Coulomb method leads to more conservative Φ's and are suggested for the soil conditions and wall heights tested.

7.2.2 Observations and Findings of MSE Wall Bearing Stability Analysis

- Observations of the models post-test indicated bearing rupture surfaces that occurred at shallower depths occurred for the higher foundation soil's friction angle. This suggested a strong influence of inclined resultant load acting on the foundation soil's surface.
- Measured soil stresses during the spin up part of all the centrifuge tests resulted in 152 measurements of vertical dead load due to the reinforced soil and a load factor, γ_D = 1.87, was calculated. AASHTO (2012) recommends γ_D for vertical earth pressure = 1.35, while Bathurst et al. (2008) proposed $\gamma_D = 1.75$ calibrated from measurements on non-extensible reinforcements in full scale MSE wall tests. The γ_D calculated herein was used in the determination of the Φ for bearing capacity of MSE walls.
- Different methods to predict the influence of load inclination and the self-weight of the foundation soil through the terms i_γ and N_γ in the general bearing capacity equation were used to calculate the respective Φ. The relative efficiency of the methods for i_γ was shown based on Φ/λ_R. The results indicate that the combination of Vesic's N_γ and a new method for i_γ are the most appropriate for the bearing capacity of MSE walls. Furthermore, the Φ's at $\beta = 3.09$ for the foundation soil's μ_ϕ = 26°-30° and 31°-33° are 0.47 and 0.45, respectively. For $\beta = 2.32$, Φ's for the proposed method range from 0.65 to 0.68.
- For design of MSE walls bearing capacity with L/H = 0.5 and built on foundation soils with μ_ϕ = 26°-30° and 31°-33°, these new recommended Φ's will result in a conservative design over the use of the current $\Phi = 0.65$.

7.2.3 Observations and Findings of Bearing Stability Analysis of MSE Walls on Slope Embankments

- Observations of the models post-test indicated rupture surfaces that were deeper than the models of MSE wall on flat ground. The passive zone present in a general bearing capacity failure could not be defined by the shape of the observed rupture surfaces.
- The observations suggested the stability was an overall stability problem. Results from Plaxis analysis verified this by looking at the Mohr's circles on the rupture surfaces from bearing failure against deeper slope type failure. The Mohr's circles had reached the failure envelope along the deeper rupture surface while those along a superimposed bearing failure surface showed they had not reached failure.
- Observed Overall stability resistance of MSE walls on embankments is greater than bearing capacity on flat ground. For this case it is recommended that slope stability analysis be performed on MSE walls on embankments.

7.3 Recommendations

Following experimental tests and analysis of MSE wall sliding and bearing stability (on flat ground and embankments), the following recommendations are made for use in design and future research:

- For design of MSE walls sliding stability with L/H = 1 and built with backfill with μ_ϕ = 32° and CV_ϕ = 11.7%, recommended LRFD Φ values are 0.74 to 0.94 for the Rankine load case, and 0.63 to 0.68 for the Coulomb load case. The wall heights tested were 8-14 ft.
- For design of MSE walls, it is recommended to use load factors for vertical earth pressure that is equal to 1.80 and for horizontal earth pressure that is equal to 1.50.

- For design of MSE walls bearing capacity, it is recommended to account for the effect of inclined load through the application of the load inclination factor using the new method presented here:

$i_\gamma = \left(1 - \frac{S_2}{V}\right)^{1.08}$, $26° < \phi_{fs} < 30°$

$i_\gamma = \left(1 - \frac{S_2}{V}\right)^{1.55}$, $31° < \phi_{fs} < 33°$

- For design of MSE walls, it is recommended to use a load factor for vertical earth pressure that is equal to 1.80.
- For design of MSE walls bearing capacity it is recommended to use Vesic's method to estimate N_γ.
- For design of MSE walls bearing capacity with L/H = 0.5 and built on foundation soils with μ_ϕ = 26°-30° and 31°-33°, recommended LRFD Φ values are 0.47 and 0.45, respectively.
- For design of MSE walls on embankments, it is recommended to perform slope stability analysis over bearing capacity analysis.
- The MSE wall and soil wedge model is recommended to estimate the applied load in a stability analysis.

It is suggested that centrifuge results for MSE walls on embankments (14 tests with same soil conditions) be used in further research to evaluate the bias and CV's associated with different slope stability methods. From this, a LRFD Φ value for overall stability could be developed.

REFERENCES

AASHTO (2012). *AASHTO LRFD Bridge Design Specifications (US Customary Units)*, Fourth Edition, AASHTO, Washington, D.C.

Allen, T.M., Nowak, A. and Bathurst, R. (2005). *Calibration to determine load and resistance factors for geotechnical and structural design*, TRB Circular E-C079, Transportation Research Board, Washington, D.C.

ASTM (2007). “Standard test methods for laboratory compaction characteristics of soil using standard effort (12,400 ft-lbf/ft^3 (600 N-m/m^3)).” *D698-00a*, West Conshohocken, PA.

ASTM (2006). “Standard practice for classification of soils for engineering purposes (unified soil classification system).” *D2487-06*, West Conshohocken, PA.

ASTM (2006). “Standard test methods for maximum index density and unit weight of soils using a vibratory table.” *D4253-00*, West Conshohocken, PA.

ASTM (2006). “Standard test methods for minimum index density and unit weight of soils and calculation of relative density.” *D4254-00*, West Conshohocken, PA.

Askegaard, V. (1963). “Measurement of pressure in solids by means of pressure cells”, *Bulletin No. 17*, Structural Research Laboratory, Technical University of Denmark, Copenhagen.

Babu, G.L.S. and Basha, B.M. (2008). “Optimum design of cantilver retaining walls using target reliability approach”, *International Journal of Geomechanics*, Vol. 8, No. 4, pp. 240-252.

Bathurst, R. J., Allen, T.M. and Nowak, A.J. (2008). “Calibration concepts for load and resistance factor design (LRFD) of reinforced soil walls”, *Canadian Geotechnical Journal*, No. 45, pp. 1377-1392.

Bolton, M.D. and Lau, C.K. (1993). “Vertical bearing capacity for circular and strip footings on Mohr-Coulomb soil”, *Canadian Geotechnical Journal*, Vol. 30, No. 6, pp. 1024-1033.

Bowles, J. E. (1997). *Foundation Analysis and Design*. McGraw-Hill, Singapore.

Chalermyanont, T. and Benson, C.H. (2005). “Reliability-based design for external stability of mechanically stabilized earth walls.” *International Journal of Geomechanics*, ASCE, Vol. 5, No. 3, pp. 196-205.

Dave, T.N. and Dasaka, S.M. (2011). “A review on pressure measurement using earth pressure cell”, *International Journal of Earth Sciences and Engineering*, Vol. 4, No. 6, pp. 1031-1034.

Dunnicliff, J. (1988). *Geotechnical Instrumentation for Monitoring Field Performance*, John Wiley and Sons, New York.

Eurocode (2005) (DIN EN 1997-1). *Geotechnical Design, Part I: General Rules*, Deutsches Institut für Normung e.v., Berlin.

FDOT SDG (2013). *FDOT Structures Design Guidelines*, Florida Department of Transportation, Tallahassee, FL.

Feld, T., Bloomquist, D. and Townsend, F.C. (1991). “Investigation of geostatic stresses in a limited sized centrifuge model container”, *Proceedings of the International Conference Centrifuge 1991*, Boulder, Colorado, pp. 569-573.

FHWA (2001). *Load and Resistance Factor Design (LRFD) for Highway Bridge Substructures*, FHWA Publication No. HI-98-032, Federal Highway Administration, Washington, D.C.

Gill, J.J. (1988). “Development and testing of a device capable of placing model piles by driving and pushing in the centrifuge”, PhD Dissertation, University of Florida

Hansen, J.B. (1970). “A revised and extended formula for bearing capacity”, *Akademiet for de Tekniske Videnskaber*, Geoteknisk Institut. Bulletin No. 28, Copenhagen, 5-11.

Hatami, K. and Bathurst, R.J. (2006). “Numerical model for reinforced soil segmental walls under surcharge loading”, *Journal of Geotechnical and Geoenvironmental Engineering*, Vol. 132, No. 6, pp. 673-684.

Labuz, J.F. and Theroux, B. (1999). Calibration of earth pressure cells, *Mn/DOT Interim Report 6*, Department of Civil Engineering, University of Minnesota.

Labuz, J.F. and Theroux, B. (2005). “Laboratory calibration of earth pressure cells”, *Geotechnical Testing Journal*, Vol. 28, No. 2, pp. 1-9.

Liang, R.Y. and Almoh’d, I.M. (2004). “Monitoring results of an instrumented MSE wall.” *Transportation Research Record: Journal of the Transportation Research Board*, No. 1868, TRB, National Research Council, Washington, D.C.

Ling, H.I., Mohri, Y., Leshchinsky, D., Burke, C., Matsushima, K. and Liu, H. (2005). “Large-scale shaking table tests on modular-block reinforced soil retaining walls”, *Journal of Geotechnical and Geoenvironmental Engineering*, Vol. 131, No. 4, pp. 456-476.

Loh, Y.C. (1954). “Internal stress gauges for cementitious materials”, *Proceedings of the Society for Experimental Stress Analysis*, Vol. 21, No. 2, pp. 13-28.

McVay, M.C, Birgisson, B., Zhang, L., Perez, A. and Putcha, S. (2000). “Load and resistance factor design (LRFD) for driven piles using dynamic methods-a Florida perspective”, *ASTM Geotechnical Testing Journal*, Vol. 23, No. 1, pp. 55-66.

McVay, M., Klammler, H., Faraone, M., Dase, K. and Jenneisch, C. (2012). *Development of variable LRFD resistance factors for deep foundation design due to site variability* FDOT Report (BDK75-977-23), Florida Department of Transportation, Tallahassee, FL.

Meyerhof, G.G. (1963). “Some recent research on the bearing capacity of foundations”, *Canadian Geotechnical Journal*, Vol. 1, No. 1, 16-26.

Michalowski, R. (1997). “An estimate of the influence of soil weight on bearing capacity using limit analysis”, *Soils and Foundation*, Vol. 37, No. 4, 57-64.

Molnit, T. (1995). *Centrifuge modeling of laterally loaded large plumb pile groups in sand*, ME Thesis, University of Florida

Monfore, G.E. (1950). *An analysis of the stress distribution in and near stress gauges embedded in elastic soils* Structural Laboratory Report (SP 26), U.S. Bureau of Reclamation, Denver, CO.

Morrison, K.F., Harrison, F.E., Collin, J.G., Dodds, A. and Arndt, B. (2006). *Shored mechanically stabilized earth design guidelines* FHWA (CFL/TD-06-001), Lakewood, CO.

Muhs, H. and Weiss, K. (1969). “The influence of the load inclination on the bearing capacity of shallow footings”, *Proceedings, Seventh International Conference on*

Soil Mechanics and Foundation Engineering, Sociedad Mexicana de Mecanica de Suelos, A.C., Mexico City, Vol. 2, pp. 187-194.

Muhs, H. (1971). Die experimentelle Untersuchung der Grenztragfaehigkeit nichtbindiger Boeden bei lotrechter Belastung. Degebo-Mitteilungen, Heft 27.

Nowak, A.S. (1995). “Calibration of LRFD bridge code.” *Journal of Structural Engineering*, ASCE, Vol. 121, No. 8, pp. 1245-1251.

Paikowsky, S.G., Canniff, M. C., Lesny, K., Kisse, A., Amatya, S. and Muganga, R. (2010). “LRFD design and construction of shallow foundations for highway bridge structures”, *NCHRP Report 651*, Transportation Research Board, Washington, D.C.

Perloff, W.H. and Baron, W. (1976). *Soil Mechanics: Principles and Applications*, John Wiley and Sons, New York.

Prandtl, L. (1920). *Ueber die Haerte plastischer Koerper*. Nachrichten der Gesellschaft der Wissenschaften, Berichte der mathem.-physikal. Klasse, pp. 74-85.

Reissner, H. (1924). “Zum erddruckproblem”, *Proceedings of 1st International Congress of Applied Mechanics*, Delft, 295-311.

Salgado, R. (2008). *The Engineering of Foundations*, McGraw Hill.

Selig, E.T. (1964). “A review of stress and strain measurements in soil”, *Proceedings of the Symposium on Soil-Structure Interaction*, University of Arizona, pp. 153-158.

Sokolovski, V.V. (1960). *Statics of Soil Media*, Butterworth, London, pp. 1-237.

Styler, M. A. (2006). *Development and implementation of the Diggs format to perform LRFD resistance factor calibration of driven concrete piles in Florida* MS thesis, Department of Civil and Coastal Engineering, University of Florida.

Taylor, D. W. (1945). “Review of pressure distribution theories. Earth pressure cell investigations, and pressure distribution data”, *Contract Report W22-053 eng-185*, U.S. Army Engineer Waterways Experiment Station, Vicksburg, MS.

Taylor, R.N. (1995). *Geotechnical Centrifuge Technology*, Chapman and Hall, London.

Tory, A.C. and Sparrow, J.W. (1967). “The influence of diaphragm flexibility on the performance of an earth pressure cell”, *Journal of Scientific Instruments*, Vol. 44, No. 9, pp. 781-785.

Vesic, A. (1973). “Analysis of ultimate loads of shallow foundations”, *Journal of Soil Mechanics and Foundations Division*, Vol. 99, No. 1, 54-73.

Vesic, A. (1975). “Bearing capacity of shallow foundations”, In *Foundaiton Engineering Handbook*, H.F. Winterjorn and H.Y. Fang, eds., Van Nostrand Reinhold, New York, 121-147.

Withiam, J.L., Voytko, E.P., Barker, R.M., Duncan, J.M., Kelly, B.C., Musser, S.C. and Elias, V. (1997). *Load and Resistance Factor Design (LRFD) for Highway Bridge Structures*, FHWA Report DTFH61-94-C-00098, Federal Highway Administration, Washington, D.C.

Yoo, Nam-Jae (1988). “Centrifuge model experiments of reinforced earth retaining walls.” PhD Dissertation, University of Colorado.

APPENDIX
ANALYTICAL EXPRESSIONS

COEFFICIENT OF VARIATION OF LOAD

The following is the derivation of CV_Q as shown by Styler (2005).

$$CV_Q^2 = \frac{\sigma_Q^2}{E[Q]^2} = \frac{var_Q}{E[Q]^2} \quad \text{(A-1)}$$

$$E[Q] = E[q_D \cdot \lambda_D] + E[q_L \cdot \lambda_L] \quad \text{(A-2)}$$

$$E[Q] = q_D \cdot E[\lambda_D] + q_L \cdot E[\lambda_L] \quad \text{(A-3)}$$

$$E[Q]^2 = q_D^2 \cdot E[\lambda_D]^2 + 2 \cdot q_D \cdot q_L \cdot E[\lambda_D] \cdot E[\lambda_L] + q_L^2 \cdot E[\lambda_L]^2 \quad \text{(A-4)}$$

$$E[Q]^2 = q_L^2 \left(\frac{q_D^2}{q_L^2} \cdot E[\lambda_D]^2 + 2 \cdot \frac{q_D}{q_L} \cdot E[\lambda_D] \cdot E[\lambda_L] + E[\lambda_L]^2\right) \quad \text{(A-5)}$$

$$var[Q] = E[(Q - E[Q])^2] \quad \text{(A-6)}$$

$$var[Q] = E[(q_D \cdot \lambda_D + q_L \cdot \lambda_L - q_D \cdot E[\lambda_D] - q_L \cdot E[\lambda_L])^2] \quad \text{(A-7)}$$

$$var[Q] = E\left[\left(q_D(\lambda_D - E[\lambda_D]) + q_L(\lambda_L - E[\lambda_L])\right)^2\right] \quad \text{(A-8)}$$

$$var[Q] = E[q_D^2(\lambda_D - E[\lambda_D])^2 + q_L^2(\lambda_L - E[\lambda_L])^2 \ldots. + 2 \cdot q_D(\lambda_D - E[\lambda_D]) \cdot$$
$$q_L(\lambda_L - E[\lambda_L])] \quad \text{(A-9)}$$

$$var[Q] = q_D^2 E[(\lambda_D - E[\lambda_D])^2] + q_L^2 E[(\lambda_L - E[\lambda_L])^2] + 2 \cdot q_D \cdot q_L E[(\lambda_D - E[\lambda_D]) \cdot$$
$$(\lambda_L - E[\lambda_L])] \quad \text{(A-10)}$$

$$var[Q] = q_D^2 \cdot var[\lambda_D] + q_L^2 \cdot var[\lambda_L] + 2 \cdot q_D \cdot q_L \cdot COV[\lambda_D, \lambda_L] \quad \text{(A-11)}$$

Substituting Equations A-5 and A-11 into Equation A-1, the CV of the load, Q, is obtained

$$CV_Q^2 = \frac{q_D^2 \cdot var[\lambda_D] + q_L^2 \cdot var[\lambda_L]}{q_L^2\left(\frac{q_D^2}{q_L^2} \cdot E[\lambda_D]^2 + 2 \cdot \frac{q_D}{q_L} \cdot E[\lambda_D] \cdot E[\lambda_L] + E[\lambda_L]^2\right)} \quad \text{(A-12)}$$

Through substitution, Equation A-12 can be expressed as

$$CV_Q^2 = \frac{q_D^2 \cdot E[\lambda_D]^2 \cdot CV_D^2 + q_L^2 \cdot E[\lambda_L]^2 \cdot CV_L^2}{q_L^2\left(\frac{q_D^2}{q_L^2} \cdot E[\lambda_D]^2 + 2 \cdot \frac{q_D}{q_L} \cdot E[\lambda_D] \cdot E[\lambda_L] + E[\lambda_L]^2\right)} \quad \text{(A-13)}$$

The last term in Equation A-11 is the covariance between the dead and live loads. In the derivation presented here, the bias of the loads are independent, thus the covariance becomes zero.

DEAD LOAD FOR SLIDING STABILITY

The following is the derivation of the CV of the dead load (horizontal earth pressure), where the active state is considered.

$$P_{EH} = \alpha \frac{1}{2} \gamma_{bf} H^2 K_a$$

$$E[P_{EH}]^2 = E\left[\alpha \frac{1}{2} \gamma H^2 K_a\right]^2$$

$$E[P_{EH}]^2 = \alpha^2 \left(\frac{1}{2}\right)^2 (H^2)^2 E[\gamma K_a]^2 \quad \text{(A-14)}$$

The expected value of dependent (correlated) random variables can be determined from the covariance, COV, of two random variables

$$COV[\gamma, K_a] = E[\gamma K_a] - E[\gamma] \cdot E[K_a]$$

$$E[\gamma K_a] = COV[\gamma, K_a] + E[\gamma] \cdot E[K_a]$$

Thus Equation A-14 becomes

$$E[P_{EH}]^2 = \alpha^2 \left(\frac{1}{2}\right)^2 (H^2)^2 (COV[\gamma, K_a]^2 + 2 \cdot COV[\gamma, K_a] \cdot E[\gamma] \cdot E[K_a] + E[\gamma]^2 \cdot E[K_a]^2) \quad \text{(A-15)}$$

The COV can be represented in terms of the correlation coefficient, ρ, which is

$$\rho_{\gamma K_a} = \frac{COV[\gamma, K_a]}{\sigma_\gamma \cdot \sigma_{K_a}} \quad \text{(A-16)}$$

Substituting Equation A-16 into Equation A-15 results in

$$E[P_{EH}]^2 = \alpha^2\left(\frac{1}{2}\right)^2 (H^2)^2\left(var[\gamma]\cdot var[K_a]\cdot {\rho_{\gamma K_a}}^2 + 2\cdot\sqrt{(var[\gamma]\cdot var[K_a])}\cdot\rho_{\gamma K_a} + E[\gamma]^2\cdot E[K_a]^2\right) \tag{A-17}$$

The variance of P_{EH} is expressed as

$$var[P_{EH}] = E[(P_{EH} - E[P_{EH}])^2]$$

$$var[P_{EH}] = E\left[\left(\alpha\frac{1}{2}\gamma H^2 K_a + E\left[\alpha\frac{1}{2}\gamma H^2 K_a\right]\right)^2\right]$$

$$var[P_{EH}] = \alpha^2\left(\frac{1}{2}\right)^2 (H^2)^2 E[(\gamma K_a - E[\gamma K_a])^2]$$

$$var[P_{EH}] = \alpha^2\left(\frac{1}{2}\right)^2 (H^2)^2 var[\gamma K_a]$$

Since there is correlation between $\tan\phi$ and γ, the variance of the product is expressed as

$$var[\gamma K_a] = COV[\gamma, K_a]^2 + 2\cdot COV[\gamma, K_a]\cdot E[\gamma]\cdot E[K_a] + E[K_a]^2\cdot var[\gamma] + E[\gamma]^2\cdot var[K_a] + var[\gamma]\cdot var[K_a] \tag{A-18}$$

Obtaining the variance in terms of the correlation coefficient from Equation 3A gives

$$var[\gamma K_a] = var[\gamma]\cdot var[K_a]\cdot {\rho_{\gamma K_a}}^2 + \ldots$$

$$2\cdot\rho_{\gamma K_a}\sqrt{(var[\gamma]\cdot var[K_a])}\cdot E[\gamma]\cdot E[K_a] + \ldots$$

$$E[K_a]^2\cdot var[\gamma] + E[\gamma]^2\cdot var[K_a] + var[\gamma]\cdot var[K_a] \tag{A-19}$$

With Equations A-17 and A-19 the CV of the load due to the horizontal soil pressure with correlated random variables can be expressed for use in the LRFD φ equation for retaining wall sliding.

$$CV_{P_{EH}}^2 = \frac{\alpha^2 \left(\frac{1}{2}\right)^2 (H^2)^2 var[\gamma K_a]}{\alpha^2 \left(\frac{1}{2}\right)^2 (H^2)^2 \left(var[\gamma] \cdot var[K_a] \cdot {\rho_{\gamma K_a}}^2 + 2 \cdot \sqrt{(var[\gamma] \cdot var[K_a])} \cdot \rho_{\gamma K_a} + E[\gamma]^2 \cdot E[K_a]^2\right)}$$

Substituting in Equation A-16 and cancelling like terms, the expression becomes

$$CV_{P_{EH}}^2 = \frac{var[\gamma] \cdot var[K_a] \cdot {\rho_{\gamma K_a}}^2 +}{\left(var[\gamma] \cdot var[K_a] \cdot {\rho_{\gamma K_a}}^2 + 2 \cdot \sqrt{(var[\gamma] \cdot var[K_a])} \cdot \rho_{\gamma K_a} + E[\gamma]^2 \cdot E[K_a]^2\right)} \cdots$$

$$\frac{2 \cdot \rho_{\gamma \tan\phi} \sqrt{(var[\gamma] \cdot var[K_a])} \cdot E[\gamma] \cdot E[K_a] +}{\left(var[\gamma] \cdot var[K_a] \cdot {\rho_{\gamma K_a}}^2 + 2 \cdot \sqrt{(var[\gamma] \cdot var[K_a])} \cdot \rho_{\gamma K_a} + E[\gamma]^2 \cdot E[K_a]^2\right)} \cdots$$

$$\frac{E[K_a]^2 \cdot var[\gamma] + E[\gamma]^2 \cdot var[K_a] + var[\gamma] \cdot var[K_a]}{\left(var[\gamma] \cdot var[K_a] \cdot {\rho_{\gamma K_a}}^2 + 2 \cdot \sqrt{(var[\gamma] \cdot var[K_a])} \cdot \rho_{\gamma K_a} + E[\gamma]^2 \cdot E[K_a]^2\right)}$$

Dividing the numerator and denominator by $E[\gamma]^2 \cdot E[K_a]^2$ simplifies the equation into terms of CV for K_a and γ.

$$CV_{P_{EH}}^2 = \frac{\rho_{\gamma K_a}^2 \cdot CV_\gamma^2 \cdot CV_{K_a}^2 + 2 \cdot \rho_{\gamma K_a} \cdot CV_\gamma \cdot CV_{K_a} + CV_\gamma^2 + CV_{K_a}^2 + CV_\gamma^2 \cdot CV_{K_a}^2}{CV_\gamma^2 \cdot CV_{K_a}^2 \cdot \rho_{\gamma K_a}^2 + 2 \cdot \rho \cdot CV_\gamma \cdot CV_{K_a} + 1}$$

If correlation doesn't exist (i.e., ρ = 0) between K_a and γ, $CV_{P_{EH}}^2$ becomes

$$CV_{P_{EH}}^2 = CV_\gamma^2 + CV_{K_a}^2 + CV_\gamma^2 \cdot CV_{K_a}^2$$

Or, in terms of the variance and mean of uncorrelated random variables

$$CV_{P_{EH}}^2 = \frac{E[K_a]^2 \cdot var[\gamma] + E[\gamma]^2 \cdot var[K_a] + var[\gamma] \cdot var[K_a]}{E[\gamma]^2 \cdot E[K_a]^2} \qquad \text{(A-20)}$$

<u>LIVE LOAD FOR SLIDING STABILITY</u>

The following is the derivation of the CV of the live load, CV_{LS} is

$$P_{LS} = \alpha q_s H K_a$$

$$E[P_{LS}] = E[\alpha q_s H K_a]$$

$$E[P_{LS}]^2 = \alpha^2 H^2 E[q_s K_a]^2$$

$$E[P_{LS}]^2 = \alpha^2 H^2 E[q_s]^2 E[K_a]^2 \quad \text{(A-21)}$$

The variance of the live load can be expressed as

$$var[P_{LS}] = E[(P_{LS} - E[P_{LS}])^2]$$

$$var[P_{LS}] = E[(\alpha q_s H K_a - E[\alpha q_s H K_a])^2]$$

$$var[P_{LS}] = E[(\alpha^2 q_s^2 H^2 K_a^2 - 2 \cdot \alpha q_s H K_a \cdot E[\alpha q_s H K_a] + E[\alpha q_s H K_a]^2)]$$

$$var[P_{LS}] = \alpha^2 H^2 (E[q_s^2 K_a^2] - E[q_s K_a]^2)$$

$$var[P_{LS}] = \alpha^2 H^2 (var[q_s] \cdot var[K_a] + 2 \cdot COV[q_s, K_a]^2 - E[q_s]^2 E[K_a]^2)$$

However, since correlation doesn't exist between the two variables, COV = 0, and the variance becomes

$$var[P_{LS}] = \alpha^2 H^2 (var[q_s] \cdot var[K_a] - COV[q_s, K_a]^2$$
$$- 2 \cdot COV[q_s, K_a] \cdot E[q_s] \cdot E[K_a] - E[q_s]^2 \cdot E[K_a]^2 \ )$$

$$CV_{LS}^2 = \frac{E[q_s]^2 \cdot var[K_a] + E[K_a]^2 \cdot var[q_s] + var[K_a] \cdot var[q_s]}{E[K_a]^2 \cdot E[q_s]^2} \quad \text{(A-22)}$$

<u>RESISTANCE FOR SLIDING STABILITY</u>

The following is the derivation of CV_R for the case of correlation.

$$CV_R^2 = \frac{\sigma_R^2}{E[R]^2} = \frac{var_R}{E[R]^2}$$

The factored resistance of a MSE wall to sliding on cohesionless soil is expressed as

$$R_{Sliding} = \alpha \gamma_{rs} H L \tan \phi$$

Where ϕ is the smallest friction angle at the sliding plane and $\tan\phi$ is dependent on γ_{rs}. Note, a load factor, α, is applied to the vertical earth pressure component of the resistance, R.

The squared mean of R is expressed as

$$E[R]^2 = E[\alpha HL\gamma \tan\phi]^2$$

$$E[R]^2 = \alpha^2 H^2 L^2 E[\gamma \tan\phi]^2 \tag{A-23}$$

The expected value of dependent (correlated) random variables can be determined from the covariance, COV, of two random variables

$$COV[\gamma, tan\phi] = E[\gamma tan\phi] - E[\gamma] \cdot E[tan\phi]$$

$$E[\gamma tan\phi] = COV[\gamma, tan\phi] + E[\gamma] \cdot E[tan\phi]$$

Thus Equation A-23 becomes

$$E[R]^2 = \alpha^2 H^2 L^2 (COV[\gamma, tan\phi]^2 + 2 \cdot COV[\gamma, tan\phi] \cdot E[\gamma] \cdot E[tan\phi] + E[\gamma]^2 \cdot E[tan\phi]^2) \tag{A-24}$$

The COV can be represented in terms of the correlation coefficient, ρ, which is

$$\rho_{\gamma \tan\phi} = \frac{COV[\gamma, \tan\phi]}{\sigma_\gamma \cdot \sigma_{\tan\phi}} \tag{A-25}$$

Squaring the terms of Equation A-25 and substituting into Equation A-24 results in

$$E[R]^2 = \alpha^2 H^2 L^2 \left(var[\gamma] \cdot var[\tan\phi] \cdot {\rho_{\gamma \tan\phi}}^2 + 2 \cdot \sqrt{(var[\gamma] \cdot var[\tan\phi])} \cdot \rho \cdot E[\gamma] \cdot E[tan\phi] + E[\gamma]^2 \cdot E[tan\phi]^2\right) \tag{A-26}$$

The variance of R is expressed as

$$var[R] = E[(R - E[R])^2]$$

$$var[R] = E[(\alpha HL\gamma \tan\phi - E[\alpha HL\gamma \tan\phi])^2]$$

$var[R] = \alpha^2 H^2 L^2 E[(\gamma \tan\phi - E[\gamma \tan\phi])^2]$

$var[R] = \alpha^2 H^2 L^2 var[\gamma \tan\phi]$ (A-27)

Since there might be correlation between tanϕ and γ, the variance of the product of two dependent variants is expressed as

$var[\gamma \tan\phi] = COV[\gamma, tan\phi]^2 + 2 \cdot COV[\gamma, tan\phi] \cdot E[\gamma] \cdot E[\tan\phi] +$

$E[\tan\phi]^2 \cdot var[\gamma] + E[\gamma]^2 \cdot var[\tan\phi] + var[\gamma] \cdot var[\tan\phi]$ (A-28)

Obtaining the variance in terms of the correlation coefficient gives

$var[\gamma \tan\phi] = {\rho_{\gamma \tan\phi}}^2 \cdot var[\gamma] \cdot var[\tan\phi] + \ldots$

$2 \cdot \rho_{\gamma \tan\phi} \sqrt{(var[\gamma] \cdot var[\tan\phi])} \cdot E[\gamma] \cdot E[\tan\phi] + \ldots$

$E[\tan\phi]^2 \cdot var[\gamma] + E[\gamma]^2 \cdot var[\tan\phi] + var[\gamma] \cdot var[\tan\phi]$ (A-29)

With Equations A-26 and A-29 the CV of the resistance with correlated random variables can be expressed for use in the LRFD φ equation for retaining wall sliding. Cancelling the constants and the equation becomes

$$CV_R^2$$

$$= \frac{{\rho_{\gamma \tan\phi}}^2 \cdot var[\gamma] \cdot var[\tan\phi] +}{\left(var[\gamma] \cdot var[\tan\phi] \cdot {\rho_{\gamma \tan\phi}}^2 + 2 \cdot \sqrt{(var[\gamma] \cdot var[\tan\phi])} \cdot \rho \cdot E[\gamma] \cdot E[tan\phi] + E[\gamma]^2 \cdot E[tan\phi]^2\right)} \ldots$$

$$\frac{2 \cdot \rho_{\gamma \tan\phi} \sqrt{(var[\gamma] \cdot var[\tan\phi])} \cdot E[\gamma] \cdot E[\tan\phi] +}{\left(var[\gamma] \cdot var[\tan\phi] \cdot {\rho_{\gamma \tan\phi}}^2 + 2 \cdot \sqrt{(var[\gamma] \cdot var[\tan\phi])} \cdot \rho \cdot E[\gamma] \cdot E[tan\phi] + E[\gamma]^2 \cdot E[tan\phi]^2\right)} \ldots$$

$$\frac{E[\tan\phi]^2 \cdot var[\gamma] + E[\gamma]^2 \cdot var[\tan\phi] + var[\gamma] \cdot var[\tan\phi]}{\left(var[\gamma] \cdot var[\tan\phi] \cdot {\rho_{\gamma \tan\phi}}^2 + 2 \cdot \sqrt{(var[\gamma] \cdot var[\tan\phi])} \cdot \rho \cdot E[\gamma] \cdot E[tan\phi] + E[\gamma]^2 \cdot E[tan\phi]^2\right)}$$

Dividing the numerator and denominator by $E[\gamma]^2 \cdot E[tan\phi]^2$ simplifies the equation into terms of CV for tanϕ and γ.

$$CV_R^2 = \frac{\rho^2_{\gamma\tan\phi} \cdot CV_\gamma^2 \cdot CV^2_{\tan\phi} + 2 \cdot \rho_{\gamma\tan\phi} \cdot CV_\gamma \cdot CV_{\tan\phi} + CV_\gamma^2 + CV^2_{\tan\phi} + CV_\gamma^2 \cdot CV^2_{\tan\phi}}{CV_\gamma^2 \cdot CV^2_{\tan\phi} \cdot \rho^2_{\gamma\tan\phi} + 2 \cdot \rho_{\gamma\tan\phi} \cdot CV_\gamma \cdot CV_{\tan\phi} + 1}$$

If correlation doesn't exist (i.e., ρ = 0) between $\tan\phi$ and γ, CV_R^2 becomes

$$CV_R^2 = CV_\gamma^2 + CV^2_{\tan\phi} + CV_\gamma^2 \cdot CV^2_{\tan\phi}$$

Or, in terms of the variance and mean of uncorrelated random variables

$$CV_R^2 = \frac{E[\tan\phi]^2 \cdot var[\gamma] + E[\gamma]^2 \cdot var[\tan\phi] + var[\gamma] \cdot var[\tan\phi]}{E[\gamma]^2 \cdot E[tan\phi]^2} \tag{A-30}$$

SURCHARGE LOAD FOR BEARING STABILITY

Derivation of the CV of the surcharge load (live load), CV_{LS} is

$$P_{LS} = (\alpha q_s H)M \tag{A-31}$$

where

$$M = \frac{\cos(\delta)}{\cos(\delta) + \frac{\sin(\delta)}{\tan(\psi)}} \tag{A-32}$$

where $\psi = \theta - \phi_{bf}$, which varies due to the variable backfill, and δ is taken as a constant.

$$E[P_{LS}] = E[\alpha q_s H M]$$

$$E[P_{LS}]^2 = \alpha^2 H^2 E[q_s M]^2$$

$$E[P_{LS}]^2 = \alpha^2 H^2 E[q_s]^2 E[M]^2 \tag{A-33}$$

Where

$$E[M]^2 = \frac{\cos(\delta)^2}{\cos(\delta)^2 + \frac{\sin(\delta)^2}{\tan\left(45° - \frac{\mu_{\phi_{bf}}}{2}\right)^2}} \tag{A-34}$$

The variance of the live load can be expressed as

$$var[P_{LS}] = E[(P_{LS} - E[P_{LS}])^2]$$

$$var[P_{LS}] = E[(\alpha q_s H M - E[\alpha q_s H M])^2]$$

$$var[P_{LS}] = E[(\alpha^2 q_s^2 H^2 M^2 - 2 \cdot \alpha q_s HM \cdot E[\alpha q_s HM] + E[\alpha q_s HM]^2)]$$

$$var[P_{LS}] = \alpha^2 H^2 (E[q_s^2 M^2] - E[q_s M]^2)$$

$$var[P_{LS}] = \alpha^2 H^2 E[(q_s M - E[q_s M])^2]$$

$$var[P_{LS}] = \alpha^2 H^2 var[q_s M]$$

$$var[q_s M] = E[q_s]^2 \cdot var[M] + E[M]^2 \cdot var[q_s] + var[M] \cdot var[q_s] \qquad \text{(A-35)}$$

where

$$var[M] = \left[\frac{\cos(\delta)\sin(\delta)\csc\left(45^\circ - \frac{\mu_{\phi_{bf}}}{2}\right)\left(\frac{1}{2}\right)}{\left(\cos(\delta) + \sin(\delta)\cot\left(45^\circ - \frac{\mu_{\phi_{bf}}}{2}\right)\right)^2} \right]^2 var_{\phi_{bf}}$$

Substituting Equations A-33 and A-35 (mean and variance of P_{LS}) into the expression for CV^2 (var/mean^2) gives

$$CV_{P_{LS}}^2 = \frac{\alpha^2 H^2 \left[E[q_s]^2 \cdot var[M] + E[M]^2 \cdot var[q_s] + var[M] \cdot var[q_s]\right]}{\alpha^2 H^2 E[q_s]^2 \cdot E[M]^2}$$

Cancelling like terms gives

$$CV_{P_{LS}}^2 = \frac{E[q_s]^2 \cdot var[M] + E[M]^2 \cdot var[q_s] + var[M] \cdot var[q_s]}{E[q_s]^2 \cdot E[M]^2}$$

$$CV_{P_{LS}}^2 = CV_{q_s}^2 + CV_M^2 + CV_{q_s}^2 \cdot CV_M^2$$